Design of pH Sensitive Electrochemical Sensor for Catecholamine Neurotransmitters Detection and the Screening Off of Ascorbic Acid

A thesis submitted for the fulfilment of requirement for the degree of

MASTER OF SCIENCE

of

RHODES UNIVERSITY

by

KEAMOGETSE TEBOGO CHARLOTTE TSHENKENG

January 2021

Dedications

This thesis is dedicated to my amazing Mom,

Mrs Kelebogile Gloria Tshenkeng

My late Father,

Mr Desmond Mokwene Tshenkeng

My younger Brother,

Tshepang Caution Tshenkeng

And my younger Sister,

Onalenna Chloe Galeboe

Trust in the Lord with all your heart and lean not on your own understanding; in all your ways acknowledge Him, and He shall direct your paths.

~ Proverbs 3:5-6

Acknowledgements

Firstly, I would like to thank God for all the opportunities and things that He has blessed me with and the lessons He has allowed me to go through in an effort to get me to become the best version of myself. Most of all, I am thankful to God for giving off His Son, Jesus Christ to die for my sins so that I may have eternal life. This is by far the greatest love that I will ever know.

I would like to extend my sincere gratitude to my supervisor, Prof P. N. Mashazi, for firstly affording me the opportunity to conduct my MSc studies in his laboratory and helping me secure funding for said studies. Also, I am thankful for his guidance throughout my studies and his willingness to share the wealth of knowledge and expertise he has gained in the field of chemistry over the years. I am also thankful for his patience and support throughout my studies as this has not been an easy journey. I wish him a long and fruitful journey as an academic and researcher.

To my Mom, Kelebogile Gloria Tshenkeng, you are grace personified! I thank God for your life and am grateful that He blessed me with a Mom such as yourself. I could not be half the person that I am had it not been for your constant love, support, encouragement and countless sacrifices. Thank you! Should I ever be blessed to become a Mom one day, I pray that I be as good a Mom to my child(ren) as you have been to me. May God grant you a life long enough to reap the seeds that you have sown.

To my brother, Tshepang Caution Tshenkeng, may you find your purpose on this Earth, fulfil it and ultimately live a life far beyond your or anyone else's imagination. To my sister, Onalenna Chloe Galeboe, for as long as I could remember, I have always longed to have a sister and in 2010 you came into our lives. You have been a

wonderful addition to our lives and I look forward to watching you grow into the woman God created you to be. I love you my Pumpkin!

I also wish to extend my gratitude to the Tshenkeng, Mentor and Galeboe families for all the support and words of encouragement throughout the years. It is truly appreciated. Additionally, I am grateful to Ntlanganiso for standing by me and supporting me during the tail-end of my Masters journey.

I am thankful to all the friendships that I gained (although some have since ended) and the wonderful people I met throughout these years: Sixolile, Zelda, Muthumuni, Omotayo, Daniel, Nnamdi, Simbongile and Thabo. Thank you for all the words of encouragement, support and advising me either academically or on a personal level. I am truly grateful.

I would also like to extend my gratitude to David, Edward and Christian for helping me with the synthesis aspect of my research. Thank you to Omotayo and Daniel for helping me with the electrochemistry technique and other aspects of my research. Thank you to Omotayo, Zelda, Asanda and Mziyanda for staying up with me on campus and walking me home when I had to work late night in the electrochemistry room. This honestly meant a great deal to me. Additionally, I am grateful to all the lab mates and interns I have had throughout the years. To Labs F3 and F5, thank you for all the fruitful group presentations that have aided my studies and for filling the laboratories with your warm spirits and endless laughter.

I would like to thank the Institute for Nanotechnology Innovation for use of their equipment and the expertise of their technical staff in certain aspects of my characterization. I would also like to thank the Rhodes University Chemistry Department and Rhodes University at large for allowing me the opportunity to be

registered at the university and for all the support structures and staff they have in place that enabled me to conduct my studies in a cohesive and well-resourced environment.

Last but certainly not least, I am grateful to the National Research Foundation (NRF) for providing me with financial support through the NRF Scarce Skills Masters Scholarship. This was greatly appreciated!

God's dream for you is greater than your dream for yourself.

~ Oprah Winfrey

Abstract

This study presents the synthesis of cobalt (II) tetra-(3-carboxyphenoxy) phthalocyanine (CoTCPhOPc) through the cyclotetramerization of 4-(3-carboxyphenoxy)phthalonitrile and its full characterization using Fourier transform infrared (FT-IR) spectroscopy, ultraviolet-visible (UV-vis) spectroscopy, magnetic circular dichroism (MCD) spectroscopy, elemental analysis and mass spectrometry. The CoTCPhOPc was then immobilized onto phenylethylamino (PEA) pre-grafted gold electrode surface, Au-PEA using amide coupling reaction through a reaction with NHS and DCC to obtain Au-PEA-CoTCPhOPc. This yielded pH sensitive thin films due to the terminal carboxylic acid (–COOH) functional groups. Electrochemical and surface characterization was conducted to confirm the modification of the bare Au with PEA thin film (Au-PEA) and amide coupling of CoTCPhOPc (Au-PEA-CoTCPhOPc). The Au-PEA-CoTCPhOPc electrode was shown to possess pH selective properties towards negatively charged $[Fe(CN)_6]^{3-/4-}$ and positively charged $[Ru(NH_3)_6]^{2+/3+}$ redox probes.

Au-PEA-CoTCPhOPc electrode surface enabled the detection of catecholamine neurotransmitters (dopamine, norepinephrine and epinephrine) and the screening off of ascorbic acid by means of pH sensitive functional groups. Bare Au and Au-PEA electrodes exhibited electro-oxidation and electroreduction of catecholamine neurotransmitters and ascorbic acid at higher potentials compared to Au-PEA-CoTCPhOPc. There was no electro-oxidation or electroreduction of ascorbic acid at Au-PEA-CoTCPhOPc. For Au-PEA-CoTCPhOPc, excellent electrocatalytic oxidation with the limit of detection (LoD) determined using 3σ was found to be 1.32 (0.95), 2.11 (1.78) and 3.08 μM for electro-oxidation and electroreduction (in brackets) of dopamine, norepinephrine and epinephrine respectively. The limit of quantification (LoQ) was

determined using 10σ and found to be 4.41 (3.17), 7.02 (5.93) and 10.3 μM electro-oxidation and electroreduction (in brackets) for dopamine, norepinephrine and epinephrine respectively. The Au-PEA-CoTCPhOPc thin film was shown to screen off ascorbic acid as no electrocatalytic oxidation was observed for up to 100.0 μM concentration.

Table of Contents

List of Abbreviations

^{13}C NMR	:	Carbon nuclear magnetic resonance
^{1}H NMR	:	Proton nuclear magnetic resonance
AA	:	Ascorbic acid
AEBD	:	4-(2-Aminoethyl)benzene diazonium salt
Ag|AgCl	:	Silver|silver chloride reference electrode
Al_2O_3	:	Aluminium oxide
Au-C	:	Gold carbide bond
Au-PEA	:	Phenylethylamine grafted gold electrode
Au-PEA-CoTCPhOPc	:	Amide coupled cobalt (II) tetra-(3-carboxyphenoxy) phthalocyanine onto phenylethylamine grafted gold electrode
Au-S	:	Gold sulphur bond
Bare Au	:	Bare gold electrode
C-C	:	Carbo-carbo
CE	:	Counter electrode
Co	:	Cobalt metal ion
$CoCl_2$	:	Cobalt (II) chloride
CoTCPhOPc	:	Cobalt (II) tetra-(3-carboxyphenoxy) phthalocyanine
$CuSO_4$	:	Copper sulphate
CV	:	Cyclic voltammetry
CV	:	Cyclic voltammogram
D_2O	:	Deuterium oxide
d_6-DMSO	:	Deuterated dimethyl sulfoxide

DA	:	Dopamine
DBU	:	1,8-Diazabicyclo(5.4.0)undec-7-ene
DCC	:	N,N’-dicyclohexylcarbodiimide
DMF	:	Dimethylformamide
DMSO	:	Dimethyl sulfoxide
DOPA	:	3,4-Dihydroxyphenylalanine
EIS	:	Electrochemical impedance spectroscopy
EP	:	Epinephrine (also adrenaline)
FT-IR	:	Fourier transform infrared
H_2O_2	:	Hydrogen peroxide
H_2Pc	:	Metal free phthalocyanine
H_2SO_4	:	Sulphuric acid
HBF_4	:	Tetrafluoroboric acid
HCl	:	Hydrochloric acid
HOMO	:	Highest occupied molecular orbital
K_2CO_3	:	Potassium carbonate
$K_3[Fe(CN)_6]$	:	Potassium ferricyanide
$K_4[Fe(CN)_6]\cdot 3H_2O$	:	Potassium hexacyanoferrate(II) trihydrate
KCl	:	Potassium chloride
KH_2PO_4	:	Potassium dihydrogen orthophosphate
KOH	:	Potassium hydroxide
LCR	:	Linear concentration range
LoD	:	Limit of detection
LoQ	:	Limit of quantification
LUMO	:	Lowest unoccupied molecular orbital

M	:	Metal
M-C	:	Metal-carbon bond
MCD	:	Magnetic circular dichroism
MeOH	:	Methanol
MPc	:	Metallophthalocyanine
Na_2HPO_4	:	Di-sodium hydrogen orthophosphate
NaCl	:	Sodium chloride
$NaNO_2$	:	Sodium nitrite
NaOH	:	Sodium hydroxide
NEP	:	Norepinephrine (also noradrenaline)
NHS	:	N-hydroxysuccinimide
NLO	:	Nonlinear optics
NT	:	Neurotransmitter
OLED	:	Organic light emitting diode
Ox	:	Oxidation
PBS	:	Phosphate buffer saline solution
Pc	:	Phthalocyanine
PDT	:	Photodynamic therapy
PEA	:	Phenylethylamine
Por	:	Porphyrin
PS	:	Photosensitizer
RE	:	Reference electrode
Red	:	Reduction
Ref	:	Reference
$Ru(NH_3)_6Cl_3$	:	Hexaaminеruthenium (III) chloride

SAM	:	Self-assembled monolayer
SCE	:	Saturated calomel electrode
SHE	:	Standard hydrogen electrode
$TBABF_4$	:	Tetrabutylammonium tetrafluoroborate
THF	:	Tetrahydrofuran
UDP	:	Under-potential separation
UV-Vis	:	Ultra violet visible
WE	:	Working electrode
XPS	:	X-ray photoelectron spectroscopy

List of Figures

List of Tables

List of Schemes

List of Symbols

A	:	Geometric surface area of gold electrode surface
C_{dl}	:	Double-layer capacitance
CPE	:	Constant phase element
e^-	:	Electron
E	:	Potential
E°	:	Standard potential
$E_{½}$	:	Half-wave potential
E_{pa}	:	Anodic peak potential
E_{pc}	:	Cathodic peak potential
eV	:	Electron volts
f	:	Frequency
F	:	Faraday's contant
H^+	:	Proton
Hz	:	Hertz
I	:	Current
I_p	:	Peak current
I_{pa}	:	Anodic peak current
I_{pa}/I_{pc}	:	Ratio of anodic to cathodic peak currents
I_{pc}	:	Cathodic peak current
n	:	Number of electrons
o	:	Octa substituted
Q	:	Charge
Q_{bare}	:	Integrated electrical charge due to bare gold electrode
$Q_{thin\ layer}$	:	Integrated electrical charge due to CoTCPhOPc modified gold electrode
r	:	Radius of electrode
R_{CT}	:	Charge transfer resistance
R_S	:	Electrolyte resistance

t	:	Tetra substituted
v	:	Scan rate
V	:	Voltage
Z	:	Impedance (or complex resistance)
Z’	:	Real component of the impedance
Z’’	:	Imaginary component of the impedance
Z_W	:	Warburg impedance
$\Gamma_{Au\text{-}PEA\text{-}CoTCPhOPc}$	:	Amount of CoTCPhOPc immobilized via amide coupling
Γ_{ibf}	:	Ion barrier factor
ΔE	:	Peak-to-peak separation
Θ	:	Phase angle
ω	:	Angular frequency
Ω	:	Ohm

Chapter One: Introduction

1. Introduction

This chapter provides an overview of the intended study. It also lays out the background and an understanding of the intended study and motivates for its necessity and contribution to the scientific field. In addition, an explanation of the concepts that will be discussed at length in the study to be conducted will also be provided.

1.1 Neurotransmitters

Neuronal networks process large amounts of information received from ones environment and from a number of senses such as eye sight, hearing, feel, emotion, touch and various other normal bodily functions. These senses are then combined with signals transmitted throughout the body. The brain utilizes neurons in order to pass information from the brain to other organs in the body and vice versa using a number of electrical impulses.[1] This transmission of messages occurs via the secretion of the neurotransmitters (NTs) from one neuron, which then binds to the specific receptor on the membrane of the target cell.[2] In essence, neurotransmitters are chemical messengers (or signals) that pass a message between neurons,[3] act on muscle cells or stimulate a response by glandular cells.[4]

The first known neurotransmitter – acetylcholine – was discovered in 1921 by the Nobel Prize winner, Otto Loewi through his work on the nervous regulation of cardiac activity.[4] Following this discovery, more than a hundred neurotransmitters have been found.[5] There are a number of classification criteria used for neurotransmitters with the most common being to classify them by the molecules they belong to.[4] Using this classification, neurotransmitters are classified into one of three groups: amino acid neurotransmitters, neuropeptides and atypical neurotransmitters.[6] The present study

investigates catecholamine neurotransmitters which form part of amino acid neurotransmitters.

1.1.1 Catecholamine Neurotransmitters

Catecholamines are neurotransmitters and/or hormones in the peripheral and central nervous system.[7] They have the means to excite, inhibit or influence the activity of cells. This class of neurotransmitters includes dopamine (DA), norepinephrine (NEP) and epinephrine (EP). Catecholamine neurotransmitters are so named because they share the catechol moiety (highlighted in red) shown in **Figure 1.1 (a)** as well as an amino group.[8] Catecholamine neurotransmitters are derived from a common precursor, namely, the amino acid tyrosine.[1] **Figure 1.1** shows the chemical structure of **(a)** catechol moiety, **(b)** dopamine, **(c)** norepinephrine and **(d)** epinephrine.

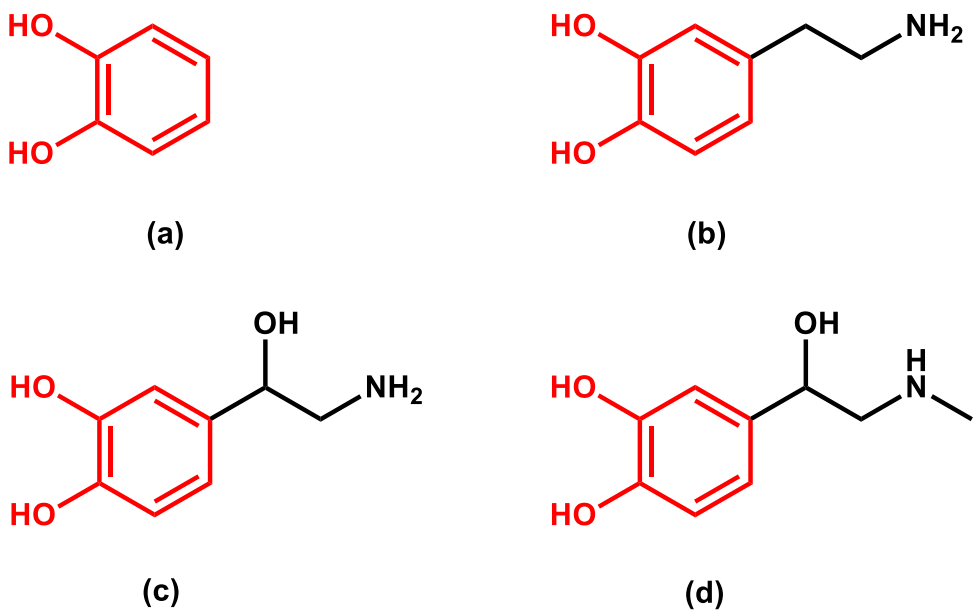

Figure 1.1: Chemical structure of **(a)** catechol moiety, **(b)** dopamine, **(c)** norepinephrine and **(d)** epinephrine.

Scheme 1.1 shows the biological synthesis of dopamine, norepinephrine and epinephrine via multiple selective enzymes. The first step in catecholamine synthesis is catalysed by tyrosine hydroxylase[1] to form 3,4-dihydroxyphenylalanine (L-DOPA), which gives origin to DA after the action of DOPA decarboxylase.[9] Dopamine plays a vital role in the function of the central nervous system, renal, hormonal and cardiovascular systems.[2] Dopamine has been shown to be associated with the bodily reward system. In the brain, dopamine is responsible for the motivation, seek out stimuli and emotions of feeling satisfied and fulfilled in one's environment. The common understanding is that this is activated by natural rewards like food, drink, pleasurable activity and possibly addictive drugs. For example, cocaine and other addictive drugs act by stimulating the release of dopamine from specific brain areas.[1] Abnormal levels of dopamine are indicative of disease states such as Parkinson's disease, senile dementia and schizophrenia.[10]

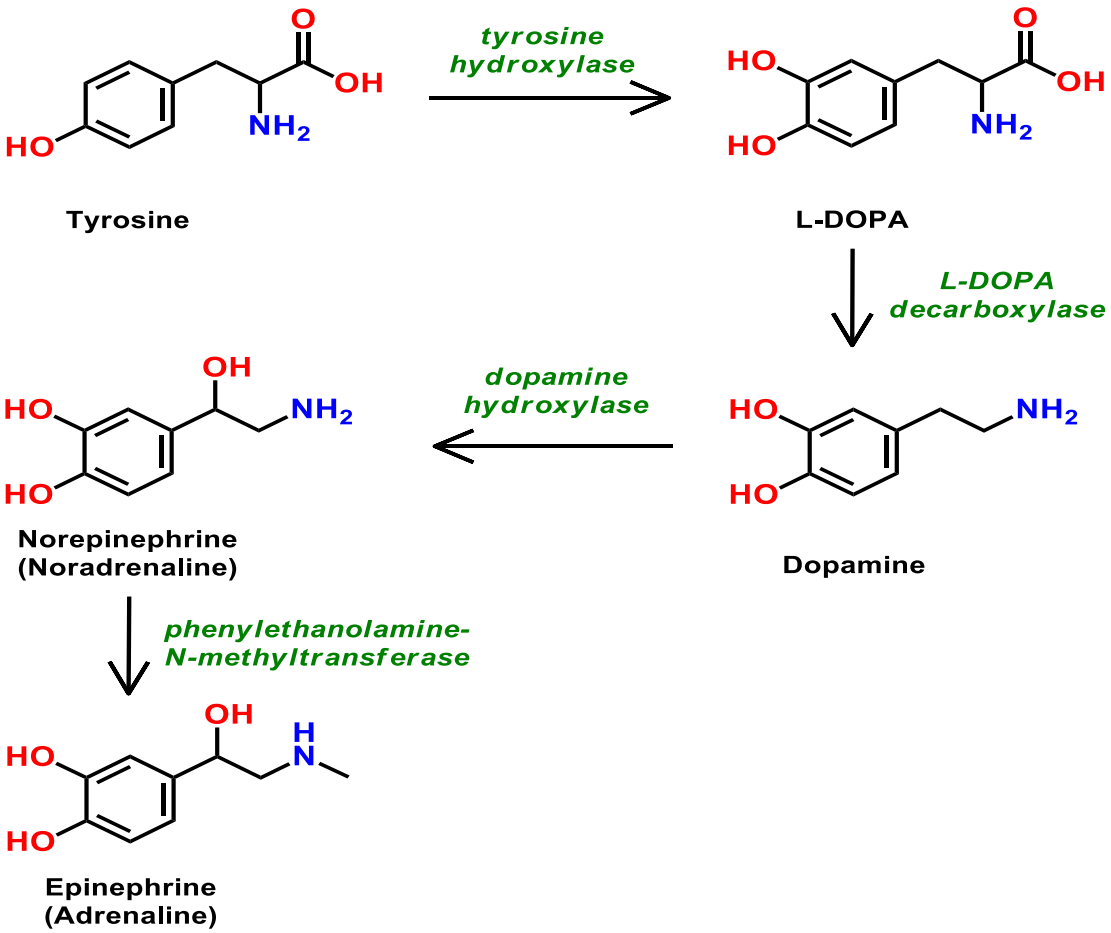

Scheme 1.1: Biological synthesis of dopamine, norepinephrine and epinephrine via multiple selective enzymes.

The synthesis of norepinephrine (also noradrenaline) involves the conversion of dopamine by dopamine β-hydroxylase enzyme. Norepinephrine is a neurotransmitter in the brain and in postganglionic sympathetic neurons. It influences sleep and wakefulness, attention, feeding behaviour, [1] stress and depression.[11] Norepinephrine can be used to treat myocardial infarction hypertension, bronchial asthma and organic heart disease. Adverse abnormalities in the levels of norepinephrine can lead to ganglia neuroblastoma, ganglion neuronal, paraganglioma and Parkinson's disease.[2]

Epinephrine (also adrenaline) is formed from norepinephrine and the enzyme involved for this transformation is phenylethanolamine-*N*-methyltransferase. Epinephrine is a hormone and neurotransmitter released from the adrenal gland and it stimulates catecholamine receptors in various organs.[1] Epinephrine is also found in the central nervous system and bodily fluids as an organic cation.[12] It plays a pivotal role in the transmission of nerve impulse,[13] during times of physical and mental stress[1] (fight-or-flight response)[5] and has been used as a common emergency healthcare medicine.[1] Abnormal levels of epinephrine have been associated with Parkingson's disease, Schizophrenia and Huntington's disease.[13] Additionally, epinephrine has also been used as a drug for the treatment of hypertension.[14]

1.1.2 Motivation for the Detection of Catecholamine Neurotransmitters

It is clear that whilst catecholamine neurotransmitters have their benefits, they can also have adverse effects on the body if not carefully monitored. Consequently, the interest in the function and measurement of catecholamine neurotransmitters is due to their potential to serve as clinical biomarkers for specific diseases or the ability to monitor the efficacy of treatments that have been administered.[1,15] As a result, a lot of research has gone into finding ways of monitoring concentration levels of catecholamine neurotransmitters.

1.1.3 Detecting Catecholamine Neurotransmitters

There are various methods that have been developed for the detection of catecholamine neurotransmitters and these include: spectrophotometry,[16] Raman spectroscopy,[8] chromatography,[17] fluorescence,[7,18] flow injection,[19] and colorimetric detection.[20-22] Whilst these methods have shown good selectivity and low levels of detection, they often need complex sample pre-treatment steps and utilize expensive instrumentation. Electrochemical sensors have also been investigated for the detection of catecholamine neurotransmitters.[9] The research interest in electrochemical sensors has increasingly grown as these are inexpensive and easy to operate analytical tools.[10] They are also sensitive, rapid[3] and afford selective detection of catecholamine neurotransmitters. Additionally, electrochemical sensors are capable of being incorporated into robust, portable and miniaturized devices for targeted applications in clinical and diagnostic fields.[1]

1.2 Electrochemical Sensors for the Detection of Catecholamine Neurotransmitters

Catecholamine neurotransmitters are electroactive and can undergo oxidation and sometimes reduction.[13] Their catechol moiety mentioned in **1.1.1** can be oxidised to form *o*-quinone moiety through the removal of the two protons.[14] The electrochemical detection of catecholamine neurotransmitters is made possible due to their ease of undergoing electrocatalytical oxidation[23] and reduction.[13] **Scheme 1.2** shows the process of the electrochemical oxidation of dopamine (with the *o*-quinone moiety highlighted in red) to serve as an illustration of how catecholamine neurotransmitters are oxidised. Electrochemistry is a strong technique to explore reactions which involve

the transfer of electrons. This is because electrochemistry associates the flow of electrons to chemical changes.[24]

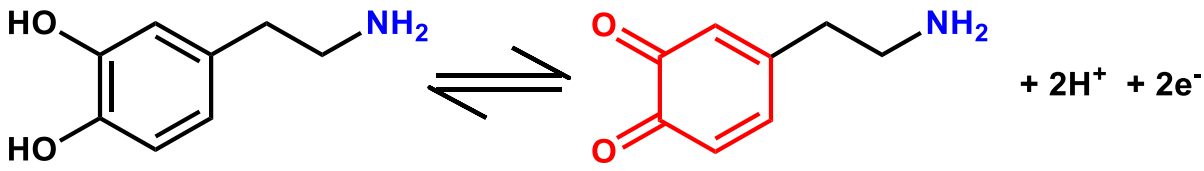

Scheme 1.2: Mechanism of dopamine oxidation with the *o*-quinone moiety highlighted in red.

Despite the numerous advantages of the electrochemical detection of catecholamine neurotransmitters stated in **1.1.3**, the technique does have its own limitations. Firstly, the electro-oxidation of neurotransmitters on bare electrode surfaces is a slow electron transfer process and occurs at high potentials. Additionally, neurotransmitters adsorb onto the bare electrode surface and this leads to the passivation of the electrode surface.[12] Also, high levels of ascorbic acid (AA), which coexist in the same environment as catecholamine neurotransmitters, serve as a strong interferent especially in biological samples. Therefore, AA interferes with the detection of catecholamine neurotransmitters in biological media.[14,25,26] AA also possesses close oxidation potentials to that of catecholamine neurotransmitters[10] on bare or unmodified electrode surfaces.

In order to overcome these drawbacks, two approaches are often taken. One approach is to improve the electrocatalytic performance on the electrode surface to enable separation of the oxidation potentials between the catecholamine neurotransmitter and ascorbic acid. The other approach is to suppress the oxidation

of ascorbic acid using pH selectivity. These two approaches have thus lead to a number of chemically modified electrodes being fabricated.[10] The surface modification of an electrode surface leads to lower over potentials and increases the electron transfer rate for desired redox reactions.[27] Incorporating a pH sensitive electroactive thin film on the electrode surface will assist with the screening off of interferents (such as ascorbic acid) by using the pH of the detecting solution.[28] A number of materials have been investigated for the modification of electrode surfaces for the detection of neurotransmitters and these include metallophthalocyanines,[12] conducting polymers,[29] nanomaterials[30,31] and conjugates of nanomaterials with metallopthalocyanines.[32] The use of metallophthalocyanines has attracted our attention and the present study investigates their fabrication as stable thin films onto gold electrode surface for the detection of catecholamine neurotransmitters.

1.3 Phthalocyanines

Phthalocyanines (Pcs) are highly coloured[33] planar aromatic macrocycles that are synthetic analogues of porphyrins (Por). They consist of four isoindole units presenting an 18 π-electron aromatic cloud delocalised over an arrangement of alternated carbon and nitrogen atoms.[34] Phthalocyanines are highly versatile[35] and possess excellent thermal and chemical stability.[34] The extensive conjugation of phthalocyanines gives rise to excellent electronic and optical properties.[36] They can exist as either metal-free phthalocyanines (H_2Pcs) or as metallophthalocyanines (MPcs). As metallophthalocyanines, numerous transition metals (M) and other metal ions can be inserted within the central cavity.[37] **Figure 1.2** shows chemical structures of **(a)** metal-free (H_2Pc) and **(b)** metallophthalocyanine (MPc) where M represents the central

metal. Phthalocyanines were accidentally discovered in the early 1900s and the full and accurate characterization thereof was only conducted in the 1930s.[38]

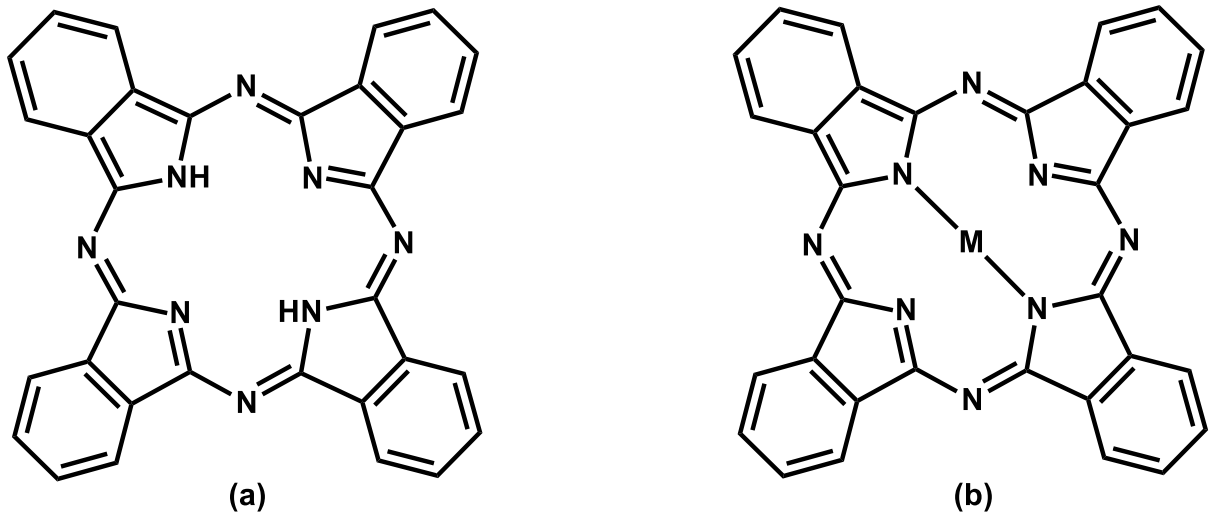

Figure 1.2: Chemical structure of **(a)** metal-free (H_2Pc) and **(b)** metallophthalocyanine (MPc) where M represents the central metal.

1.3.1 Nomenclature of Phthalocyanines

The naming of phthalocyanines is derived from the formula a-$(L)_n$MPc-n&p-S as shown in **Figure 1.3 (c)**. The numbers on the phthalocyanine ring represent the 16 possible sites or positions for substitution. The α-positions are associated with the carbons at positions (1, 4, 8, 11, 15, 18, 22 and 25) and are also referred to as non-peripheral positions. The β-positions sometimes referred to as peripheral positions are associated with the carbons at positions (2, 3, 9, 10, 16, 17, 23 and 24). Phthalocyanines that possess four substituents at either the peripheral or non-peripheral positions are called tetra (*t*) substituted. Alternatively, phthalocyanines that have eight substituents at either the periphery or the non-periphery are regarded as

being octa (*o*) substituted.[33] Tetra substituted phthalocyanines are generally more soluble than their octa substituted counterparts and this is due to the formation of constitutional isomers and their high dipole moments.[38] As previously mentioned, the central cavity of a phthalocyanine can accommodate several metal ions. In addition, axial ligands can also be introduced to the central metal ion of a phthalocyanine molecule.[33] **Figure 1.3** shows the structure of a metallophthalocyanine with **(a)** and **(b)** the possible positions for substitution and **(c)** the notation for naming phthalocyanines.

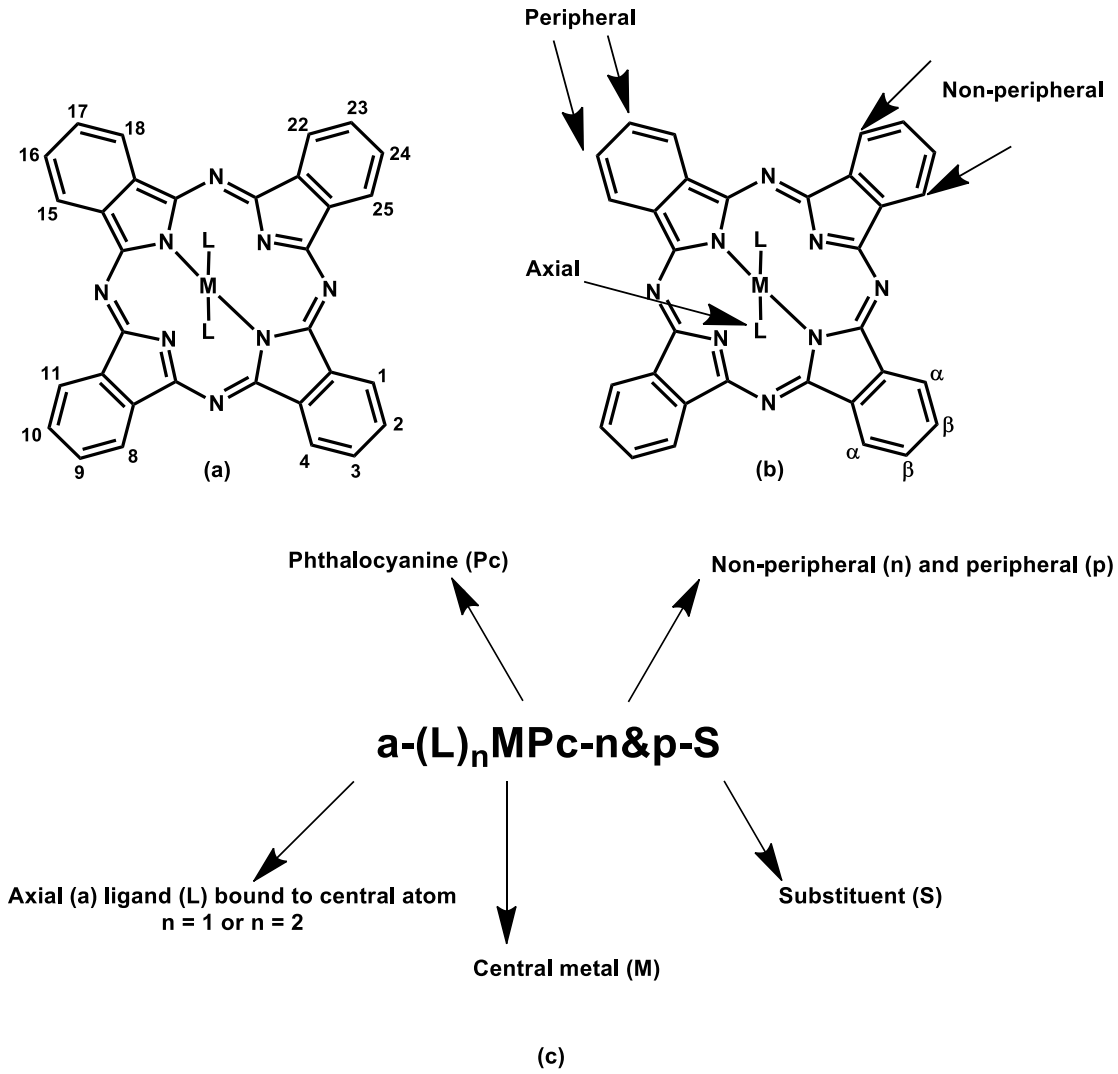

Figure 1.3: The structure of a metallophthalocyanine with **(a)** and **(b)** the possible positions for substitution and **(c)** the notation for naming phthalocyanines.

1.3.2 Properties of Phthalocyanines

The UV-vis spectra of phthalocyanines exhibits a typical electronic spectra with two strong absorption bands known as Q and B bands. The Q band is located in the visible region at 600 – 750 nm. It is attributed to the a_{1u} – e_g transition from the highest occupied molecular orbital (HOMO) to the lowest unoccupied molecular orbital (LUMO) of the Pc ring.[36,39,40] Metallophthalocyanines have a single Q-band and

corresponding metal-free phthalocyanines have a split Q-bands owing to their lower symmetry.[41] The B-band on the other hand is located in the ultraviolet region at 300 – 400 nm and is attributed to the transition from the deeper lying b_{1u} orbital levels of the HOMO.[36,39,40] **Figure 1.4** shows the UV-vis spectra of a metal-free phthalocyanine (red line) and a metallophthalocyanine (black line).

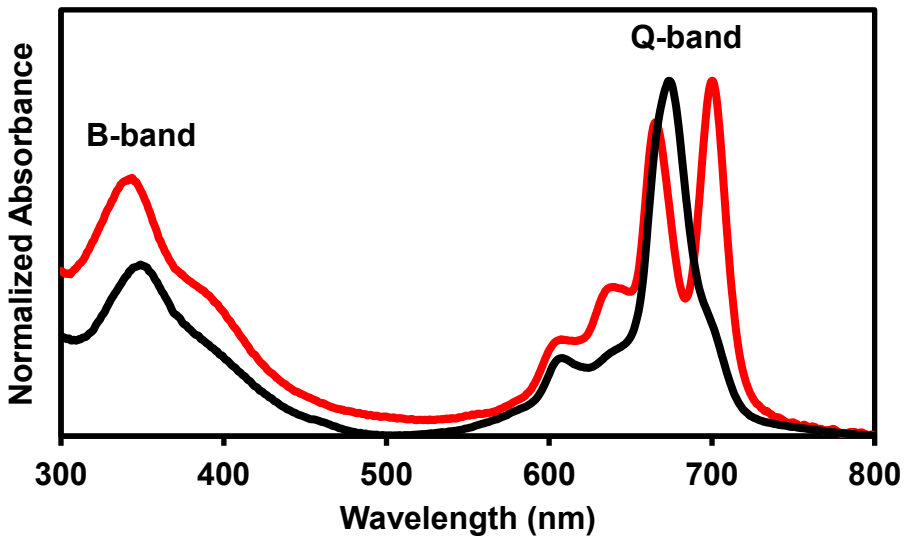

Figure 1.4: UV-vis spectra of a metal-free phthalocyanine (red line) and a metallophthalocyanine (black line).

1.3.3 Synthesis of Phthalocyanines

The most common method utilized for the synthesis of phthalocyanines involves the cyclotetramerization of phthalonitriles.[42] However, other precursors that can be utilized include: phthalic acids,[43] phthalic anhydrides,[44] phthalamides,[43] o-cyanobenzamide[33] and 1,3-diiminoisoindolines.[45] The synthesis of MPcs can be achieved directly through the incorporation of the desired metal salt in the cyclotetramerization reaction.[33] The

general synthetic route of metallophthalocyanines is shown in **Scheme 1.3.** Alternatively, the desired metal salt can be reacted with a H_2Pc in order to achieve metallation. When synthesizing H_2Pc the cyclotetramerization reaction is conducted in the absence of a metal salt.[33] It is also possible to remove the metal (demetallate) from a MPc in order to form H_2Pc.[45] The introduction of substituents onto the periphery (α and β positions) of the phthalocyanine can be conducted through the modification of an already existing phthalocyanine core. Otherwise, cyclotetramerization of a substituted phthalocyanine precursor can be utilized.[43] In the present study, the desired phthalocyanine, cobalt (II) tetra-(3-carboxyphenoxy) phthalocyanine, was directly synthesized by cyclotetramerization of an appropriate phthalonitrile derivative, namely, 4-(3-carboxyphenoxy)phthalonitrile.

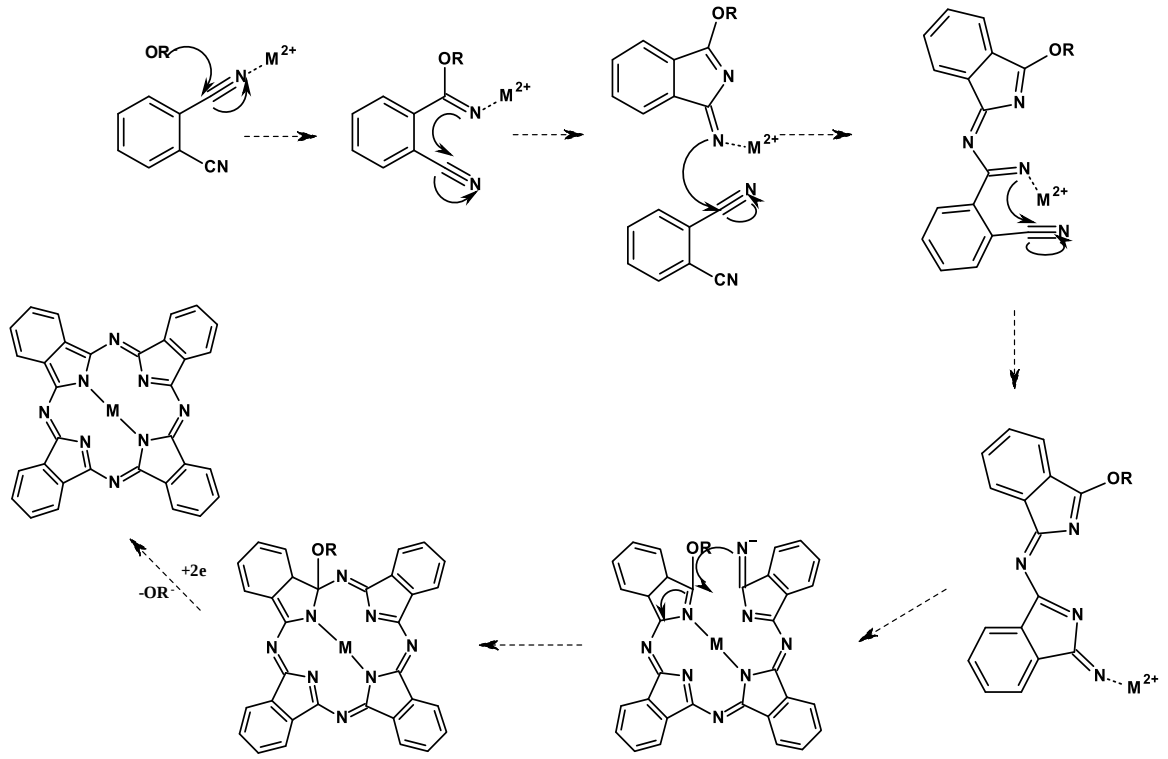

Scheme 1.3: The general synthetic route of metallophthalocyanines.

1.3.4 Phthalocyanine Synthesized in this Study

Cobalt (II) tetra-(3-carboxyphenoxy) phthalocyanine (CoTCPhOPc) was synthesized in the present study and the chemical structure thereof is shown in **Figure 1.5**. The choice of metal centre, namely cobalt is due to its excellent electrocatalytic properties.[46] The choice of carboxylic acid functional group on the synthesized phthalocyanine molecule is due to its pH sensitivity and will afford the pH-selectivity of the modified electrodes towards the catecholamine neurotransmitters and screen off ascorbic acid. This is because catecholamine neurotransmitters are cationic at physiological pH conditions[47] whilst ascorbic acid is anionic at physiological pH conditions.[3] This manner of electrode modification will enable one to selectively detect the catecholamine neurotransmitters of interest on the electrode surface without interference from ascorbic acid.[10] The synthesized metallophthalocyanine will be highly soluble due to the substituents that are attached to the phthalocyanine ring. The tetra substitution affords the formation of constitutional isomers and high dipole moments.[38]

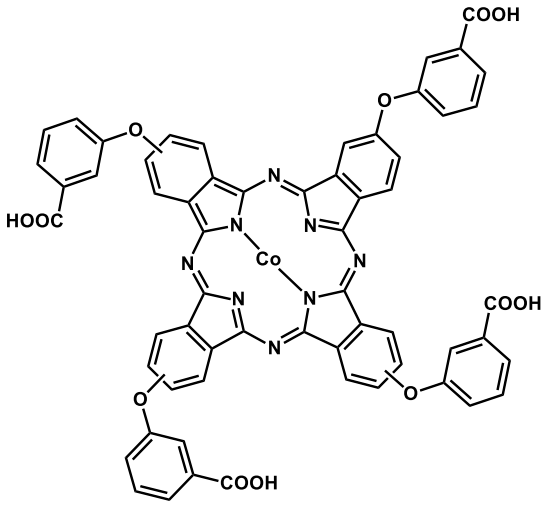

Figure 1.5: Chemical structure of cobalt (II) tetra-(3-carboxyphenoxy) phthalocyanine (CoTCPhOPc).

1.3.5 Applications of Phthalocyanines

Whilst the phthalocyanine synthesized in the present study will used as an electrochemical sensor, it is also interesting to note the various applications of phthalocyanine molecules. It is quite rare in history to find a single type of molecule that has the wide applicability that the phthalocyanine molecule possesses.[28] The wide applications of phthalocyanines are due to their chemical structure, high level of aromaticity, characteristic electronic spectra and the ease of adaptability of their synthesis.[38] Some of the applications for phthalocyanines include: photosensitizers (PS) for photodynamic therapy (PDT) of cancer,[48] semiconductors[49] or photocatalysis.[50] Phthalocyanines have also been investigated for their potential application in electrocatalysis,[32] catalysis,[51] organic light emitting diodes (OLEDs)[52] and nonlinear optical (NLO) materials.[34] The present study focuses on their application as electrocatalysts.

1.3.6 Phthalocyanines as Electrochemical Sensors

The modification of electrodes with metallophthalocyanines enhances electron transfer reactions. In addition, the electrochemical behaviour of metallophthalocyanines is determined by their metal centres, the number, type and position of substituents. The planar structure of metallophthalocyanines enables them to undergo redox processes without losing their stability.[46] The utilization of metallophthalocyanine molecules in electrocatalysis involves their immobilization onto solid surfaces such as electrodes. Once immobilized onto an electrode surface, the electrode takes the properties of the metallophthalocyanine and forms electroactive interfaces. Metallophthalocyanines on an electrode surface act as electron mediators

thus allowing redox reactions to occur with the target analyte in solution. During the interaction between the surface confined metallophthalocyanine complex and the analyte of interest in the solution, the metallophthalocyanine changes its oxidation states. Thereafter recovering its initial oxidation state. The changes in oxidation states are either due to the metal ion at the centre of the phthalocyanine ring or the conjugated ring itself. It is also interesting to note that complexes with non-electroactive central metal ions can undergo redox processes emanating or mediated by the ring system.[53]

The reduction of an analyte dependents on the energy level of the lowest unoccupied molecular orbitals (LUMO) and the oxidation dependents on the energy level of the highest occupied molecular orbitals (HOMO). Redox processes of phthalocyanines take place through successive one electron transfer between the working electrode and the π-conjugated ring system. Normally, a redox reaction gives rise to a long-lived anion or cation radical in non-aqueous solutions. The redox processes in metallophthalocyanines also occur on the central metal ion if the metal d-orbitals or energy level lie between the HOMO and LUMO gap of the phthalocyanine ring.[40] A phthalocyanine complex with Co as a central metal ion, has d-orbitals between HOMO-LUMO gap of the phthalocyanine ring.[54] The cobalt metal ion within the phthalocyanine has a Co^{2+} oxidation state[33] whilst the phthalocyanine ring has Pc^{-2} oxidation state.[54] The first reduction of the cobalt metal ion within the phthalocyanine ring is always metal-based,[40] that is, (Co^{II}/Co^{I}). The first oxidation is Co^{II}/Co^{III}.[54] Both these redox processes dependent on the solvent used.[40] The known oxidation processes for the ring are Pc^{-2}/Pc^{-1} and Pc^{-1}/Pc^{0} and these are from the HOMO orbitals. The reduction processes of the ring occur in the LUMO orbitals (e_g) which is

doubly degenerate and can accept 4 electrons leading to the following oxidation states, Pc^{-2}/Pc^{-3}, Pc^{-3}/Pc^{-4}, Pc^{-4}/Pc^{-5} and Pc^{-5}/Pc^{-6}.[45,54,55]

1.4 Electrode Modification and Drawbacks with Current Studies

There are various methods used to modify different electrode surfaces with metallophthalocyanines and these include drop dry,[46] electropolymerization,[56] self-assembly method[57] and electrochemical grafting[58] to name but a few. Using the drop dry method, the research takes advantage of the delocalized and conjugated phthalocyanine ring system and forms π-π interaction with glassy carbon electrode.[59] Using the drop-dry method is relatively easy in that a solution of known concentration of phthalocyanines is dropped onto the active electrode surface and left to dry (drop-dry).[46] The disadvantage of this method is the lack of reproducibility and also only conjugated carbon based electrodes can be studied using this method for π-π interaction to occur.[46,59] Electropolymerization of phthalocyanines requires the substituents to have polymer-forming functional groups such as morpholine,[60] dimethylamine[61] and azole[62] to name but a few. The advantage of this method is that various electrodes (platinum[56] and carbon) can be used for the electropolymerization studies. The method is excellent as some control of film thickness can be achieved.[63] The limitation is the complex synthesis of metallophthalocyanines bearing polymer-forming functional groups.[60-62] The self-assembly method is one of the easiest methods of immobilizing phthalocyanines especially on coinage metal surfaces. However, the phthalocyanine must have substituents or functional groups that have a strong affinity towards the active electrode surface (coinage metals surfaces). This results in self-assembled monolayer (SAM) thin films. For gold electrode, the

phthalocyanine functional groups should contain sulphur[64, 65] or amine[66] groups for self-assembly to occur. The disadvantage of the method is the environmental stability and mobility of the SAM thin film under storage.[28] This method is easy to use in that the solution of phthalocyanine is left to deposit over time and the phthalocyanines self-assemble onto the electrode surface. SAMs are specific to gold or coinage metal electrodes.[64] Self-assembly method has been used for the immobilization of metallophthalocyanines with pre-modification of the gold electrode with terminal functionalized thiol SAMs. The terminal functional groups can react with metallophthalocyanine substituents.[57] The reaction between functionalized thiol SAMs that has been investigated is via carbodiimide chemistry,[28] ester formation[57] and axial ligation on the central metal ion.[67] Due to the instability of thiol SAMs,[68] the research continues to seek other methods for forming stable thin monolayer metallophthalo-cyanine films. In the present study, the use of the electrochemical grafting method which results in the formation of stable Au-C (gold carbide bond)[69] was investigated.

Electrochemical grafting refers to an electrochemical reaction that allows the binding of an organic layer to a solid conducting surface. An aryldiazonium salt, $ArN_2^+X^-$, is utilized in electrochemical grafting.[68] The electrochemical grafting process involves one electron reduction of the diazonium salt and the cleavage of nitrogen which is then followed by the attachment of the aryl radical to the surface through a metal-carbon (M-C) or carbo-carbo (C-C) covalent bond.[70] The use of electrochemical grafting in order to modify an electrode surface has received great research attention.[71] This is due to its ease of preparation, rapid electroreduction and the formation of a strong covalent bond.[72] The metal-carbon bond formed due to diazonium grafted layers is stable relative to the metal-sulphur bond produced by SAMs.[73] For the modification of a gold surface, the electrochemical grafting results in the formation of an

environmentally and electrically stable gold carbide (Au-C) bond with a bond energy of 317 kJ.mol^{-1},[71] which is stronger than the gold-sulphur (Au-S) bond (184 kJ.mol^{-1}) obtained using SAMs.[74] Whilst the electrochemical grafting of an aryldiazonium salt can be conducted in situ, the approach of using the aryldiazonium salt directly is advantageous. The latter method allows you to accurately determine the amount of aryldiazonium salt introduced to the solution and consequently control the electrochemical grafting conditions. Additionally, the approach enables researchers to use either organic or aqueous solvents for the electrochemical grafting.[69]

The present study investigates the use of electrochemical grafting method of the diazonium salt directly. The electrochemical grafting of diazonium salts has been shown to have a blocking effect on the electrode surface especially when the grafted layer is well-packed. This blocking effect can thus be used to determine whether the layer is pinhole free or if there are any defects in the coverage.[53] In the present study, 4-(2-aminoethyl)benzene diazonium (AEBD) salt was electrochemically grafted onto gold electrode surface. **Scheme 1.4** shows the electrode functionalization of gold electrode using the electrochemical grafting of AEBD.

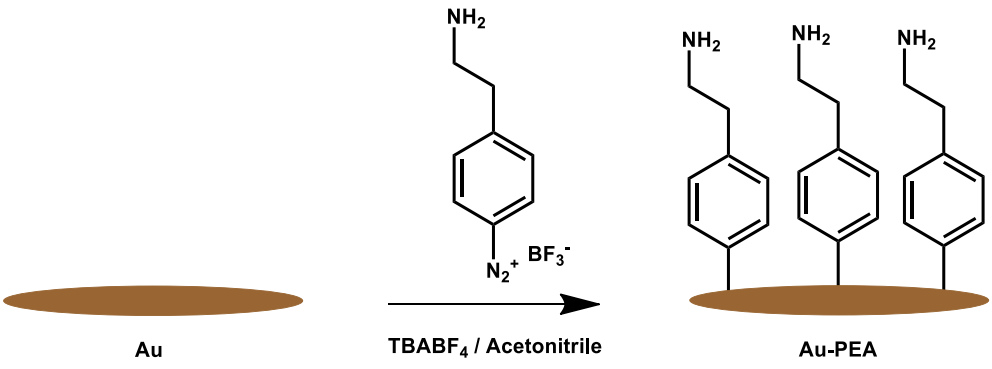

Scheme 1.4: Electrode functionalization of gold electrode using the electrochemical grafting of AEBD.

The electrografted surface should contain functional groups capable of reacting with substituents on the metallophthalocyanine ring. Most of the research conducted on gold electrodes has focused on electrografting and coupling reaction using Click chemistry (alkyne-azide reaction),[58] and Schiff-reaction (aldehyde-amine reaction).[75] The electrochemical grafting reaction yields very stable metallophthalocyanine thin films.[58]

1.5 Phthalocyanine Modified Electrodes for Catecholamine Neurotransmitters Detection

There are several studies that have been reported for the detection of catecholamine neurotransmitters (dopamine, norepinephrine and epinephrine) that involve the use of phthalocyanine modified electrode surfaces. From these studies, the use of cobalt phthalocyanines has also been reported. **Table 1.1** shows the summary of the research that has been conducted thus far for the detection of catecholamine neurotransmitters using phthalocyanine modified electrodes.

Table 1.1: Metallophthalocyanine modified electrodes used for the detection of catecholamine neurotransmitters: dopamine (DA), norepinephrine (NEP) and epinephrine (EP).

Analyte	Electrode	Method of Modification	E_p (V)	LoD	LoQ	LCR	Sensitivity	Refs
DA	[a]GCE-pCoTABAPc	Electropolymerization	0.300 0.300	20 nM 30 nM	- -	0.10 – 1.0 µM 0.10 – 0.40 µM	0.024 µA.nM^{-1} (CA) 0.016 µA.nM^{-1} (CV)	76
DA	[b]GCE-MWCNT-CoTMBANAPc	Drop-dry	0.490	0.33 nM	10.0 nM	7.5 – 67.5 nM	1.07 µA.µM^{-1}	77
DA	[c]GCE-CoTGPc	Drop-dry	0.245	0.030 µM	-	2.0 – 10	2.54 µA.µM^{-1}	78
DA	[d]GCE-Graphene-CoTSPc	Electrochemical deposition	0.280	0.87 nM	-	20 – 220 nM	0.302 µA.nM^{-1}	79
NEP	[e]GCE-MWCNT-ZnO-29H,31H-Pc	Drop-dry	0.208	1.7 µM	-	7.5 – 56 µM	-	80
EP	[f]Au-Cys-FeOCPc	SAM	0.200	13.8 nM	45.8 nM	Up to 300 nM	0.53 ± 0.01 nA.nM^{-1}	12
EP	[g]GCE-SWCNT-CoTSPc	Drop-dry and electrochemical deposition	-	45.17 µM	150.56 µM	2.44 – 3.00 µM	0.132 ± 0.003 A.M^{-1}	14
EP	[h]MWCNT-CoPc	Paste	0.250	15.6 nM	-	1.33 – 5.5 µM	-	15

Table 1.1 (Continued)

Analyte	Electrode	Method of Modification	E_p (V)	LoD	LoQ	LCR	Sensitivity	Refs
EP	[i]Au-Cys-SWCNT-CoTAPc	SAM	0.200	6.0 µM	-	Up to 130 µM	9.4 $mA.mM^{-1}$	[32]

[a]GCE-pCoTABAPc – Cobalt (II) tetra-[*β*-N-(4-aminophenyl)benzamide] phthalocyanine

[b]GCE-MWCNT-CoTMBANAPc – Cobalt (II) tetra[(*E)*-(4-methoxybenzylidene) amino] naphthalene-1-amine phthalocyanine

[c]GCE-CoTGPc – Cobalt (II) tetra-ganciclovir phthalocyanine

[d]GCE-Graphene-CoTSPc – Cobalt (II) tetrasulfonated phthalocyanine

[e]GCE-MWCNT-ZnO-29H,31H-Pc – 29*H*,31*H*-Phthalocyanine

[f]Au-Cys-FeOCPc – Iron (II) octacarboxy phthalocyanine

[g]GCE-SWCNT-CoTSPc – Cobalt (II) tetrasulfophthalocyanine

[h]MWCNT-CoPc – Cobalt (II) phthalocyanine

[i]Au-Cys-SWCNT-CoTAPc – Cobalt (II) tetra-amino phthalocyanine

CA – Chronoamperommetry

CV – Cyclic voltammetry

1.6 Electrochemical Methods and Surface Characterization Techniques

The electrochemical properties of the modified electrode surfaces will be investigated with cyclic voltammetry (CV) and electrochemical impedance spectroscopy (EIS) as electrochemical methods.

An electrochemical cell is used to conduct electrochemical methods such as CV and EIS.[24] **Figure 1.6** shows a representation of an electrochemical cell utilized for CV and EIS. The electrochemical cell consists of the working electrode (WE), reference electrode (RE), and counter electrode (CE). The working electrode ought to be made of inert conducting or semi-conducting material with no redox activity in the potential range being studied. The working electrode is responsible for conducting electrons.[24] Some examples of working electrodes are gold[58] and glassy carbon.[81] The reference electrode possesses a known and stable equilibrium potential. It is utilized as a point of reference against which the potential of the other electrodes can be measured within an electrochemical cell.[24] Common reference electrodes include the saturated calomel electrode (SCE),[82] standard hydrogen electrode (SHE)[24] and the Ag|AgCl electrode.[71,83] The role of the counter electrode is to complete the electrical circuit and also act as an electron sink or source depending on the reduction or oxidation electrochemical reaction investigated.[24] A platinum wire is typically used as a counter electrode.[46] In the present study a gold electrode was used as the WE, Ag|AgCl as the RE and platinum wire used as the CE. An external power source was supplied by the Potentio-Galvanostat Electrochemistry Workstation to the working electrode to modulate the energy of the electrons in the electrode.[24]

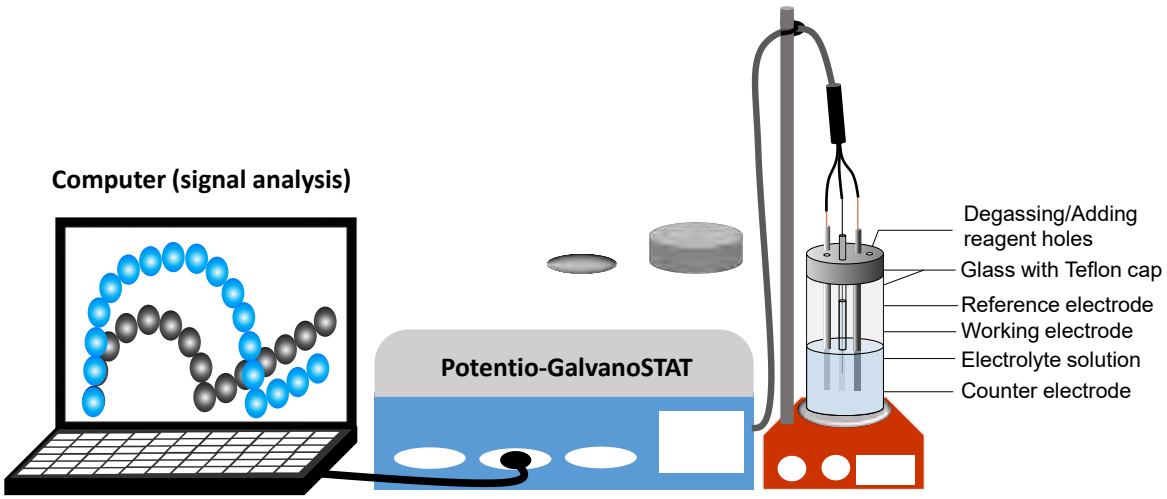

Figure 1.6: A schematic representation of an electrochemical cell utilized for CV and EIS.

In addition to the electrochemical characterization, the surface characterization will be conducted using X-ray photoelectron spectroscopy (XPS) on gold-coated quartz crystal. This method is used to confirm the formation of the functionalized surfaces. The interest in the XPS is due to the fact that covalent functionalization of the electrocatalysts (MPcs) will be studied and these need to be confirmed spectroscopically. XPS is a technique that can be used to characterize the modified electrode surfaces.[53] XPS is utilized to identify the presence of various elements, functional groups and the surface compositions[83] through the observation of peak positions and peak shapes.[84] During XPS analysis, a sample is irradiated by photons of a known energy, resulting in the photoelectric effect. A portion of the electrons generated close to the surface leaves the sample into vacuum and enters the analyser slit of the spectrometer, which is able to measure the electron current (which corresponds to the number of electrons per time unit) as a function of their energy. The XPS spectrum is a plot of intensity (amount of substance on the surface) versus

the binding energy. The specificity of the technique is realized due to its sensitivity to binding properties of the elements which can be analysed using high resolution elemental and core-level spectrum.[85] **Figure 1.7** illustrates **(a)** XPS experimental set-up, the photoelectron spectrometer with a hemispherical electron energy analyser, **(b)** survey and **(c)** high-resolution core-level spectra (results indication). In the present study, XPS was utilized to characterize the following electrode surfaces: bare Au, Au-PEA and Au-PEA-CoTCPhOPc.

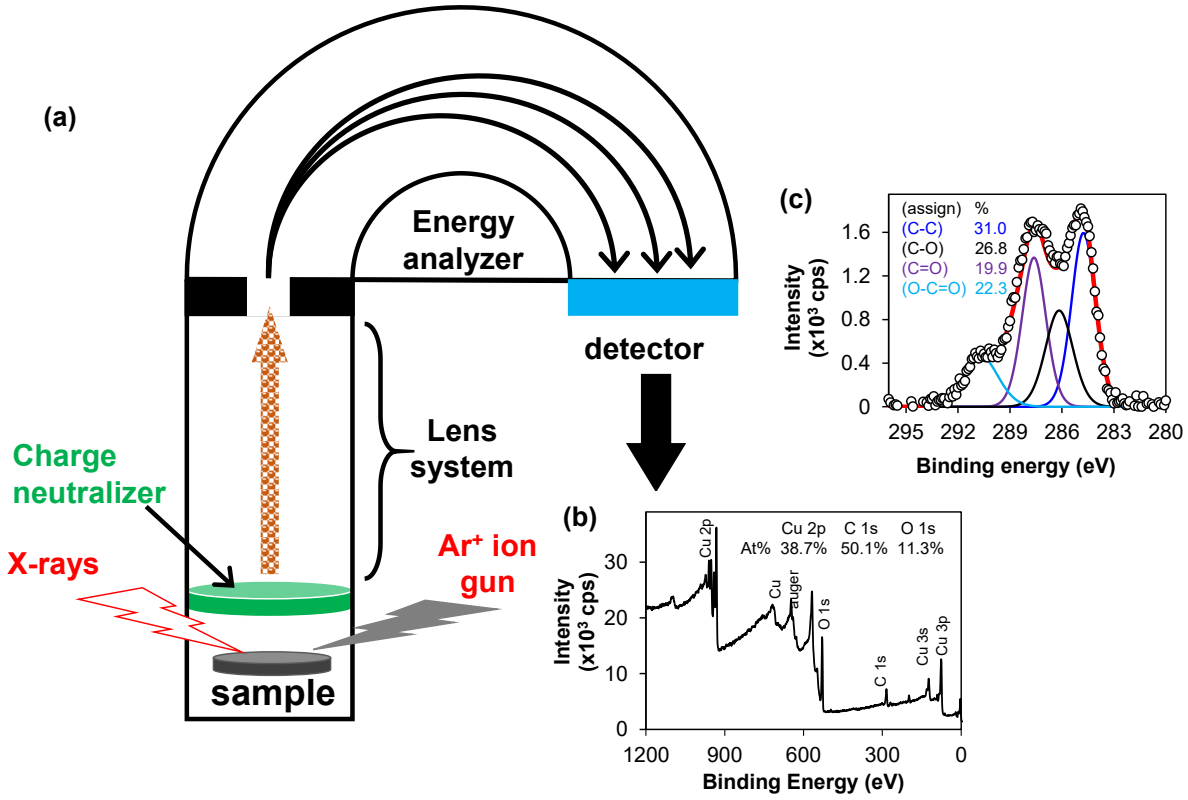

Figure 1.7: (a) XPS experimental set-up, the photoelectron spectrometer with a hemispherical electron energy analyser, **(b)** survey and **(c)** high-resolution core-level spectra (results indication).

1.6.1 Cyclic Voltammetry

Cyclic voltammetry (CV) is a commonly utilized method for studying electrochemical properties in solution.[40] It has been shown to be a useful tool for studying surface chemistry[53] and can provide insight into the structure of an electroactive film adsorbed onto an electrode surface.[86] CV is an electrochemical technique that measures the amount of current generated in an electrochemical cell under conditions where the voltage supplied is greater than that predicted by the Nernst equation.[83] The Nernst equation relates the potential of an electrochemical cell (E) to the standard potential of a species (Eº) and the relative activities of the oxidised (Ox) and reduced (Red) analytes in the system at equilibrium.[24] The formal redox potential situated between the anodic peak potential (E_{pa}) and cathodic peak potential (E_{pc}) is approximately equal to the half-wave potential, $E_{½}$, which is expressed in **equation 1.1**:

$$E_{\frac{1}{2}} = \frac{E_{pa} + E_{pc}}{2} \qquad \textbf{(1.1)}$$

CV is an invaluable and common electrochemical technique used to study the oxidation and reduction processes of molecular species[83] and the electron transfer-initiated by chemical reactions.[24] A CV scan is conducted by applying the potential on a working electrode and measuring the resultant current in a cyclic manner (forward and reverse potential is scanned).[83] The potential of the working electrode is changed linearly with time, starting at a potential where no electrode reaction takes place. The potential is then changed to values where oxidation or reduction of the adsorbed species takes place followed by a reverse scan to the initial potential.[87] This process results in the generation of a cyclic voltammogram (CV) as illustrated in **Figure 1.8**. The current axis is at times not labelled on a cyclic voltammogram and instead a scale bar is inset to the graph[24] as is the case in the aforementioned figure. Vital information

can be obtained from a cyclic voltammogram. This includes: the amount of adsorbed material, the formal potential of the analyte involved in the redox couples and the kinetics of the electron transfer.[87] In the present study, CV was utilized to electrochemically graft AEBD onto bare gold (Au) electrode. The technique was also used to characterize the following electrode surfaces: bare Au, Au-PEA and Au-PEA-CoTCPhOPc. In addition, CV was also utilized to investigate the effect of pH on Au-PEA-CoTCPhOPc in the presence of negative and positively charged redox probing species. Lastly, CV was used for the electrocatalytic and electroanalytical detection of the catecholamine neurotransmitters and ascorbic acid.

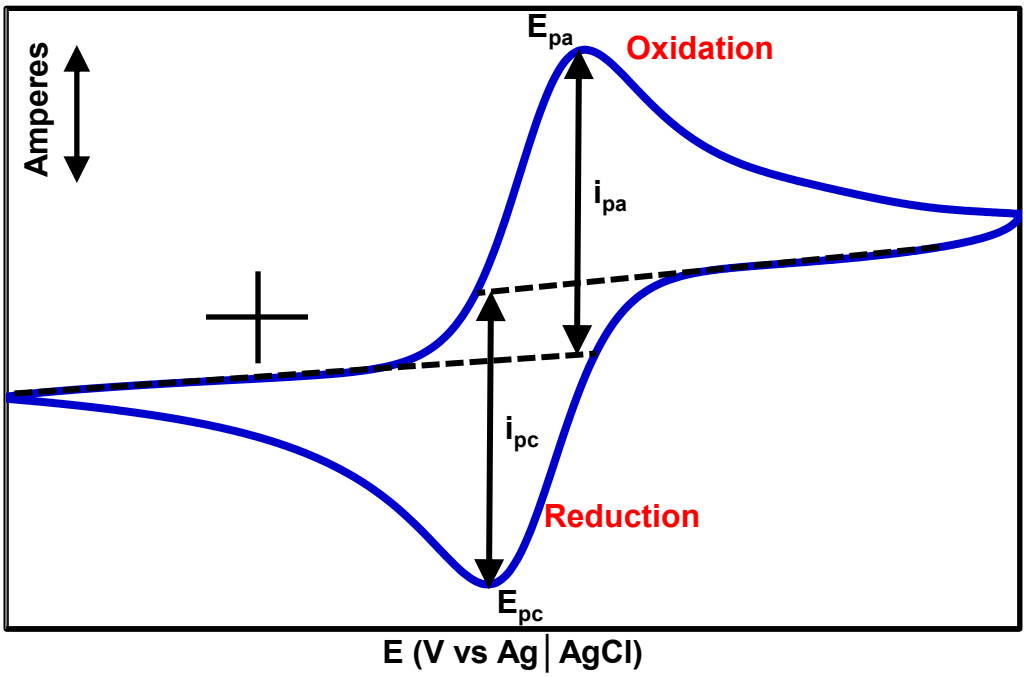

Figure 1.8: Typical cyclic voltammogram for a redox reaction showing the oxidation (E_{pa}) and reduction (E_{pc}) peak potential and the corresponding currents (I_{pa} and I_{pc}). The cross represents the (0,0) co-ordinate of the x- and y-axes.

1.6.2 Electrochemical Impedance Spectroscopy

Electrochemical impedance spectroscopy (EIS) is a non-destructive and informative electrochemical method for probing adsorption and interfacial surface properties.[9] It provides critical information about the electrochemical processes that occur at the electrode|electrolyte interface.[88] During an EIS measurement, a small sinusoidal varying voltage V(ω,t) is applied to the electrochemical system under study and the resulting current I(ω,t) is measured. Through the variation of the excitation frequency (f) of the applied voltage over a range of frequencies, the complex impedance can be calculated. The complex impedance is a sum of the real (Z' (ω)) and imaginary (Z'' (ω)) impedance components of the system as a function of the frequency (i.e. angular frequency ω).[89] Consequently, EIS combines the analysis of both the real and imaginary components of the impedance, which stem from the resistance and capacitance.[30] This is illustrated in **equation 1.2 – 1.4**.

$$Z(\omega) = \frac{V(\omega,t)}{I(\omega,t)} \qquad \textbf{(1.2)}$$

$$Z(\omega) = Z'(\omega) + Z''(\omega) \qquad \textbf{(1.3)}$$

$$\omega = 2\pi f \qquad \textbf{(1.4)}$$

EIS data can be represented in two different ways: the Nyquist plot and the Bode plot. With the Nyquist plot, the data is represented as Z'' as a function of Z' in the complex plane. The Bode plots however, are a pair of graphs depicting log $|Z|$ and θ (phase angle, º) as a function of log (f).[89] In the present study the Nyquist plot will be utilized to illustrate EIS data. The shape of the Nyquist plot can provide information about the electron-transfer kinetics and diffusion characteristics.[30] The Nyquist plot is divided into two frequency regions, the kinetically controlled (high frequency) region where the

semi-circle is observed and the diffusion controlled (low frequency) region where the Warburg line is observed. On a Nyquist plot, the infinite Warburg impedance (Z_W) appears as a diagonal line.[53] The semicircle diameter in the Nyquist plot is a measure of a charge transfer resistance (R_{CT}) and can be utilized to describe the interfacial properties at different stages of the electrode modification. R_{CT} directly affects the electron transfer process of the redox couple at the interface.[83] The experimental data of the Nyquist plot can be fitted with a Randles equivalent circuit model. In the Randles equivalent circuit model, R_S is the electrolyte resistance, R_{CT} is the electron transfer resistance, C_{dl} is the double-layer capacitance and Z_W is the Warburg impedance.[9] **Figure 1.9 (a)** illustrates a Nyquist plot with the experimental data represented as diamond shapes and the fitted data as a solid line and **(b)** a Randles equivalent circuit model.

In the present study, EIS will be utilized to characterize the following electrode surfaces: bare Au, Au-PEA and Au-PEA-CoTCPhOPc. In addition, EIS will also be used to investigate the effect of pH on Au-PEA-CoTCPhOPc in a negative and positively charged redox probing species.

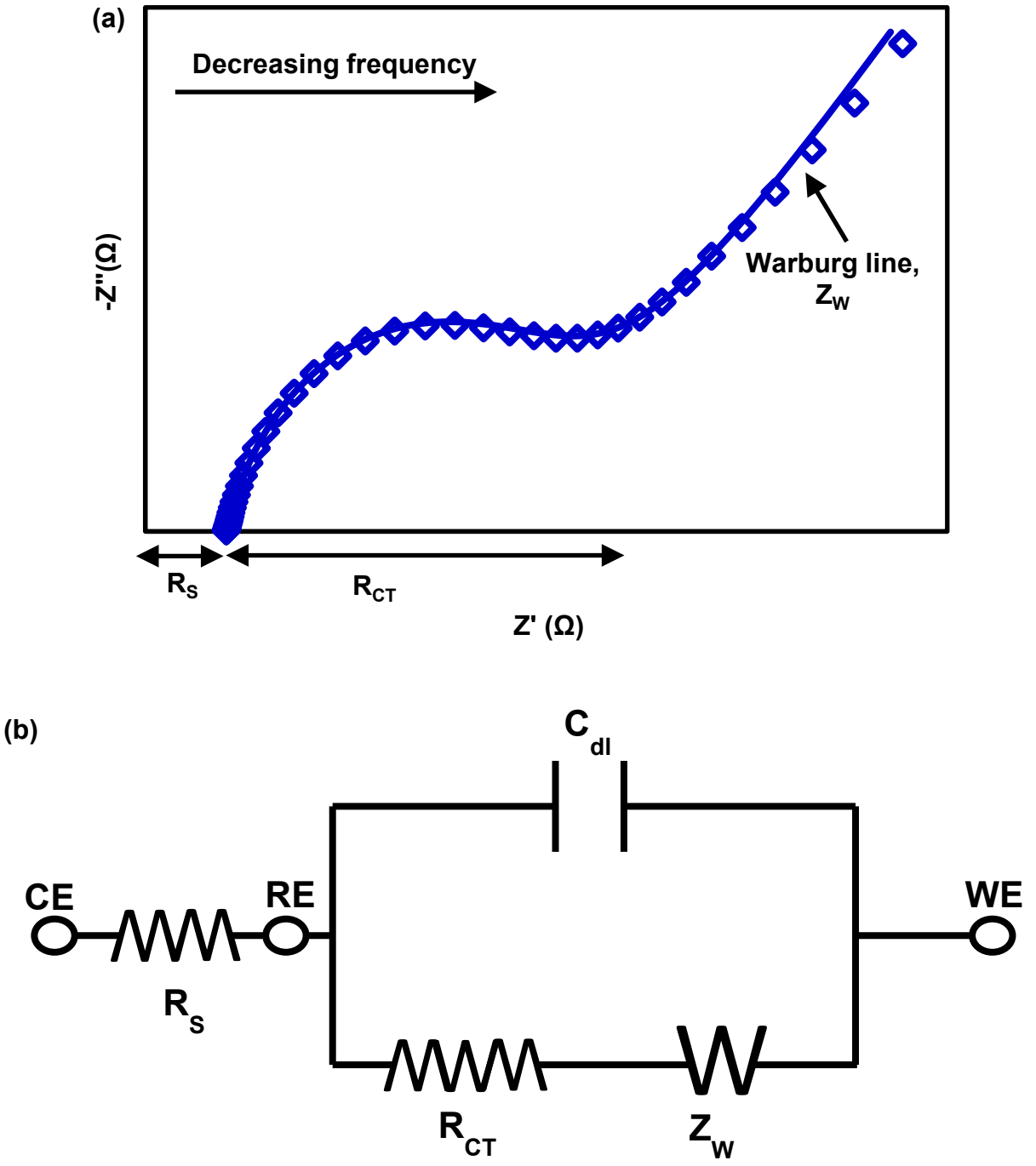

Figure 1.9: (a) Nyquist plot for an electrochemical system with diffusion-limited behaviour with the experimental data represented as diamond shapes and the fitted data as a solid line and **(b)** a Randles equivalent circuit model.

1.7 Problem Statement and Hypothesis

Catecholamine neurotransmitters play a vital role in the human body. However, they can also have adverse effects on the body if not properly monitored. A variety of methods have been utilized for the detection of catecholamine neurotransmitters. This is because catecholamine neurotransmitters play an important role due to their potential to serve as clinical biomarkers for specific disease states or their ability to be monitored in order to evaluate the efficacy of treatments that have been administered.

Electrochemical detection of catecholamine neurotransmitters is a viable method due to the advantage of the method being inexpensive and easy to operate. The drawback of the electrochemical detection of catecholamine neurotransmitters is the interference from ascorbic acid as it co-exists with catecholamine neurotransmitters in biological samples. This limitation can be overcome by modifying the electrode surface to enable the detection of catecholamine and screen off ascorbic acid.

The present study hypothesizes that an electrode surface modified with CoTCPhOPc will enable the detection of catecholamine neurotransmitters and screen off ascorbic acid by means of pH sensitive properties.

1.8 Aims and Objectives of the Thesis

The **aim of this thesis** study is to design a pH sensitive electrochemical sensor for the detection of catecholamine neurotransmitters (dopamine, norepinephrine and epinephrine) and the screening off of ascorbic acid.

The **objectives** of this thesis include:

(i) To synthesize and fully characterize cobalt (II) tetra-(3-carboxyphenoxy) phthalocyanine (CoTCPhOPc) using Fourier transform infrared (FT-IR) spectroscopy, UV-vis spectroscopy, magnetic circular dichroism (MCD), nuclear magnetic resonance (NMR), elemental analysis (CHN), mass spectroscopy (MS) and elemental analysis (CHN).

(ii) To synthesize and fully characterize 4-(2-aminoethyl)benzene diazonium salt (AEBD) with FT-IR spectroscopy, NMR and elemental analysis (CHN). Also to investigate its electrografting onto gold electrode surface.

(iii) To study the immobilization of CoTCPhOPc onto electrochemically grafted phenylethylamine gold electrode to form Au-PEA-CoTCPhOPc.

(iv) To characterize the modified electrode surface using various surface sensitive techniques such as cyclic voltammetry (CV), electrochemical impedance spectroscopy (EIS) and X-ray photoelectron spectroscopy (XPS).

(v) To investigate the modified gold electrodes towards the detection of catecholamine neurotransmitters (dopamine, norepinephrine and epinephrine) and ascorbic acid.

(vi) To evaluate the efficiency of the modified electrode to screen off ascorbic acid.

1.9 Thesis Outline

The present thesis deals with the design of a pH sensitive electrochemical sensor utilized for the detection catecholamine neurotransmitters and the screening off of ascorbic acid.

The thesis comprises of five chapters.

- **Chapter One**: gives a background and an understanding of the intended study. It provides a brief literature review, states the problem statement and hypothesis and defines the aims and objectives of the study.
- **Chapter Two**: outlines the experimental design of the present study and the method of electrode preparation and modification.
- **Chapter Three**: reports on the synthesis of CoTCPhOPc and AEBD and discusses at length the various techniques used for characterization.
- **Chapter Four**: reports on the surface modification and formation of Au-PEA-CoTCPhOPc. The electrochemical and spectroscopic characterization of the various electrode surfaces. The electrocatalysis and electroanalysis of dopamine, norepinephrine, epinephrine and ascorbic acid is conducted.
- **Chapter Five**: provides a comprehensive summary of the present study and provides an outlook for future studies aimed at carrying the study forward.

Chapter Two: Experimental

2. Experimental

This chapter reports on the chemical reagents, apparatus and experimental methods utilized for the synthesis of the complexes presented in the present study. It also reports on the method of electrode preparation and modification.

2.1 Chemical Reagents

Deuterium oxide (D_2O), deuterated dimethyl sulfoxide (d_6-DMSO), dimethyl sulfoxide (DMSO), tetrahydrofuran (THF), 1,8-diazabicyclo(5.4.0)undec-7-ene (DBU), sodium nitrite ($NaNO_2$) and potassium hydroxide (KOH) were purchased from Merck chemicals. 3-Hydroxybenzoic acid, 1-pentanol, potassium carbonate (K_2CO_3), cobalt (II) chloride ($CoCl_2$), tetrafluoroboric acid (HBF_4), 4-(2-aminoethyl)aniline, N-hydroxysuccinimide (NHS), tetrabutylammonium tetrafluoroborate ($TBABF_4$), α-cyano-4-hydroxycinnamic acid, potassium ferricyanide ($K_3[Fe(CN)_6]$), potassium hexacyanoferrate(II) trihydrate ($K_4[Fe(CN)_6]\cdot 3H_2O$), acetonitrile (ACN), hexaammineruthenium (III) chloride [($Ru(NH_3)_6Cl_3$], dopamine hydrochloride (DA), (-)-norepinephrine (NEP), (-)-epinephrine (EP), L-ascorbic acid (AA) and N,N'-dicyclohexylcarbodiimide (DCC) were purchased from Sigma-Aldrich. Aluminium oxide (Al_2CO_3, 1.0 μm, 0.30 μm and 0.05 μm) was purchased from Allied High Tech Inc. 32% Hydrochloric acid (HCl), 30% hydrogen peroxide (H_2O_2), 32% sulphuric acid (H_2SO_4), potassium chloride (KCl) and sodium chloride (NaCl) were purchased from Spellbound Laboratory Solutions. Sodium hydroxide (NaOH) was purchased from B & M Scientific.

Petroleum ether, methanol (MeOH), dimethylformamide (DMF), potassium dihydrogen orthophosphate (KH_2PO_4) and di-sodium hydrogen orthophosphate (Na_2HPO_4) were purchased from Associated Chemical Enterprises (ACE). Copper sulphate ($CuSO_4$)

was purchased from AIP Chemicals. Phosphate buffer saline solution (PBS, pH 7.4) was prepared using appropriate amounts of Na_2HPO_4 (1.44 g, 10.14 mmol), KH_2PO_4 (0.24 g, 1.76 mmol), NaCl (8.0 g, 0.17 mol) and KCl (0.2 g, 2.68 mmol) dissolved in 1.0 L of ultrapure (Milli-Q) water. Sodium hydroxide (NaOH, 1.0 M) and hydrochloric acid (HCl, 1.0 M) were used to adjust the pH of the PBS solution to appropriate values. DMF and 1-pentanol were dried over molecular sieves for a minimum of 12 hours before use. Solutions in the electrochemical cell were de-aerated by bubbling argon or nitrogen prior to every experiment and the electrochemical cell was kept under argon atmosphere.

All aqueous solutions were prepared using ultrapure water obtained from purification through a Milli-Q Water System (Millipore Corp. Bedford, MA, USA). With the exception of DMF and 1-pentanol, all chemicals were of analytical reagent grade and were utilised as received from the suppliers without any further purification. 4-Nitrophthalonitrile was synthesized from phthalimide following a previously reported method.[90]

2.2 Apparatus

Fourier transform infrared spectra were obtained on a Perkin-Elmer Universal ATR Sampling accessory spectrum 100 FT-IR spectrometer. Proton Nuclear Magnetic Resonance (^{1}H NMR) and Carbon Nuclear Magnetic Resonance (^{13}C NMR) data was obtained using either a Bruker 300 MHz or a Bruker 600 MHz NMR spectrometer in d_6-DMSO or D_2O. The choice of NMR solvent depended on the solubility of the compound being analysed. The NMR data was analysed using MestReNova software for integration and peak picking. Ultraviolet-visible (UV-vis) electronic absorption

spectra were obtained on a Thermo Scientific Multiskan Sky Microplate spectrophotometer. Magnetic circular dichroism (MCD) spectrum was measured on a Chirascan Plus spectropolarimeter equipped with a permanent magnet which produces a magnetic field of 1 Tesla (1 T). Mass spectrum was collected on a Bruker Auto FLEX III smart-beam MALDI-TOF mass spectrometer using α-cyano-4-hydroxycinnamic as the matrix in positive ion mode. Elemental (CHN) analysis were conducted using a Vario-Elementar Microcube ELIII.

An electrochemical cell containing an analytical solution and three electrodes consisting of a working electrode (WE), a counter electrode (CE), and a reference electrode (RE), was used for all the electrochemical measurements. The gold WE had a geometric surface of 0.0201 cm^2. The CE was the platinum wire and RE was silver-silver chloride in 3.0 M solution of potasium chloride (Ag│AgCl, 3.0 M KCl). Cyclic voltammetry (CV) and electrochemical impedance spectroscopy (EIS) experiments were performed on an AUTOLAB PGSTAT302N potentiostat/galvanostat workstation interfaced to a Proline desktop computer equipped with a 1.10 version NOVA software. The EIS experiments were recorded in the frequency of range between 10 kHz to 100 MHz at a formal potential of $E_{1/2}$ of the $[Fe(CN)_6]^{3-/4-}$ and $[Ru(NH_3)_6]^{2+/3+}$ redox couple for a bare gold electrode and with an amplitude 5 mV rms sinusoidal modulation. Measurements of pH were conducted using a Metrohm 827 pH lab, 230 V, EU with Primatrode.

X-ray photoelectron spectroscopy (XPS) was measured using a Kratos Axis Ultra DLD, with the Al (monochromatic) anode, equipped with a charge neutralizer. For wide or survey XPS scans, the following parameters were used: emission 10 mA, anode (HT): 13.5 kV, operating pressure below 5 x 10^{-9} Torr, hybrid lens, and resolution to acquire scans was at 80 eV pass energy in slot mode. The centre used for the scans

was at 590 eV and the width at 1205 eV, with steps at 1 eV and dwell time at 100 ms. For the high-resolution scans, the resolution was changed to 40 eV pass energy in slot mode. Centre was at 402 eV and width at 12 eV for N 1s, with step size at 0.05 eV and dwell time at 500 ms.

2.3 Synthesis

2.3.1 Synthesis of 4-(3-Carboxyphenoxy)phthalonitrile (3)

4-(3-Carboxyphenoxy)phthalonitrile (**3**) was synthesized following a previously reported method[39] with slight modifications.

Briefly, 4-nitrophthalonitrile (**1**, 1.51 g, 8.70 mmol) and 3-hydroxybenzoic acid (**2**, 1.22 g, 8.70 mmol) were dissolved in dry DMF (75 mL) under argon at room temperature. After 30 minutes of continuous stirring, excess K_2CO_3 (10.12 g, 73.22 mmol) was added to the reaction mixture in approximately 5 equal portions over 30 minute intervals. After 4 days of stirring at room temperature, the reaction mixture was added to ice water. Once the ice had melted, concentrated HCl (32%) was added dropwise to the solution to precipitate out the desired product, that is, 4-(3-carboxyphenoxy)phthalonitrile (**3**). The product was then filtered off and washed with acidified (HCl) ice water. The residue was then left to dry in vacuum.

Yield: 1.90 g (82%). FT-IR γ (cm^{-1}): 3076 (C-H); 2552 (O-H); 2235 (CN); 1691 (C=O); 1479 (C=C); 1300 (C-O-C); 1246 (C-O). Anal. calc. for $C_{15}H_8N_2O_3$: C 68.18, H 3.05, N 10.60%; found: C 67.83, H 2.87, N 10.54%. ^{1}H NMR (600 MHz, d_6-DMSO, δ (ppm)): 7.41 – 7.45 (m, 2H, Ar-H); 7.60 – 7.63 (m, 2H, Ar-H); 7.76 (d, 1H, Ar-H); 7.85 – 7.87 (d, 1H, Ar-H); 8.05 – 8.07 (d, 1H, Ar-H). ^{13}C NMR (600 MHz, d_6-DMSO, δ (ppm)): 109.04 (CH=<u>C</u>-CN); 115.84 (CH=<u>C</u>-CN); 116.33 (C-<u>C</u>N); 117.22 (C-<u>C</u>N); 121.04

(C=CH-CO); 122.91 (OC-CH=C); 123.42 (OC-CH=CH); 125.28 (C=CH-CH); 126.90 (CH=CH-CO); 131.55 (CH=CH-CH); 133.73 (HOOC-C=CH); 136.79 (HC=CH-C); 154.47 (HC=C-O); 161.03 (O-C=CH); 166.82 (C-COOH).

2.3.2 Synthesis of Cobalt Tetra (3-Carboxyphenoxy) Phthalocyanine (4)

Cobalt tetra (3-carboxyphenoxy) phthalocyanine (CoTCPhOPc, **4**) was synthesized following a previously reported method[91-93] with slight modifications:

Briefly, 4-(3-carboxyphenoxy)phthalonitrile (**3**, 0.60 g, 2.28 mmol) was suspended in 1-pentanol (5.0 mL) in the presence of cobalt (II) chloride (0.15 g, 1.13 mmol) and DBU (35.0 µL). The solution was heated to 140 ^{o}C under argon atmosphere. The solution turned blue and was left to stir under reflux for 48 hours. Upon cooling to room temperature, a mixture of methanol and THF was added to the reaction vessel. The resultant precipitate was then collected by centrifugation and washed several times with a mixture of methanol and THF and then finally with 1.0 M HCl. The resultant product, CoTCPhOPc (**4**) was then left to dry in the oven.

Yield: 198.10 mg (31%). FT-IR γ (cm^{-1}): 2953 (O-H); 1716 (C=O); 1434 (C=C); 1268 (C-O-C); 1229 (C-O). Anal. calc. for $6H_2O{\cdot}C_{60}H_{32}CoN_8O_{12}$ C 58.88, H 3.62, N 9.16%; found C 58.96, H 3.21, N 8.83%. MS (MALDI-TOF) m/z: Calc. for $C_{60}H_{32}CoN_8O_{12}$ [M + H]$^+$ 1116.15; found 1116.42 [M + H]$^+$. UV-vis, λ_{max} (nm), (log ε): 660 (4.77), 602 (1.22), 336 (3.61).

2.3.3 Synthesis of 4-(2-Aminoethyl)benzene Diazonium Salt (6)

The synthesis of 4-(2-aminoethyl)benzene diazonium (AEBD) salt has been reported before[69] and we have modified it slightly for our research:

Briefly, 4-(2-aminoethyl)aniline (**5**, 0.5084 g, 3.73 mmol) was added to tetrafluoroboric acid (1.0 mL) and the solution was cooled for 15 minutes while stirring vigorously. To this solution, ice cold sodium nitrite dissolved in water (**6**, 0.5186 g, 6.10 mmol) was added drop wise and the solution stirred vigorously. The mixture was allowed to react for 40 minutes after which the precipitate formed. The resultant precipitate, AEBD, was filtered and washed with petroleum ether, left to air dry and stored in the freezer.

Yield: 0.76 g (86%). FT-IR γ (cm^{-1}): 3268, 3206 (N-H); 3111 (C-H); 2286 (N≡N); 1268 (C-N). ^{1}H NMR (300 MHz, D_2O, δ (ppm)): 2.90 – 2.95 (t, 2H, Ali-H); 3.22 – 3.27 (t, 2H, Ali-H); 6.89 – 6.90 (d, 2H, Ar-H); 7.20 – 7.23 (d, 2H, Ar-H). ^{13}C NMR (300 MHz, D_2O, δ (ppm)): 31.83 (H_2C-$\underline{C}H_2$-NH_2); 40.22 (C-$\underline{C}H_2$-CH_2); 115.86 (HC-$\underline{C}$-CH_2); 127.79 (HC-$\underline{C}$H-C); 130.29 (HC-$\underline{C}$H-CH); 154.58 (HC-$\underline{C}$-N_2).

2.4 Electrode Modification

2.4.1 Electrode Cleaning

A clean electrode surface was achieved by following the established method[64] with slight modifications. Briefly, the gold electrode (Au) was polished by mirror-finish on a Beuhler felt pad using an aqueous slurry of aluminium oxide (1.0 μm, 0.30 μm and 0.05 μm). The polished gold electrode was then chemically treated by etching for about 2 minutes in a “Piranha” solution [3:1 (v/v) concentrated (32%) sulphuric acid (H_2SO_4) and 30% hydrogen peroxide (H_2O_2)] and was rinsed with copious amounts of ultra-

pure Milli-Q water. The cleaned electrode was dried in a continuous stream of nitrogen. The cleanliness of the bare gold electrode surface was established by placing the electrode in 0.50 M H_2SO_4 and scanning the potential between -0.20 V and 1.50 V (versus Ag│AgCl in 3.0 M KCl) at a scan rate of 100 $mV.s^{-1}$ until reproducible scans were obtained. Following this pre-treatment, the gold electrode was modified following the method below.

2.4.2 PEA Electrochemical Grafting and Immobilization of CoTCPhOPc (4)

Prior to the immobilization of the CoTCPhOPc complex, the gold electrode (Au) was first modified with phenylethylamine (PEA) using electrochemical grafting. The AEBD salt (1.0 mM) was dissolved in 5.0 mL acetonitrile solution containing 0.10 M $TBABF_4$. A reductive electrochemical process was conducted at a potential window starting from +0.40 V to -0.40 V at a scan rate of 100 $mV.s^{-1}$. After the electrografting, the Au-PEA electrode was rinsed with acetonitrile to remove any unreacted and physically adsorbed AEBD. The Au-PEA electrode was immersed in 1.0 mL DMF solution containing CoTCPhOPc (**4**, 1.0 mg, 0.89 µmol), NHS (11.5 mg, 0.10 mmol) and DCC (25.52 mg, 0.12 mmol) which had been left for an hour to stir. The reaction was allowed to occur for 3 hours. The formation of Au-PEA-CoTCPhOPc thin film was accomplished following a carboxylic activation and amide coupling onto Au-PEA. The Au-PEA-CoTCPhOPc electrode was rinsed with DMF to remove any unreacted and physically adsorbed CoTCPhOPc and then finally with PBS buffer, pH 7.4.

Publication

The results discussed in this thesis are based on the work published in a peer review international journal which will not be referenced any further.

Publication details:

K. Tshenkeng and P. Mashazi, *Electrochimica Acta*, 2020, **360**, 137015. DOI: 10.1016/j.electacta.2020.137015.

Impact Factor **= 6.215**

Author contributions:

Keamogeste Tshenkeng (MSc Candidate): Idea generation from concept, data collection and analysis, results interpretation and drafting of the original manuscript.

Philani Mashazi (Supervisor): Research supervisor, resources, idea generation from concept, support and guidance of the research, data collection and analysis, results interpretation, drafting and finalization of the manuscript and corresponding with the journal.

Results and Discussion

This section is divided into two chapters which are:

Chapter 3: Synthesis and Characterization

Chapter 4: Modification, Characterization and Electroanalysis

Chapter Three: Synthesis and Characterization

3. Synthesis and Characterization

This chapter reports on the synthesis of CoTCPhOPc and AEBD. The results obtained from the various techniques used for characterization are also discussed at length.

3.1 Synthesis and Characterization of CoTCPhOPc (4), Scheme 3.1

Similar phthalocyanine complexes to the one reported in the present study have been reported containing peripherally substituents, indium (InTCPhOPc)[91] and zinc (ZnTCPhOPc),[92] and also non-peripherally substituted ZnTCPhOPc.[93] A similar procedure was followed for the synthesis of CoTCPhOPc (**4**) and this is illustrated in **Scheme 3.1**. The formation of compound (**3**) was achieved via a base (K_2CO_3) catalysed Williamson ether synthesis between 4-nitrophthalonitrile (**1**) and 3-hydroxybenzoic acid (**2**). Dry solvent was used as the acid produced was neutralized by the base to produce an ether product (**3**). The reaction was achieved in 82% yields. The synthesized compound (**3**) was cyclotetramerized in the presence of $CoCl_2$ to obtain a pure CoTCPhOPc (**4**) in 31% yields. The successful synthesis of CoTCPhOPc (**4**) was then analyzed using varies characterization techniques.

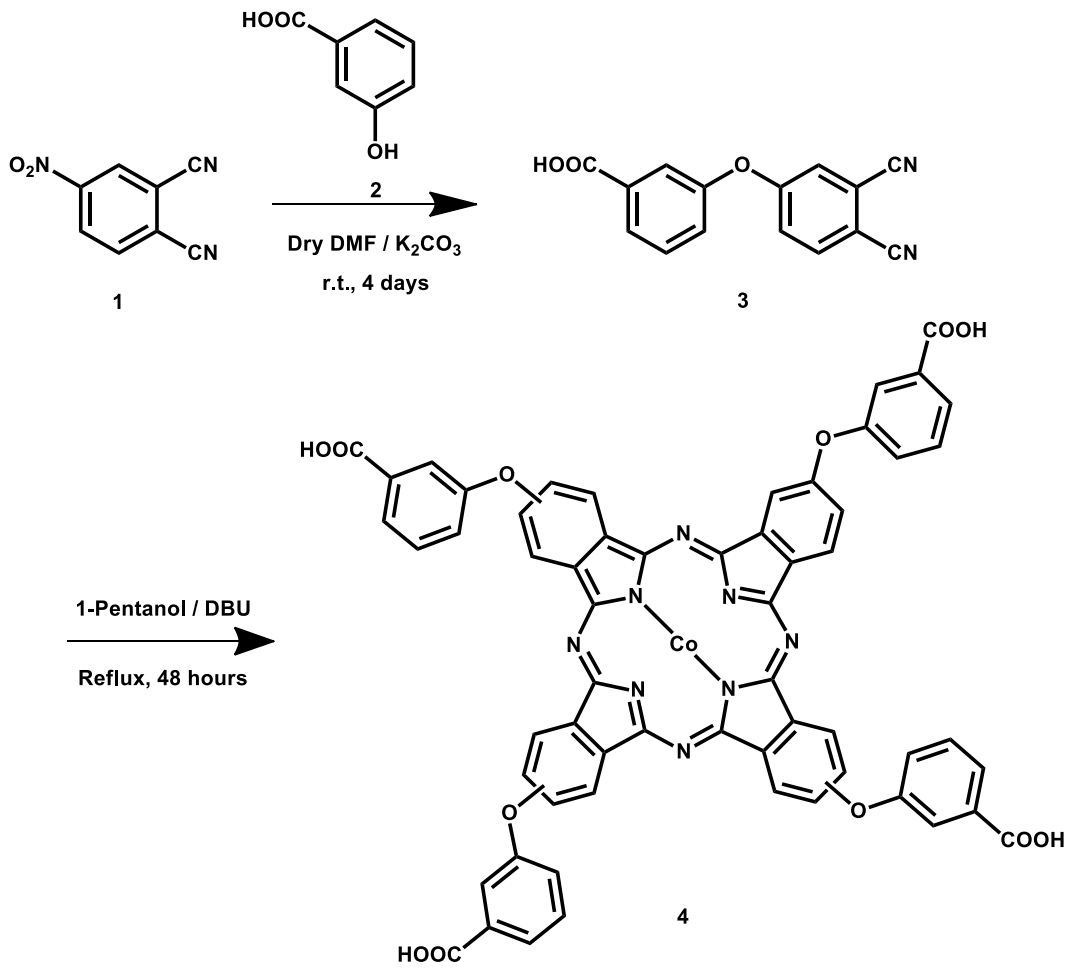

Scheme 3.1: Synthesis procedure for the formation of CoTCPhOPc (**4**) from 4-(3-carboxyphenoxy)phthalonitrile (**3**).

Figure 3.1 shows the FT-IR spectra of **(i)** 4-nitrophthalonitrile (**1**), **(ii)** 3-hydroxybenzoic acid (**2**) and **(iii)** 4-(3-carboxyphenoxy)phthalonitrile (**3**). A sharp absorption at 3076 cm^{-1} was observed due to the presence of the aromatic C-H (φC-H) stretch on 4-(3-carboxyphenoxy)phthalonitrile (**3**). This sharp aromatic C-H (φC-H) stretch was also observed in 4-nitrophthalonitrile (**1**) at 3088 cm^{-1}. A sharp absorption at 2235 cm^{-1} was observed for the nitrile (C≡N) stretch from 4-(3-carboxyphenoxy)phthalonitrile (**3**) and a similar peak was observed on 4-nitrophthalonitrile (**1**) at 2243 cm^{-1}. The carbonyl (C=O) group presents a sharp stretch

at 1691 cm^{-1} and a ring C=C stretch at 1479 cm^{-1} due to the aromaticity of 4-(3-carboxyphenoxy)phthalonitrile (**3**). The formation of an ether (C-O-C) was observed as a stretch at 1300 cm^{-1} for compound (**3**). The absence of the alcohol (O-H) group from 3-hydroxybenzoic acid (**2**) at 3317 cm^{-1} was observed. A broad O-H absorption for COOH was not observed due to the formation of ($–COO^-K^+$) from the excess potassium carbonate base added to neutralize the acid produced by the reaction. In addition, the nitro groups at 1519 and 1348 cm^{-1} from 4-nitrophthalonitrile (**1**) disappeared further confirming the formation of compound (**3**). Elemental analysis was also conducted in order to investigate the purity of compound (**3**). The elemental analysis of the calculated CHN was similar to the found CHN values and within 0.35% for compound (**3**), thus confirming successful synthesis.

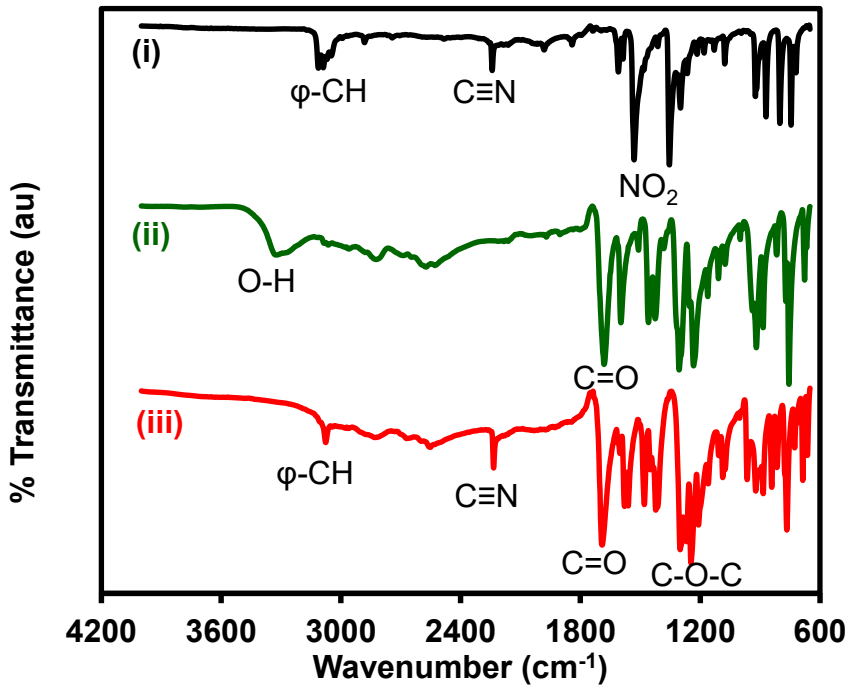

Figure 3.1: FT-IR spectra of **(i)** 4-nitrophthalonitrile (**1**), **(ii)** 3-hydroxybenzoic acid (**2**) and **(iii)** 4-(3-carboxyphenoxy)phthalonitrile (**3**).

The formation of and purity of 4-(3-carboxyphenoxy)phthalonitrile (**3**) was further investigated using ^{1}H and ^{13}C NMR. **Figure 3.2** shows ^{1}H NMR spectrum of 4-(3-carboxyphenoxy)phthalonitrile (**3**) measured in d_6-DMSO. The ^{1}H NMR exhibited a spectrum which integrated for seven protons instead of the expected eight protons. The seven protons observed in **Figure 3.2** were in the aromatic region between 7.41 – 8.07 ppm. The four protons (labeled 1 – 2) in the region 7.41 to 7.63 ppm are attributed to the 3-carboxyphenoxy substituent. The additional three protons (labeled 3 – 5) in the region 7.76 to 8.07 ppm are attributed to protons from the phthalonitrile. However, the proton due to the carboxylic acid on the 3-carboxyphenoxy substituent which would have given a total of eight protons, did not appear on the spectrum. This is due to the compound forming a potassium carbonate salt ($–COO^{-}K^{+}$) as discussed in the aforementioned FT-IR spectrum. Given this, the protons integrated for the correct amount of aromatic protons for the proposed structure in **Scheme 3.1**.

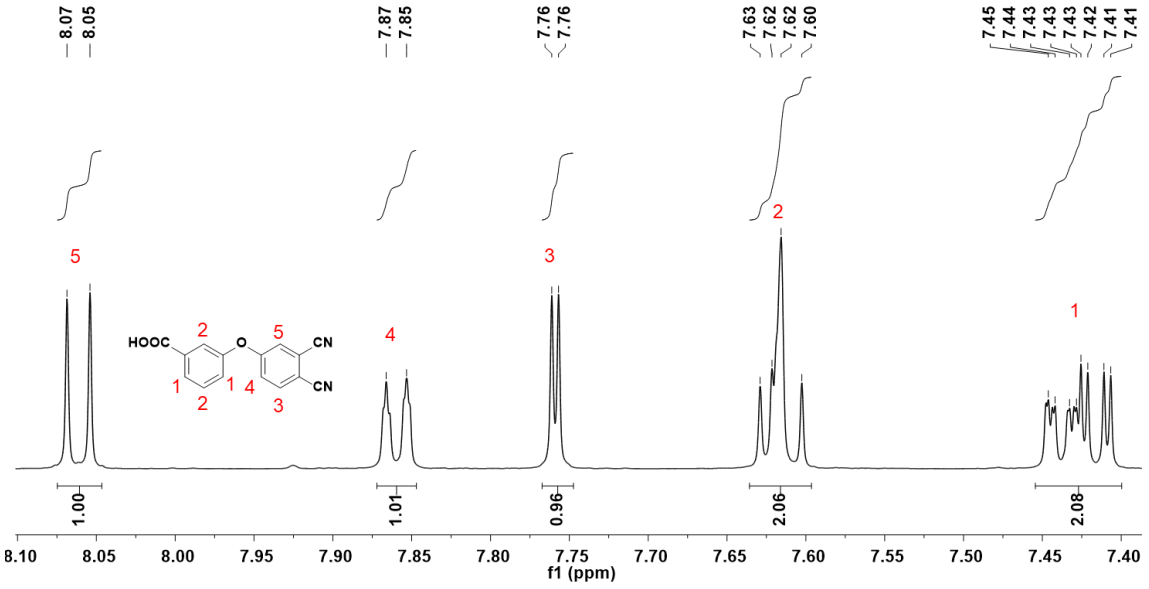

Figure 3.2: Proton ^{1}H NMR spectrum of 4-(3-carboxyphenoxy)phthalonitrile (**3**) measured in d_6-DMSO.

Figure 3.3 shows FT-IR spectra of **(i)** 4-(3-carboxyphenoxy)phthalonitrile (**3**) and **(ii)** CoTCPhOPc (**4**). The FT-IR spectrum of (**3**) in **Figure 3.3 (i)** is similar to the previously mentioned **Figure 3.1 (iii)** and was discussed. The synthesis of CoTCPhOPc (**4**) was determined by the disappearance of the C≡N vibrational stretch of 4-(3-carboxyphenoxy)phthalonitrile (**3**) at 2235 cm^{-1} in **Figure 3.3 (i)** as a result of the cyclotetramerization reaction. A broad absorption was observed at about 3200 – 3300 cm^{-1} due to the presence of carboxylic acid alcohol (O-H) group on CoTCPhOPc (**4**) in **Figure 3.3 (ii)**. The carbonyl (C=O) stretch was retained from 4-(3-carboxyphenoxy)phthalonitrile (**3**) at 1717 cm^{-1}. The presence of an ether (C-O-C) was observed as a stretch at 1234 cm^{-1} further confirming the formation of compound (**4**). In addition, the solution turned green during the cyclotetramerization reaction confirming the formation of CoTCPhOPc (**4**).

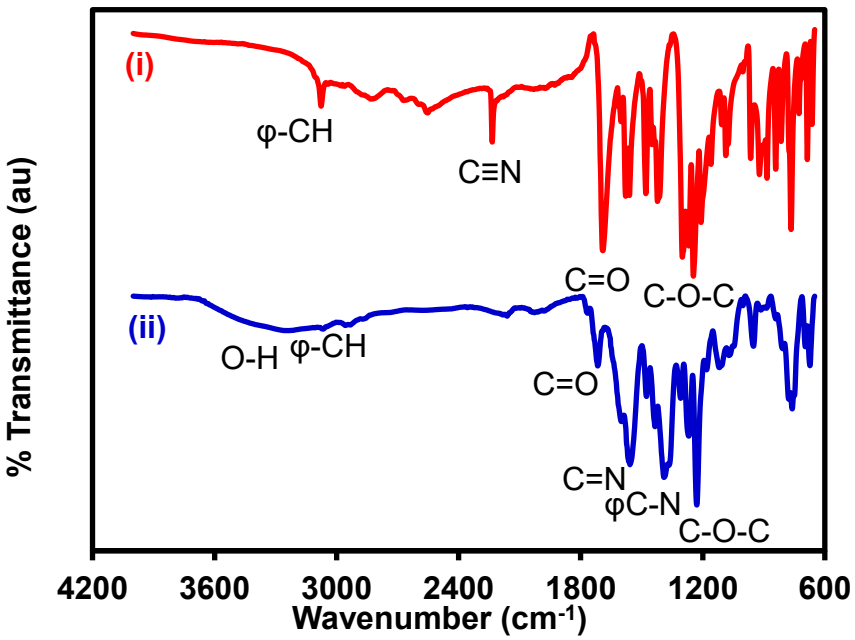

Figure 3.3: FT-IR spectra of **(i)** 4-(3-carboxyphenoxy)phthalonitrile (**3**) and **(ii)** CoTCPhOPc (**4**).

The formation of CoTCPhOPc (**4**) was further characterized using Magnetic Circular Dichroism (MCD) and UV-vis spectroscopy. MCD spectroscopy affords information about the spin and orbital angular momenta linked with ground and excited electronic states of molecules.[94,95] In MCD, the compounds need not necessarily be optically active. The MCD signal arises from the same transitions as those seen in UV-vis absorption spectrum. However, whilst UV-vis absorption intensity utilizes solely dipole moment, MCD utilizes both the dipole moment and the magnetic dipole moment making the two techniques complementary to one another. MCD provides ground and excited state degeneracy information which is essential in understanding the electronic structure of molecules of high symmetry. MCD also provides the Faraday *A*, *B* and *C* terms[96] which can be used to identify the main electronic Q and B bands in UV-vis spectrum.[97]

Figure 3.4 shows the **(a)** MCD and **(b)** UV-vis spectra of 1.0 mM CoTCPhOPc (**4**) measured in DMSO. In **Figure 3.4 (a)** the MCD spectra shows the Faraday *A1* terms observed at 663 nm which can be readily assigned to Q-band transitions on the basis of Gouterman's 4-orbital model. The Q-band of CoTCPhOPc (**4**) in the UV-vis spectrum has an inflection point in the MCD spectrum at 663 nm. This inflection point corresponds to the absorption maximum of the Q-band hence, it is assigned a Faraday *A1* term. The same was observed for the B-band which exhibited an inflection point at the absorption maximum (339 nm) for Faraday *A* term. **Figure 3.4 (b)** shows the UV-vis spectra of CoTCPhOPc (**4**) measured in DMSO. Generally, the UV-vis spectra of phthalocyanine complexes is characterized by the presence of two strong absorption bands, namely, the B- and Q-bands.[40] The B-band is located in the UV region between 300 – 400 nm and occurs due to deeper lying b_{1u} orbital levels of the HOMO. The Q-band on the other hand is found in the visible region between 600 – 750 nm and is a

result of a_{1u} – e_g transitions. Both B- and Q-bands are generally characterized as transitions from the highest occupied molecular orbital (HOMO) to the lowest unoccupied molecular orbital (LUMO) of the phthalocyanine ring.[37,98] The UV-vis spectra of CoTCPhOPc (**4**) was conducted in DMSO and showed a B-band at 339 nm and a Q-band at 663 nm respectively.

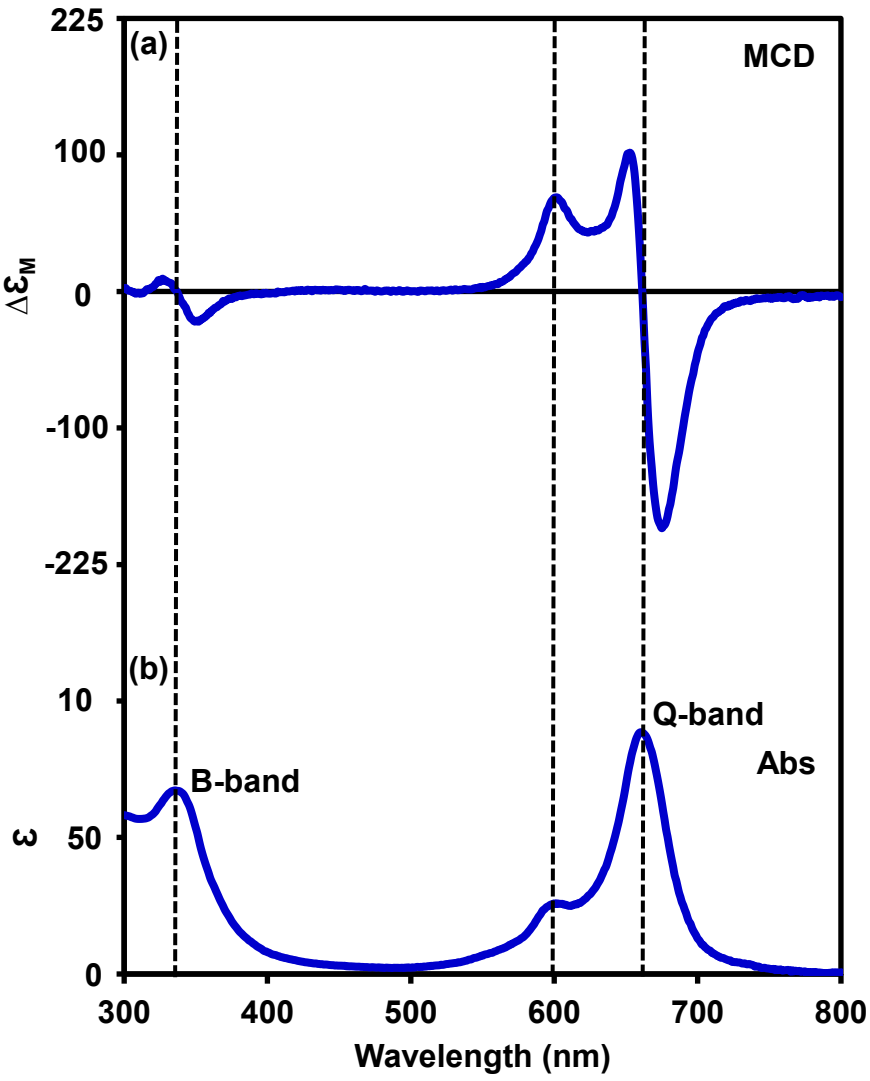

Figure 3.4: (a) MCD and **(b)** UV-vis spectra of 1.0 mM CoTCPhOPc (**4**) measured in DMSO.

The mass spectra was utilized for the confirmation of CoTCPhOPc (**4**) and **Figure 3.5** shows the mass spectra and chemical structure of CoTCPhOPc (**4**). Studies have shown that phthalocyanine complexes can degrade with the molecular ion peaks $[M]^+$, $[M \pm nH]^+$ where n = 1 – 3.[99,100] The mass spectrometric analysis showed the corresponding molecular ions at *m/z* = 1116.42 for $[M + H]^+$ for CoTCPhOPc (**4**) which is one hydrogen ion higher than the expected *m/z* = 1115.15 confirming the $[M + H]^+$ molecular ion with about 1.27 *m/z* difference. Elemental analysis was also conducted in order to investigate the purity of CoTCPhOPc (**4**). The elemental CHN analysis calculated for hydrated molecules and found CHN values were within 0.41%, thus confirming the synthesis of and CoTCPhOPc (**4**).

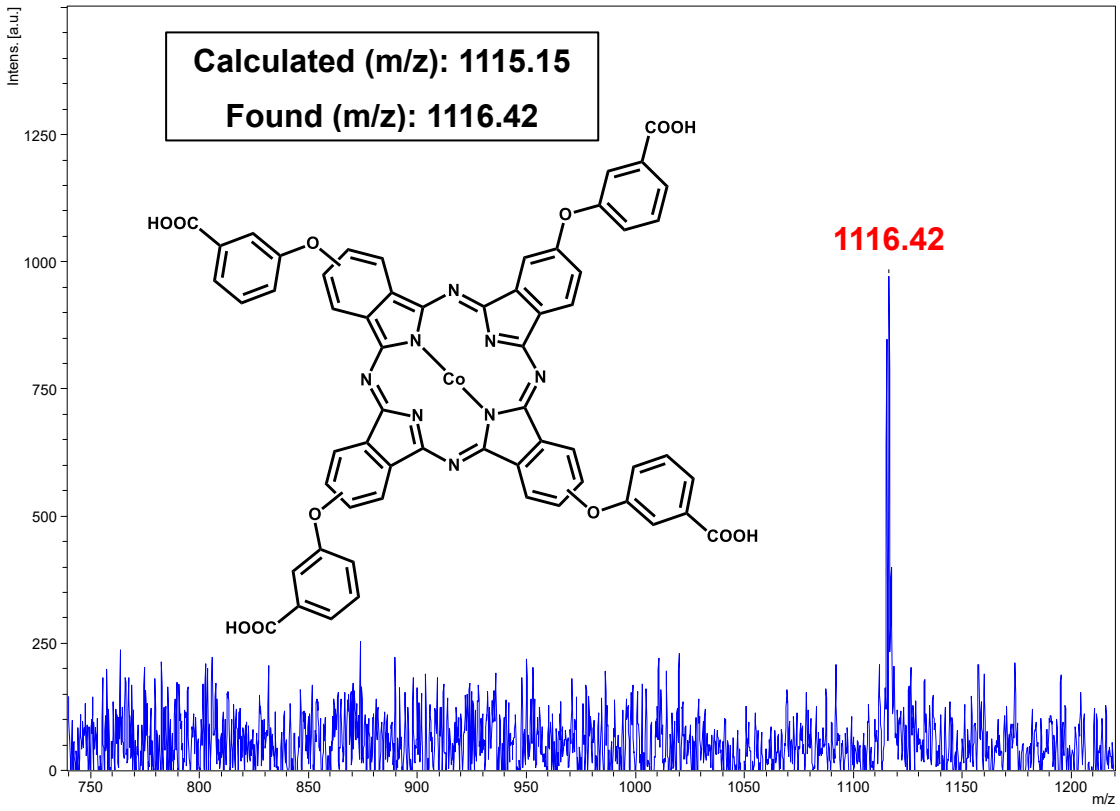

Figure 3.5: Mass spectra and chemical structure of CoTCPhOPc (**4**).

3.2 Synthesis and Characterization of 4-(2-Aminoethyl)benzene Diazonium Salt (6), Scheme 3.2

The synthesis of AEBD was conducted according to established procedure[69] as is described in the experimental sub-section, **2.3.3**. **Scheme 3.2** illustrates the synthetic route of 4-(2-aminoethyl)benzene diazonium salt (**6**). Briefly, 4-(2-aminoethyl)aniline (**5**) and sodium nitrite were reacted in the presence of tetrafluoroboric acid to yield 4-(2-aminoethylbenzene diazonium salt (**6**).

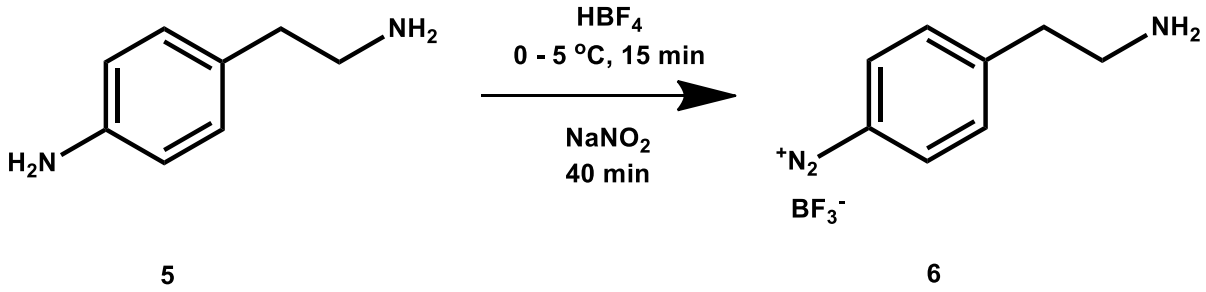

Scheme 3.2: Synthesis of 4-(2-aminoethyl)benzene diazonium salt (**6**).

The successful synthesis of the desired compound was investigated with varies characterization techniques. **Figure 3.6** shows the FT-IR spectra of **(i)** 4-(2-aminoethyl)aniline (**5**) and **(ii)** 4-(2-aminoethyl)benzene diazonium (AEBD) salt (**6**). The successful formation of the AEBD salt was confirmed by the appearance of the intense N_2^+ (N≡N) stretch at 2286 cm^{-1}. This is due to the aromatic amine at 3345 cm^{-1} for compound (**5**) being converted to the diazonium (N≡N) functional group for 4-(2-aminoethyl)benzene diazonium (AEBD) salt (**6**). The aliphatic amine however, was not converted to the N≡N functional group and this is due to the specificity of the diazonium reaction to the arylamine ($Ar\text{-}NH_2$).[69] As a result, the aliphatic C-N groups at 1000 cm^{-}

[1] are retained and the aromatic C-N at 1271 cm^{-1} disappeared. Following this, the successful synthesis of the compound was further investigated with ^{1}H and ^{13}C NMR spectroscopy.

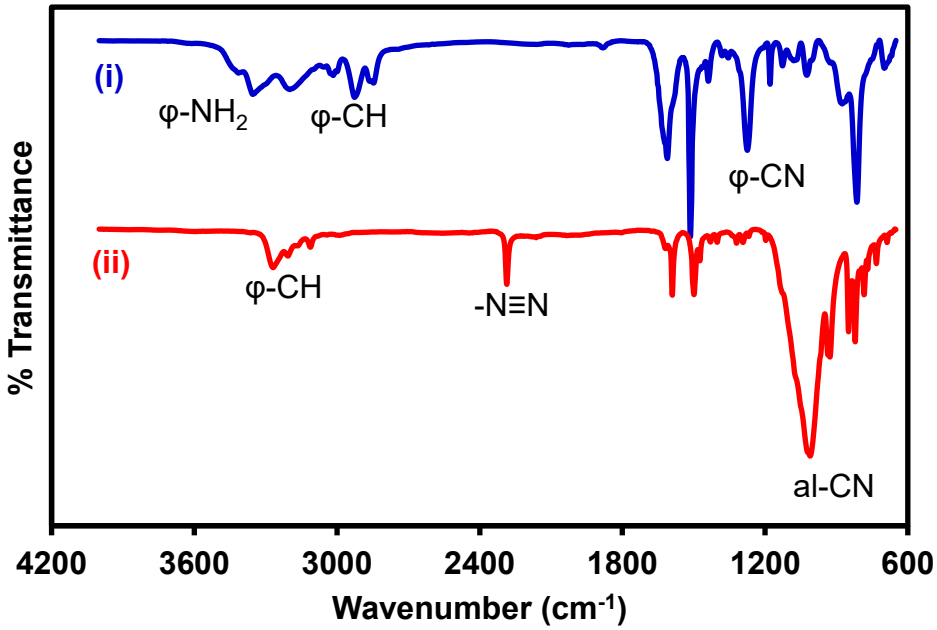

Figure 3.6: FT-IR spectra of **(i)** 4-(2-aminoethyl)aniline (**5**) and **(ii)** 4-(2-aminoethyl)benzene diazonium (AEBD) salt (**6**).

Figures 3.7 shows the **(a)** proton (^{1}H) and **(b)** carbon (^{13}C) NMR spectra of 4-(2-aminoethyl)benzene diazonium (AEBD) salt (**6**) measured in D_2O. The ^{1}H NMR spectra showed the purity of the product (**6**) as the integration showed the aromatic and aliphatic protons as expected. The four aliphatic protons were observed between 2.89 and 3.26 ppm whilst the four aromatic protons were observed between 6.87 and 7.22 ppm. The carbons observed on the ^{13}C NMR spectra were assigned accordingly as discussed in the experimental sub-section, **2.3.3**. This, in conjunction with the FT-IR data that showed the successful synthesis of the desired compound, 4-(2-

aminoethyl)benzene diazonium (AEBD) salt (**6**). The electrochemical grafting of the AEBD (**6**) molecule onto the gold electrode surface then followed.

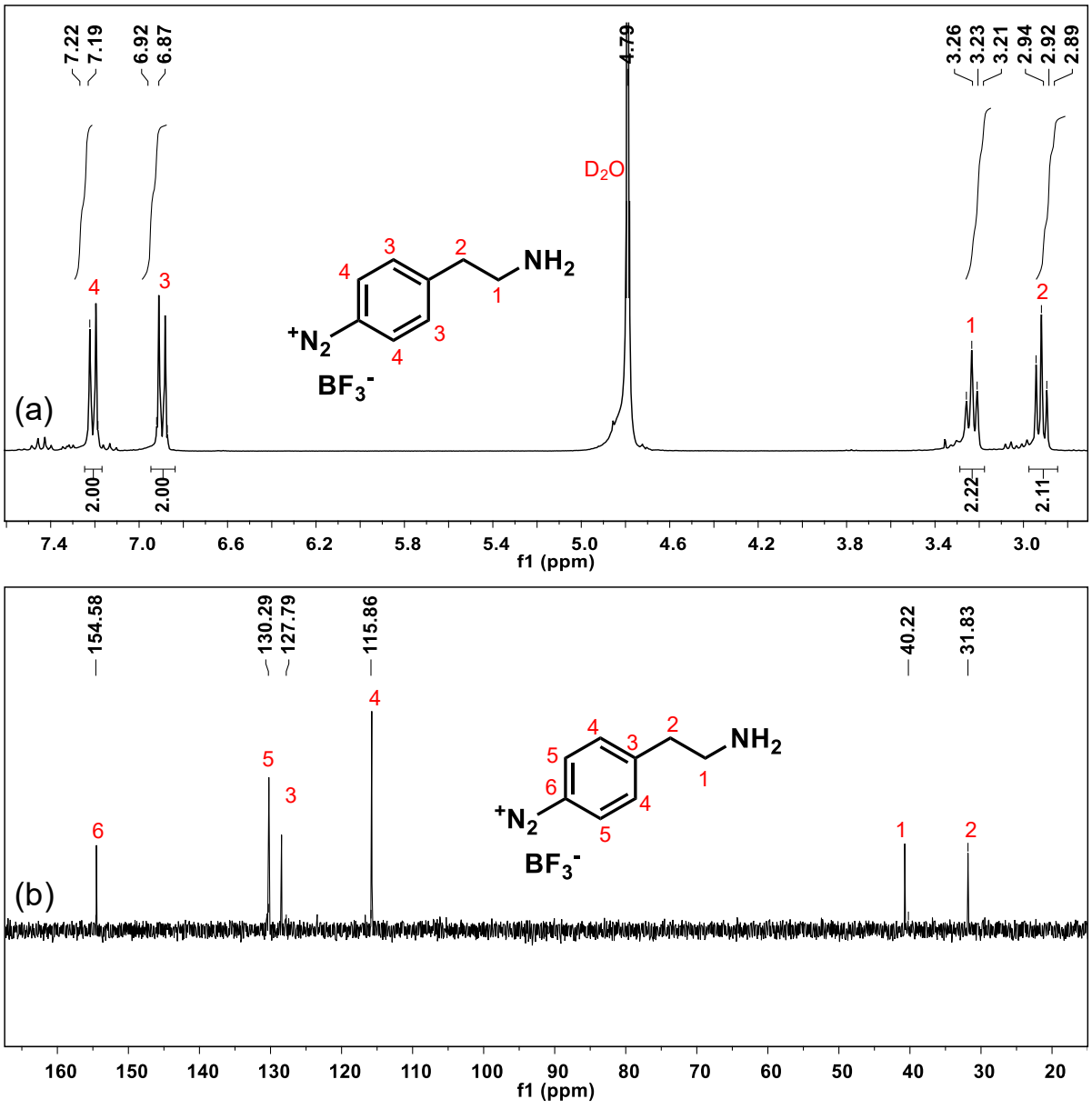

Figure 3.7: (a) Proton (^{1}H) and **(b)** carbon (^{13}C) NMR spectra of 4-(2-aminoethyl)benzene diazonium (AEBD) (**6**) salt measured in D_2O.

Chapter Four:

Modification, Characterization and Electroanalysis

4. Modification, Characterization and Electroanalysis

This chapter reports on the results and discussion of the surface modification and formation of Au-PEA-CoTCPhOPc. The electrochemical and spectroscopic characterization of the various electrode surfaces will also be discussed at length. Finally, the electrocatalysis and electroanalysis of catecholamine neurotransmitters (dopamine, norepinephrine and epinephrine) and ascorbic acid is conducted.

4.1 Electrochemical Grafting of AEBD (6) and Amide Coupling of CoTCPhOPc (4), Scheme 4.1

The first step in gold electrode modification involved electrochemical grafting of the bare gold electrode with AEBD (**6**), which produces the phenylethylamino (PEA) radical. The formation of the phenylethlamino thin film has been previously reported[68,69] and its controlled formation was achieved in the present study through utilizing 1.0 mM AEBD and two reductive cycles as per previous studies.[71] This radical species is then covalently attached onto the gold electrode surface (represented as Au-PEA). Subsequently, CoTCPhOPc (**4**) was immobilized onto PEA grafted gold electrode surface by means of amide coupling (represented as Au-PEA-CoTCPhOPc). **Scheme 4.1** illustrates the electrochemical grafting of bare Au with AEBD (Au-PEA) and the subsequent immobilization of CoTCPhOPc (Au-PEA-CoTCPhOPc).

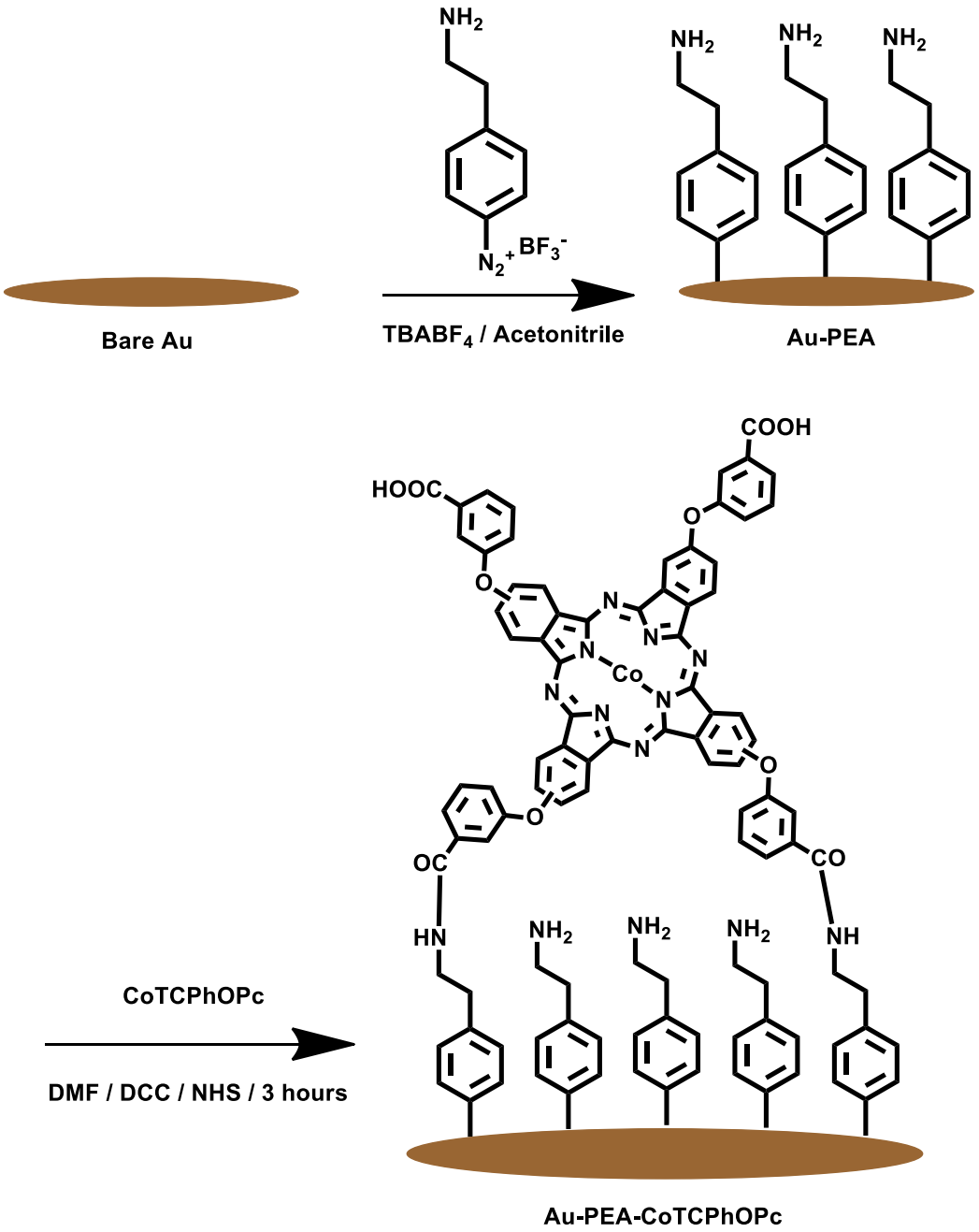

Scheme 4.1: The electrochemical grafting of AEBD (**6**) onto Au forming Au-PEA and subsequent immobilization of CoTCPhOPc (**4**) to form Au-PEA-CoTCPhOPc.

Cyclic voltammetry (CV) was utilized for the electrochemical grafting of the bare gold electrode surface. CV is an electrochemical technique which measures the current generated in an electrochemical cell where the voltage is in surplus of that predicted

by the Nernst equation. This technique is often used to investigate the oxidation and reduction processes of molecular species in solution or adsorbed onto conducting electrode surfaces. CV is also beneficial in the study of electron transfer chemical reactions, electrocatalysis.[83] **Figure 4.1** shows the CVs obtained for the electrochemical grafting of 1.0 mM AEBD salt in ACN solution containing 0.10 M $TBABF_4$ at a scan rate of 100 $mV.s^{-1}$. The first cycle shows a reduction peak at +0.20 V corresponding to the reduction of the diazonium salt and the generation of the phenylethylamine (PEA) radical. Upon scanning further, an additional broad reduction peak was observed at -0.38 V. The latter reduction peak was due to the covalent attachment of the PEA radical onto the gold electrode surface. The second cycle showed no reduction peaks and this is due to the blockage of the electrode surface by the PEA thin film after the formation of Au-PEA.

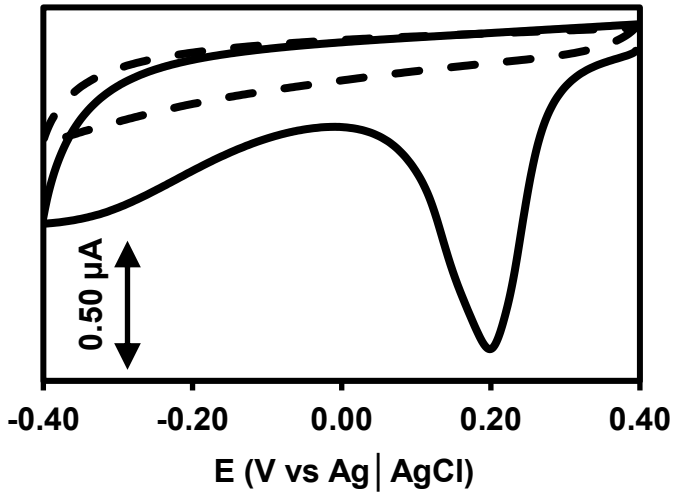

Figure 4.1: Cyclic voltammograms obtained for the electrochemical grafting of 1.0 mM AEBD salt in ACN solution containing 0.10 M $TBABF_4$ at a scan rate of 100 $mV.s^{-1}$.

After the successful electrochemical grafting of the PEA thin film, a mixture of CoTCPhOPc (**4**), NHS and DCC was dissolved in DMF and left to stir for an hour. The conversion of the carboxylic acid groups on the CoTCPhOPc (**4**) into amine reactive carbodiimide esters occurred. Thereafter, the Au-PEA electrode was immersed into the aforementioned solution and kept in the dark for 3 hours. This time was important for the immobilization to yield the best results. The amide coupling reaction between the –COOH functional groups of the CoTCPhOPc (**4**) with the $–NH_2$ groups of the AEBD (**6**) took place. This resulted in the immobilization of CoTCPhOPc (**4**), forming Au-PEA-CoTCPhOPc thin film. The Au-PEA-CoTCPhOPc electrode was then rinsed with DMF to remove any physically adsorbed and unreacted CoTCPhOPc (**4**). The Au-PEA-CoTCPhOPc electrode was finally rinsed with PBS buffer pH 7.4 in order to hydrate the carbodiimide esters and stored at room temperature. The electrochemical characterization of the bare Au, Au-PEA and Au-PEA-CoTCPhOPc thin films was then conducted.

4.2 Electrochemical Characterization of Bare and Modified Gold Surfaces

In the present study, bare Au, Au-PEA and Au-PEA-CoTCPhOPc thin films were investigated for their electrochemical properties. The following Faradaic processes were investigated: the oxidation and reduction of solution species, gold oxidation and the under-potential deposition (UDP) of metals.[101] The initial studies involved the cyclic voltammetry and electrochemical impedance spectroscopy (EIS) of the negatively charged, $[Fe(CN)_6]^{3-/4-}$ and positively charged, $[Ru(NH_3)_6]^{2+/3+}$ as electroactive redox probes. **Figure 4.2** shows the CVs and their corresponding Nyquist plots for **(i)** bare Au, **(ii)** Au-PEA and **(iii)** Au-PEA-CoTCPhOPc measured in 1.0 mM of **(a)** $[Fe(CN)_6]^{3-/4-}$ and **(b)** $[Ru(NH_3)_6]^{2+/3+}$ solution containing 0.10 M KCl at a scan rate of 50 $mV.s^{-1}$.

The CV response recorded for bare Au in $[Fe(CN)_6]^{3-/4-}$, **Figure 4.2 (a) (i)**, shows a couple of redox waves with a peak-to-peak separation (ΔE) of 73 ± 4.5 mV and a ratio of anodic to cathodic peak currents (I_{pa}/I_{pc}) of 1.0. These results confirmed high reversibility expected for such redox couple on Au electrodes.

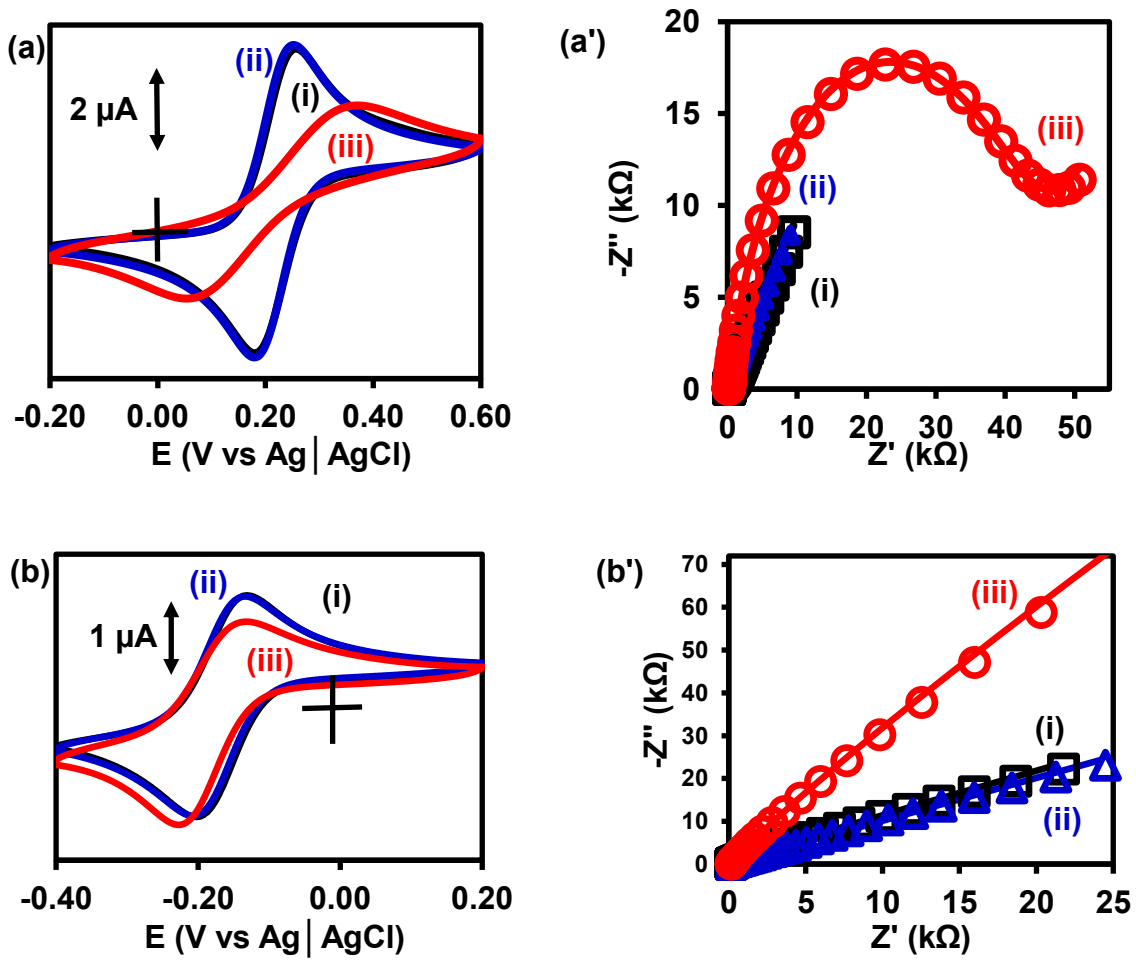

Figure 4.2: Cyclic voltammograms and their corresponding Nyquist plots for **(i)** bare Au, **(ii)** Au-PEA and **(iii)** Au-PEA-CoTCPhOPc measured in 1.0 mM of **(a)** $[Fe(CN)_6]^{3-/4-}$ and **(b)** $[Ru(NH_3)_6]^{2+/3+}$ solution containing 0.10 M KCl. Scan rate = 50 $mV.s^{-1}$. For EIS, a formal potential ($E_{½}$) for $[Fe(CN_6)]^{3-/4-}$ (220 mV) and for $[Ru(NH_3)_6]^{2+/3+}$ (-160 mV) for bare Au was used.

Although the theoretical value for a fully reversible pair is ΔE = 59.2 mV, values in the range 68.5 – 77.5 mV as observed in the current study are acceptable in practice due to slight irreproducibility in the order and cleanliness of the electrode surface and ohmic drop. The CV for the Au-PEA electrode was identical to that of bare Au, **Figure 4.2 (a) (ii)**, with ΔE = 73 ± 2.4 mV. The range of ΔE was narrow 70.6 – 75.4 mV confirming the charged PEA layer as previously reported.[68,71] The Au-PEA-CoTCPhOPc thin film in **Figure 4.2 (a) (iii)**, showed the $[Fe(CN)_6]^{3-/4-}$ redox couple to be to some extent suppressed. An increase in ΔE to 307 ± 10 mV and a decrease in the redox peak currents was observed at the Au-PEA-CoTCPhOPc thin film due to the immobilization of CoTCPhOPc (**4**). The Au-PEA-CoTCPhOPc thin film possesses carboxylic acid (–COOH) functional groups with a pKa value of 3.4 which is negatively charged at pH 7.4 of 1.0 mM $[Fe(CN)_6]^{3-/4-}$ solution containing 0.10 M KCl. The negatively charged Au-PEA-CoTCPhOPc thus repels the negatively charged $[Fe(CN)_6]^{3-/4-}$.

The bare Au, Au-PEA and Au-PEA-CoTCPhOPc electrodes in the presence of $[Ru(NH_3)_6]^{2+/3+}$ were also studied in **Figure 4.2 (b)**. The bare Au in **Figure 4.2 (b) (i)** exhibited a redox peak with ΔE = 63 ± 3.5 mV which is closer to the ideal value (59.2 mV). The Au-PEA in **Figure 4.2 (b) (ii)** showed an even smaller ΔE of 61 ± 2.5 mV compared to the bare Au owing to the PEA thin film bearing hydrophilic functional groups and permeable to electrolyte ions. **Figure 4.2 (b) (iii)** for Au-PEA-CoTCPhOPc gave ΔE of 95 ± 5.5 mV and this was due to electrode kinetics which slowed the diffusion of $[Ru(NH_3)_6]^{2+/3+}$. When comparing the two redox probes, the $[Ru(NH_3)_6]^{2+/3+}$ showed better conductivity of the Au-PEA-CoTCPhOPc than the $[Fe(CN)_6]^{3-/4-}$. The effect of the surface charge due to terminal COOH functional groups played a role in the observed changes in the electrochemical properties. That is, the negatively

charged probe was repelled by the negatively charged surface. Conversely, the positively charged probe was attracted onto the negatively charged surface resulting in the decrease in ΔE from 307 ± 10 mV for $[Fe(CN)_6]^{3-/4-}$ to 95 ± 5.5 mV for $[Ru(NH_3)_6]^{2+/3+}$. The experiment also confirms the effect of pH on the Au-PEA-CoTCPhOPc response to positive and negatively charged redox probes. Additional studies of pH effect will be discussed at length in the present study in sub-section **4.4**.

The bare Au **(i)**, modified gold surfaces with PEA **(ii)** and Au-PEA-CoTCPhOPc **(iii)** thin films were studied for their electron transfer properties using EIS in the presence of 1.0 mM of $[Fe(CN)_6]^{3-/4-}$ in **Figure 4.2 (a')** and $[Ru(NH_3)_6]^{2+/3+}$ containing 0.10 M KCl solution in **Figure 4.2 (b')** as redox probes. EIS is an effective characterization technique for investigating the charge transfer properties at the electrode|solution interface.[83,102] The Nyquist plot was used to represent the data.

Figure 4.2 (a') illustrates the Nyquist plots of **(i)** bare Au, **(ii)** Au-PEA and **(iii)** Au-PEA-CoTCPhOPc in $[Fe(CN)_6]^{3-/4-}$ containing 0.10 M KCl solution, the applied potential was at $E_{½}$ (220 mV) for bare Au. The raw data was fitted using Randles equivalent circuit with R_S (solution resistance) in series with a parallel combination of Q (constant phase element, CPE) and R_{CT} charge transfer resistance in series to Z_W (Warburg impedance). The solid line in the EIS represents the fitted data and was only accepted when the fitting error was < 5% for all the circuit components. Two regions were of importance in the Nyquist plot, that is the high frequency region which represents the kinetic region with R_S and the low frequency region where both the R_{CT} and Z_W are obtained. Upon fitting, the Nyquist plot of bare Au in **Figure 4.2 (a') (i)** showed a small semi-circle with $R_{CT} \approx 0.61 \pm 0.14$ kΩ which disappeared at the Au-PEA thin film in **Figure 4.2 (a') (ii)**. The Au-PEA-CoTCPhOPc modified thin film however, showed a large semi-circle with $R_{CT} \approx 47 \pm 4.3$ kΩ. The pronounced semi-circle in the Au-PEA-

CoTCPhOPc thin film is due to the $–COO^-$ of immobilized CoTCPhOPc (**4**) repelling the negatively charged $[Fe(CN)_6]^{3-/4-}$ inline and confirming the observed CV studies.

Figure 4.2 (b') shows the Nyquist plots for **(i)** bare Au, **(ii)** Au-PEA and **(iii)** Au-PEA-CoTCPhOPc measured in $[Ru(NH_3)_6]^{2+/3+}$ containing 0.10 M KCl solution, the applied potential was at $E_{½}$ (-160 mV) for bare Au. The Nyquist plot for **(i)** bare Au and **(ii)** Au-PEA were similar with $R_{CT} \approx 0.51 \pm 0.21$ kΩ in **Figure 4.2 (b')**. At the Au-PEA-CoTCPhOPc in **Figure 4.2 (b') (iii)**, the R_{CT} increased from 0.51 ± 0.21 kΩ to 5.3 ± 1.5 kΩ. The increase in R_{CT} value was attributed to the formation of the Au-PEA-CoTCPhOPc as an additional layer onto Au-PEA thus slowing the solution kinetics confirming the attachment of CoTCPhOPc onto Au-PEA via amide coupling. The R_{CT} values for $[Ru(NH_3)_6]^{2+/3+}$ were smaller than those of $[Fe(CN)_6]^{3-/4-}$ at Au-PEA-CoTCPhOPc thin film surface due to the electrostatic repulsion between the $–COO^-$ charge repelling the $[Fe(CN)_6]^{3-/4-}$. The observed effect of pH conditions were observed on the Au-PEA-CoTCPhOPc with –COOH functional groups.

Additional electrochemical experiments were investigated for the characterization of bare and modified gold electrode surfaces. Amongst these processes were gold redox processes in KOH, H_2SO_4 containing $CuSO_4$ (under-potential deposition solutions) and in phosphate buffer (PBS, pH 7.4) solution.[101,103] **Figure 4.3** shows CVs of **(i)** bare Au, **(ii)** Au-PEA and **(iii)** Au-PEA-CoTCPhOPc measured in **(a)** 0.010 M KOH, **(b)** 0.50 M H_2SO_4 containing 1.0 mM $CuSO_4$ and **(c)** 1.0 mM PBS buffer (pH 7.4) solutions at a scan rate of 50 $mV.s^{-1}$. The gold oxidation and reduction reactions on the bare and modified gold electrode surfaces were studied in order to verify the successful modification with PEA and CoTCPhOPc thin films respectively. **Figure 4.3 (a)** shows that the gold oxidation and reduction peaks were both present on the bare Au **(i)** electrode surface. These redox peaks decreased upon the functionalization of the gold

surface with PEA thin film **(ii)**. The aforementioned gold peaks decreased further at the Au-PEA-CoTCPhOPc **(iii)**.

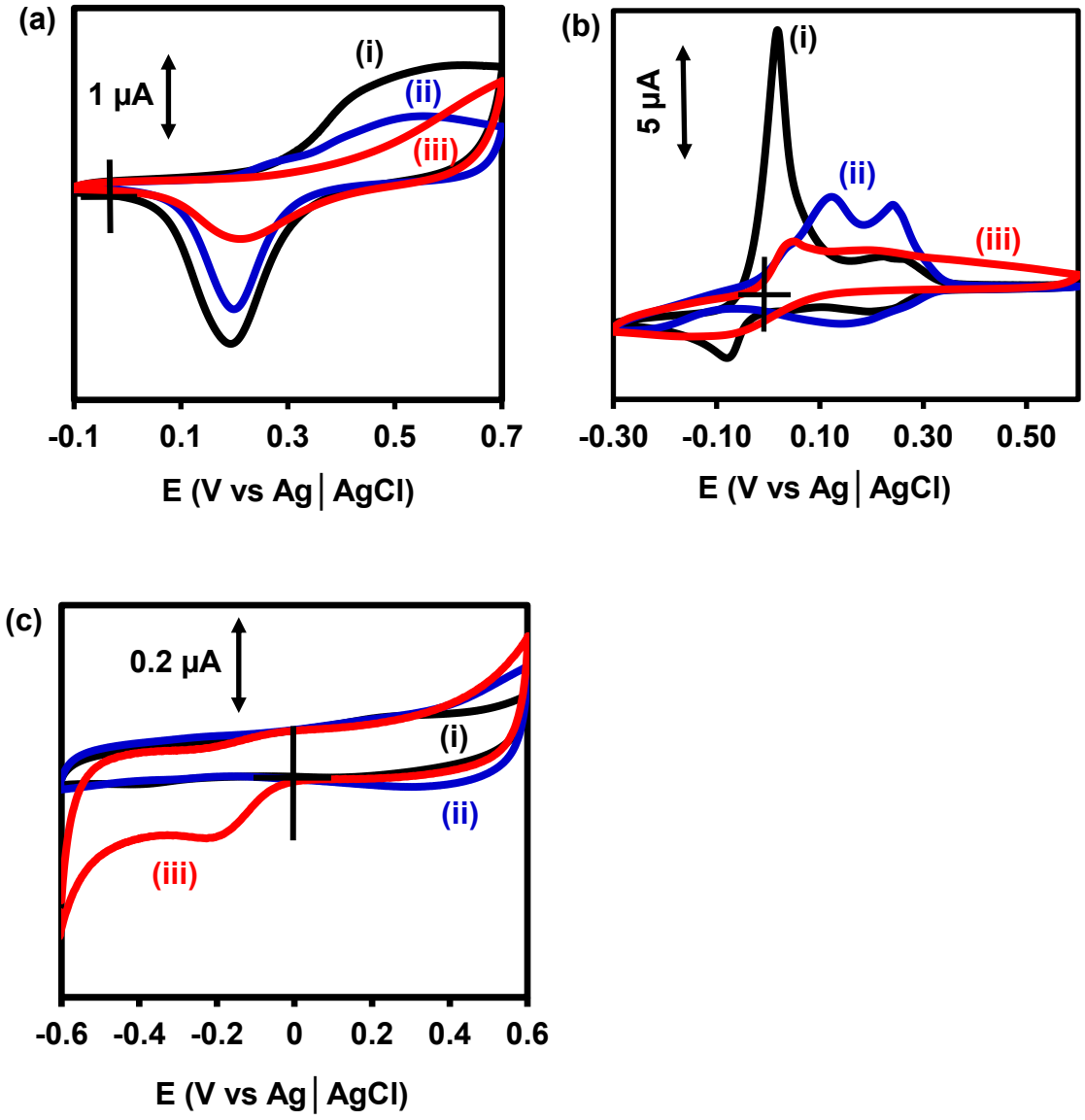

Figure 4.3: Cyclic voltammograms of **(i)** bare Au, **(ii)** Au-PEA and **(iii)** Au-PEA-CoTCPhOPc measured in **(a)** 0.010 M KOH solution, **(b)** 0.50 M H_2SO_4 solution containing 1.0 mM $CuSO_4$ and **(c)** 1.0 mM PBS buffer solution (pH 7.4). Scan rate of 50 $mV.s^{-1}$.

The decrease in the gold oxidation and reduction peaks confirmed the functionalization of the gold electrode surface by PEA and CoTCPhOPc thin films. A measure of the surface coverage is important in ascertaining the extent of electrode modification. The film 'ion barrier factor' (Γ_{ibf}) was used to determine the extent of surface coverage with the PEA for Au-PEA and PEA-CoTCPhOPc for Au-PEA-CoTCPhOPc. The **equation 4.1** was used to calculate the Γ_{ibf}:

$$\Gamma_{ibf} = 1 - \frac{Q_{thin\ layer}}{Q_{bare}} \qquad \textbf{(4.1)}$$

Where $Q_{thin\ layer}$ is the charge under the peak of Au-PEA or Au-PEA-CoTCPhOPc and Q_{bare} is the charge under the unmodified gold electrode. Ozoemena and Nyokong[101] showed that Γ_{ibf} could be up to unity for a close packed monolayer confirming the complete passivation of the gold electrode. In their work, the alkanethiols self-assembled monolayers were used which rendered the surface completely passivated and blocked electrolyte ions from reaching the surface. In the present study, gold modified with thin monolayer films of PEA and PEA-CoTCPhOPc were investigated. The Γ_{ibf} was obtained to be 0.90 for Au-PEA and 0.75 for Au-PEA-CoTCPhOPc. The higher Γ_{ibf} (close to unity) the higher the extent of blocking of electrolyte ions to react with the underlying gold surface. The Au-PEA formed as a thin layer could block 90% of oxygen as a source for gold oxidation and reduction. The Au-PEA-CoTCPhOPc could block 75% oxygen. This is attributed to the thin layer of less than C6 in chain length and a functional group that is hydrophilic making it permeable to solution ions.[104] Ozoemena et al.[101,105] showed that a monolayer with hydrophobic terminal groups blocks 100% of the gold surface whilst that with hydrophilic groups was permeable to solution ions. The thin films studied in the present study contain hydrophilic groups and are permeable to solution ions. The functional groups such as

–NH_3 for Au-PEA and –COOH for Au-PEA-CoTCPhOPc allowed oxygen and Cu^{2+} ion to permeate through the hydrophilic thin films and react at the underlying gold surface.

The gold modified with thin films were further investigated using the H_2SO_4 solution containing $CuSO_4$ for under-potential deposition (UDP) of Cu metal to form an ad-atom onto the gold surface. This method can be used to study the surface properties of the gold electrode surface post-modification.[101,103] **Figure 4.3 (b)** shows the CVs of **(i)** bare Au, **(ii)** Au-PEA and **(iii)** Au-PEA-CoTCPhOPc in 0.50 M H_2SO_4 solution containing 1.0 mM $CuSO_4$. The bare gold surface showed a broad reduction peak for Cu^{II} to Cu^0 at -70 mV and Cu^0 was deposited forming Au(Cu) ad-atom. On return scan the oxidation peak was observed at 20 mV for Cu^0 to Cu^{II} and Cu^{II} stripping and dissolving back into solution. At the Au-PEA and Au-PEA-CoTCPhOPc, the reduction peaks shifted to 150 mV and -56 mV respectively for Cu^{II} to Cu^0. Au-PEA exhibited two oxidation peaks at 130 mV and 250 mV whilst Au-PEA-CoTCPhOPc showed an oxidation peak at 42 mV for Cu^0 to Cu^{II}. The reduction and oxidation peaks still present in Au-PEA and Au-PEA-CoTCPhOPc are owing to Cu reduction and oxidation due to the hydrophilic groups being permeable to the solution ions.

In PBS buffer (pH 7.4), **Figure 4.3 (c)**, no oxidation and reduction peaks were observed for both the **(i)** bare Au and **(ii)** Au-PEA thin film. At the **(iii)** Au-PEA-CoTCPhOPc surface, a small oxidation peak is observed at 0.0 mV due to Co^{I}/Co^{II} and its corresponding reduction peak at -202 mV attributed to Co^{II}/Co^{I}. The reduction peak was pronounced and this is due to the electrolyte solution used. To observe a well-defined redox peak an organic solution containing tetrabutylammonium perchlorate should be used.[101] In the present study the observed oxidation and reduction peak confirmed the immobilization of CoTCPhOPc (**4**). The appearance of the metal reduction peak in the CV obtained on Au-PEA-CoTCPhOPc thin film, is

indicative of the successful immobilization of CoTCPhOPc (**4**) onto the pre-grafted Au-PEA surface. The amount of CoTCPhOPc immobilized via amide coupling was determined by integrating the charge under the reduction peak using the **equation 4.2**:

$$\Gamma_{\mathrm{Au-PEA-CoTCPhOPc}} = \frac{\mathrm{Q}}{\mathrm{nFA}} = \frac{\int \mathrm{Idt}}{\mathrm{nFA}} \qquad \textbf{(4.2)}$$

where Q (0.158 μF) is total charge under the reduction peak, n = 1 (number of electrons), A = 0.0201 cm^2 (geometric surface area of gold electrode surface with diameter 1.6 mm) and F = 96485 $C.mol^{-1}$ (Faradays constant). The surface coverage for the Au-PEA-CoTCPhOPc was found to be 8.14 x 10^{-11} $mol.cm^{-2}$ in line with a vertically aligned CoTCPhOPc (**4**) complex and confirming the surface functionalization. The phthalocyanine lying flat (octopus/umbrella orientation) on gold electrode surface occupies 1.0 x 10^{-10} $mol.cm^{-2}$ surface.[102] In the present study, the CoTCPhOPc (**4**) occupied a smaller surface area 8.14 x 10^{-11} $mol.cm^{-2}$ than that of the MPc lying flat in an octopus or umbrella orientation. This supported a conclusion that CoTCPhOPc was covalently attached onto Au-PEA with one or two COOH functional groups exposing the unreacted COOH functional groups onto the electrolyte, hence the perpendicular orientation.

4.3 Surface Characterization of Au-PEA-CoTCPhOPc

The XPS characterization of bare Au and Au-PEA was accomplished as previously reported.[71] The analysis of Au-PEA-CoTCPhOPc in **Figure 4.4** shows **(a)** the survey spectrum with peaks due to underlying gold surface as Au 4f, Au 4d, C 1s, N 1s and O 1s. The observed elemental composition especially the C 1s, N 1s and O 1s were from the immobilized PEA-CoTCPhOPc. The percentage atomic composition (% At)

was obtained to the 5.3% for Au 4f, 57.8% for C 1s, 12.5% N 1s and 24.3% O 1s. The decrease in Au 4f was accompanied by the increase in C 1s, N 1s and O1s in the Au-PEA-CoTCPhOPc confirming the electrode fabrication.

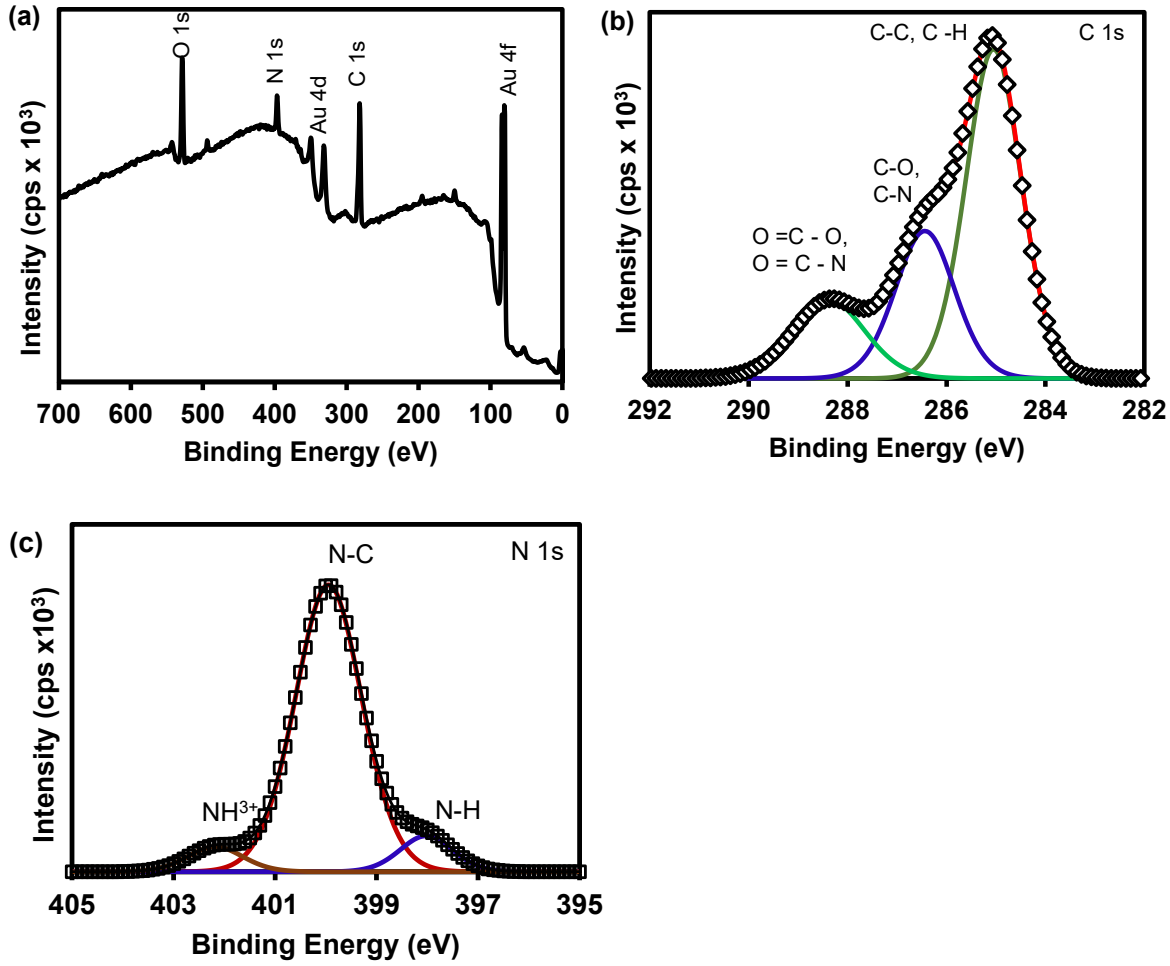

Figure 4.4: X-ray photoelectron spectroscopy characterization for Au-PEA-CoTCPhOPc **(a)** survey spectrum and high resolution of **(b)** C 1 s and **(c)** N 1 s.

The high resolution of C 1s in **Figure 4.4 (b)** and N 1s in **Figure 4.4 (c)** were investigated. The chosen high resolution spectra were for the functional groups involved in the amide coupling reaction. The O 1s was not involved and hence not reported. The C 1s was devonvoluted into 3 components at 385.0 eV (C-C, C-H), 286.8

eV (C-O, C-N) and 288.8 eV (O=C-O, N-C=O). The observed peak at 288.8 eV confirmed the amide coupling and the carboxylic acid functional group on the PEA-CoTCPhOPc. The high resolution of N 1s exhibited three components at 397.9 eV for N-H, 399.8 eV for N-C and 402.2 eV for NH_3^+. The N-C component is from the amide and isoindole ring and azobridge in the core of the CoTCPhOPc (**4**). The N-H component from the amide bond between NH_2 of a thin PEA layer and carboxylic group of the CoTCPhOPc (**4**). The NH_3^+ component is from the unreacted amine terminal functional group from the Au-PEA.[71]

4.4 Effect of pH on the Au-PEA-CoTCPhOPc Against Charged Redox Probes

The effect of pH was investigated as a preliminary study before the detection of catecholamine neurotransmitters and the screening off of ascorbic acid. The redox probing species, $[Fe(CN)_6]^{3-/4-}$ and $[Ru(NH_3)_6]^{2+/3+}$, were investigated at different pH conditions against the pH sensitive –COOH functional group of the Au-PEA-CoTCPhOPc. **Figure 4.5** shows the **(a)** and **(b)** CVs, **(a')** and **(b')** Nyquist plots and **(a")** correlation of ΔE and R_{CT} vs pH for 1.0 mM of **(a)** $[Fe(CN)_6]^{3-/4-}$ and **(b)** $[Ru(NH_3)_6]^{2+/3+}$ both containing 0.10 M KCl. In **Figure 4.5 (a)** the electrochemical signal of the $[Fe(CN)_6]^{3-/4-}$ exhibited a decrease in peak currents as the pH increased and this was accompanied by an increasing peak-to-peak separation (ΔE). The observed changes were due to the electrostatic repulsion of the negatively charged $–COO^-$ functional group of Au-PEA-CoTCPhOPc and $[Fe(CN)_6]^{3-/4-}$. As previously stated the pKa of the –COOH is 3.4, therefore at pH 3.0 the carboxylic acid group is protonated and is neutral (–COOH). This results in a thin film with zero net charge (neutral) and

thus no effect on the negatively charged redox probe, $[Fe(CN)_6]^{3-/4-}$ as shown in **Figure 4.5 (a) (i)**.

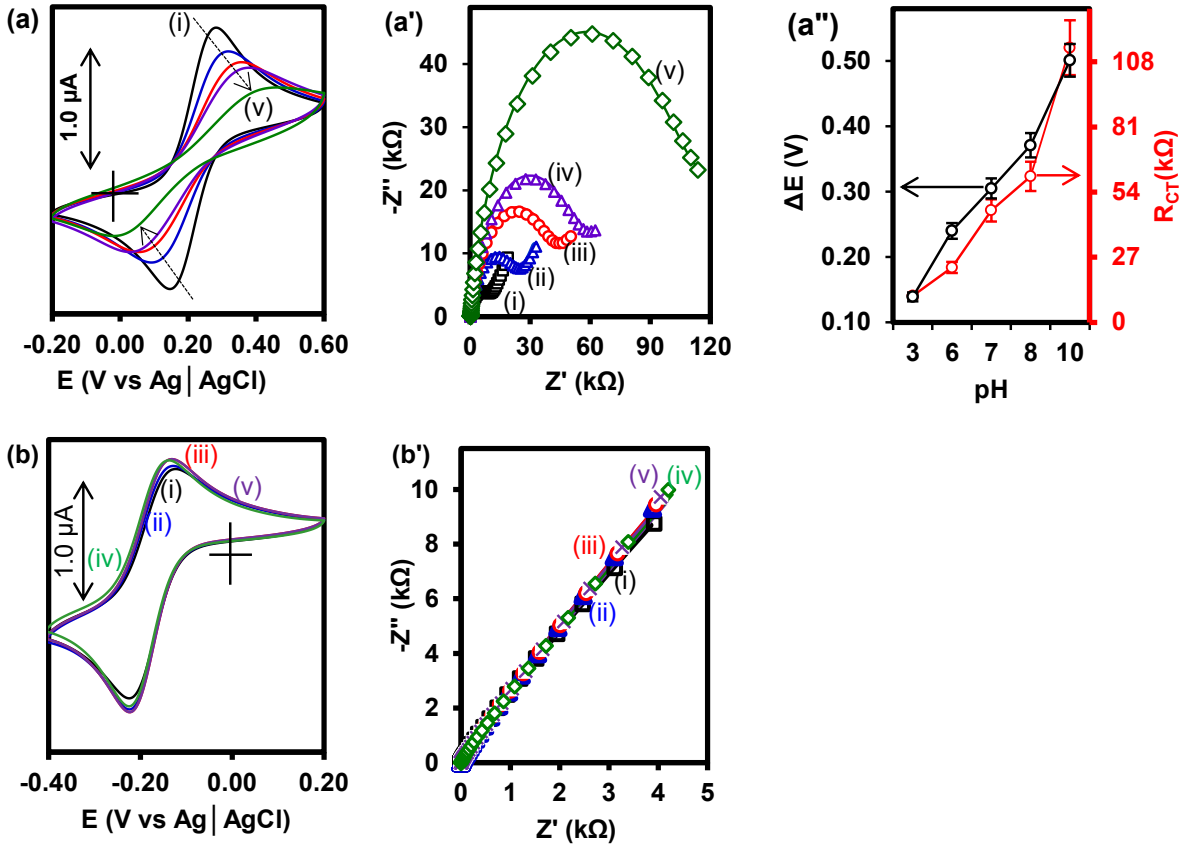

Figure 4.5: (a) and **(b)** Cyclic voltammograms, **(a')** and **(b')** Nyquist plots and **(a'')** correlation of ΔE and R_{CT} vs pH of Au-PEA-CoTCPhOPc measured in 1.0 mM of **(a)** $[Fe(CN)_6]^{3-/4-}$ and **(b)** $[Ru(NH_3)_6]^{2+/3+}$ containing 0.10 M KCl solution at pH **(i)** 3.0, **(ii)** 6.0, **(iii)** 7.0, **(iv)** 8.0 and **(v)** 10.0. Scan rate = 50 $mV.s^{-1}$. For EIS, a formal potential ($E_{½}$) for $[Fe(CN_6)]^{3-/4-}$ (220 mV) and for $[Ru(NH_3)_6]^{2+/3+}$ (-160 mV) for bare Au was used.

When the pH increased to above 3.4, the net charge of Au-PEA-CoTCPhOPc is negative due to the deprotonation of the carboxylic acid group ($–COO^-$). The result of this negative net charge is the electrostatic repulsion and hence an increase in ΔE and decrease in peak currents, as observed in **Figure 4.5 (a) (ii) – (v)**. Similarly, the

Nyquist plot in **Figure 4.5 (a')** for the $[Fe(CN)_6]^{3-/4-}$ an increase in R_{CT} signal was observed as the pH increased further confirming the net electrostatic repulsion. The data of ΔE and R_{CT} vs pH was shown in **Figure 4.5 (a'')** for $[Fe(CN)_6]^{3-/4-}$. The effect of pH in **Figure 4.5 (a'')** clearly shows the increase in the peak-to-peak separation and also charge transfer resistance due to electrostatic repulsion. The probe was changed from the negatively charged $[Fe(CN)_6]^{3-/4-}$ to the positively charged $[Ru(NH_3)_6]^{2+/3+}$. The effect of pH (3.0 to 10.0) was investigated. There was no observed changes for the cyclic voltammetry (ΔE) in **Figure 4.5 (b)** and Nyquist plot (R_{CT}) in **Figure 4.5 (b')**. There was a slight decrease in ΔE and slight increase in peak currents as the pH increased from 3.0 – 10.0 but the changes were very small, that is, 175 ± 5 mV. The observed response of Au-PEA-CoTCPhOPc towards negative and positively charged redox species indicates that pH can be used for selective detection of catecholamine neurotransmitters with the screening off of ascorbic acid.

4.5 Electrocatalytic Detection of Catecholamine Neurotransmitters and Ascorbic Acid

The Au-PEA-CoTCPhOPc electrode exhibited excellent electrocatalysis towards dopamine (DA), norepinephrine (NEP) and epinephrine (EP). **Figure 4.6** shows the CVs of Au-PEA-CoTCPhOPc in the **(i)** absence and **(ii)** presence of 0.10 mM **(a)** dopamine, **(b)** norepinephrine, **(c)** epinephrine and **(d)** ascorbic acid in pH 7.4 PBS solution. The CV response in the absence of dopamine, norepinephrine, epinephrine and ascorbic acid exhibited no oxidation or reduction peaks, **Figure 4.6 (i)**. However, in the presence of 0.10 mM dopamine in pH 7.4 PBS solution, oxidation and reduction peaks were observed at 0.264 V and 0.110 V respectively, **Figure 4.6 (a) (ii)**. Norepinephrine (0.10 mM) in pH 7.4 PBS solution exhibited oxidation and reduction

peaks at 0.269 V and 0.130 V respectively, **Figure 4.6 (b) (ii)**. In a PBS solution containing 0.10 mM epinephrine, an oxidation peak at 0.271 V was observed and no reduction peak, **Figure 4.6 (c) (ii)**. Ascorbic acid, 0.10 mM in pH 7.4 PBS exhibited no peak within the studied potential range, **Figure 4.6 (d) (ii)**. Epinephrine exhibited a single oxidation peak in the potential window studied whilst dopamine and norepinephrine exhibited oxidation and reduction peaks. The observed electrocatalytic oxidation potentials are within the potential for Co^{II}/Co^{III} oxidation and the metal induces electrocatalytic oxidation and reduction of the catecholamine neurotransmitters. Ascorbic acid was completely blocked and this was attributed to the carboxylic acid functional group of the immobilized phthalocyanine molecule being oriented outwardly and deprotonated at pH 7.4 resulting in electrostatic repulsion. Ascorbic acid has two pKa values at 4.17 and 11.6, therefore at pH > 4.17 ascorbate anion forms with a net negative charge resulting in electrostatic repulsion with the Au-PEA-CoTCPhOPc electrode. Dopamine, norepinephrine and epinephrine have pKa values > 8 and therefore have a net positive charge at pH 7.4. The negatively charged $–COO^-$ of Au-PEA-CoTCPhOPc attracts the positively charged catecholamine neurotransmitters and their electrocatalysis occurs. The electrocatalytic oxidation current densities ($\mu A.cm^{-2}$) decreased following this trend: 58.7 > 41.3 > 36.4 for dopamine > norepinephrine > epinephrine respectively.

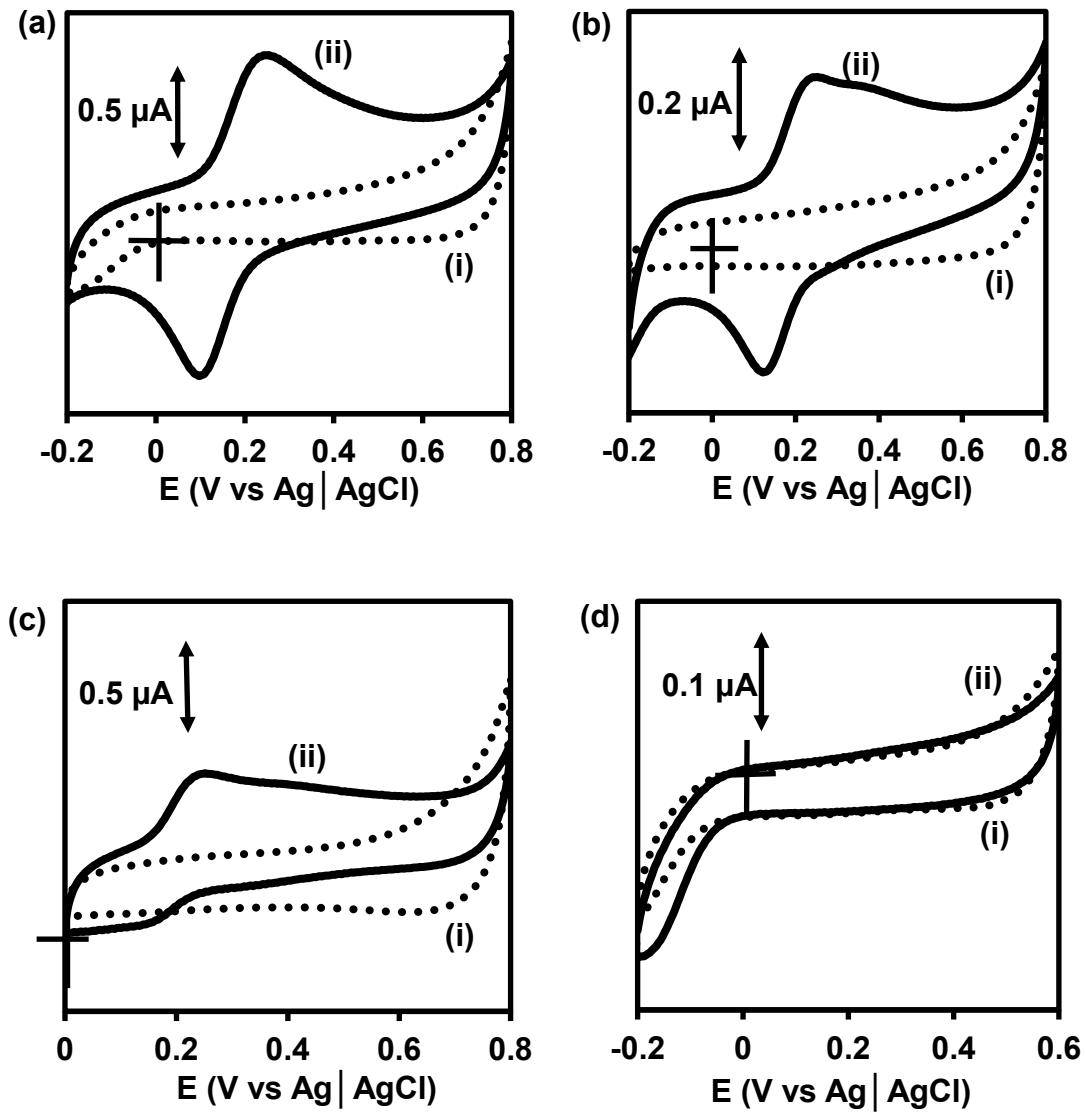

Figure 4.6: Cyclic voltammograms of Au-PEA-CoTCPhOPc in the **(i)** absence and **(ii)** presence of 0.10 mM **(a)** dopamine, **(b)** norepinephrine, **(c)** epinephrine and **(d)** ascorbic acid in pH 7.4 phosphate buffer solution at scan rate 50 $mV.s^{-1}$.

The electrochemical detection of 1.0 mM in pH 7.4 PBS solution of **(a)** dopamine, **(b)** norepinephrine, **(c)** epinephrine and **(d)** ascorbic acid were investigated on **(i)** bare Au and **(ii)** Au-PEA in **Figure 4.7**. The oxidation on both the electrodes occurred at much higher potentials, between 0.366 V – 0.569 V at Au and between 0.483 V – 0.601 V at

Au-PEA. For Au-PEA-CoTCPhOPc, the oxidation potentials were observed between 0.264 V – 0.271 V. Furthermore, the bare Au and Au-PEA electrodes showed oxidation due to the strong catecholamine neurotransmitter interferent, ascorbic acid at 0.366 V for bare Au and at 0.520 V for Au-PEA.

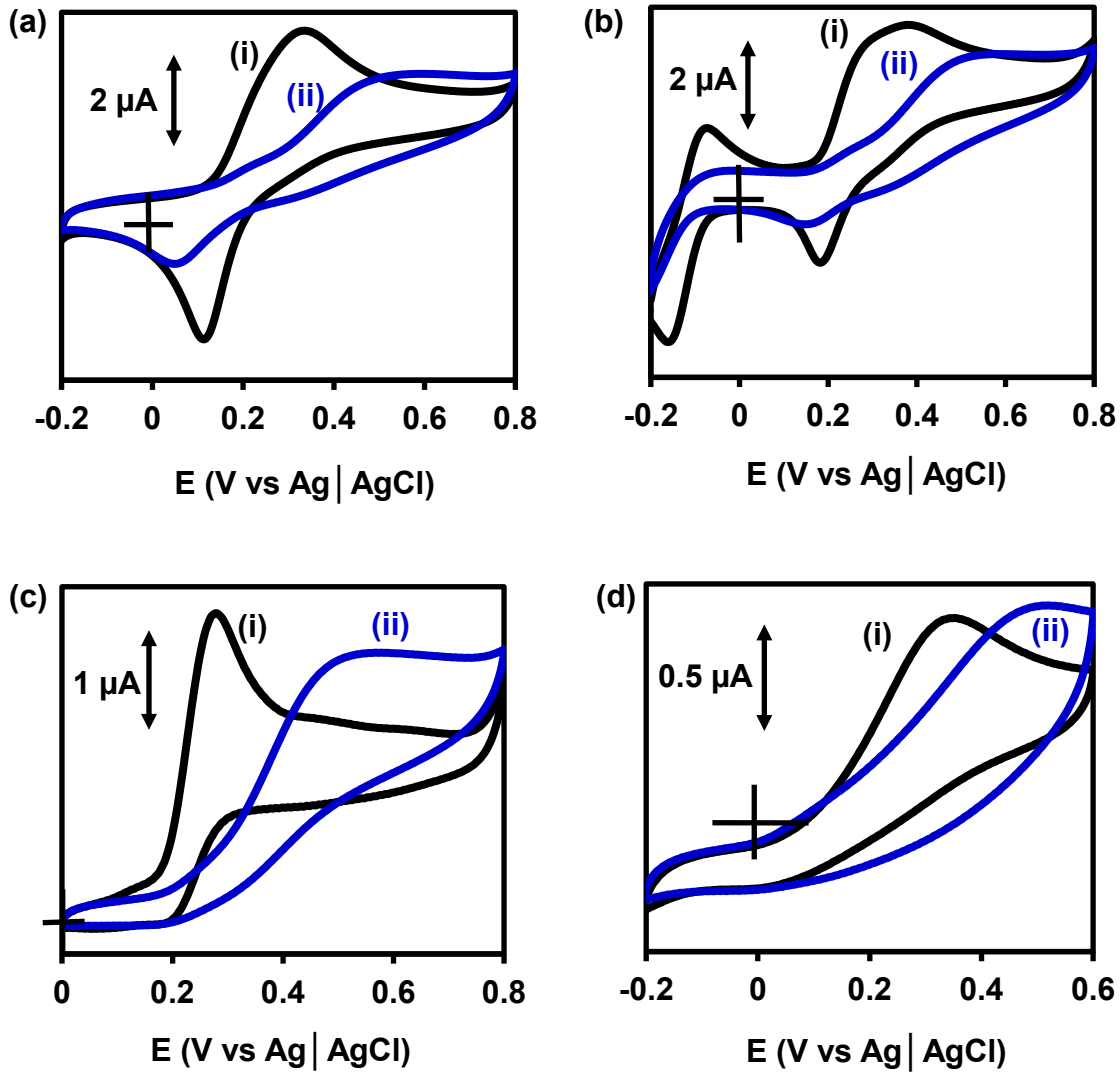

Figure 4.7: Cyclic voltammograms of **(i)** bare Au and **(ii**) Au-PEA in the presence of 1.0 mM **(a)** dopamine, **(b)** norepinephrine, **(c)** epinephrine and **(d)** ascorbic acid in pH 7.4 phosphate buffer solution at scan rate 50 $mV.s^{-1}$.

No oxidation of ascorbic acid was observed on Au-PEA-CoTCPhOPc. The lack of oxidation of ascorbic acid on Au-PEA-CoTCPhOPc electrode was attributed to the pH selectivity at pH 7.4 due to the deprotonated $–COO^-$ functional groups. A summary of the electrocatalytic detection (oxidation potentials, E_{ap}) of 1.0 mM (0.10 mM in the case of Au-PEA-CoTCPhOPc) DA, NEP, EP and AA concentrations for bare Au, Au-PEA and Au-PEA-CoTCPhOPc are summarized in **Table 4.1**.

Table 4.1: Summary of the electrocatalytic detection (oxidation potentials, E_{ap}) of 1.0 mM (0.10 mM in the case of Au-PEA-CoTCPhOPc) DA, NEP, EP and AA concentrations for bare Au, Au-PEA and Au-PEA-CoTCPhOPc.

	DA (E_{pa}/V)	**NEP (E_{pa}/V)**	**EP (E_{pa}/V)**	**AA (E_{pa}/V)**
Au	0.420	0.569	0.552	0.366
Au-PEA	0.601	0.552	0.483	0.520
Au-PEA-CoTCPhOPc	0.264	0.269	0.271	-

4.6 Electroanalytical Detection of Catecholamine Neurotransmitters and Ascorbic Acid

The electrocatalysis of dopamine (DA), norepinephrine (NEP) and epinephrine (EP) exhibited excellent electrocatalysis at Au-PEA-CoTCPhOPc and were analysed further. **Figure 4.8** shows the CVs and the corresponding calibration curve of Au-PEA-CoTCPhOPc in the presence of **(i)** 5.0 µM, **(ii)** 10.0 µM, **(iii)** 25.0 µM, **(iv)** 50.0 µM, **(v)** 75.0 µM and **(vi)** 100.0 µM of **(a)** dopamine, **(b)** norepinephrine, **(c)** epinephrine and **(d)** ascorbic acid in pH 7.4 PBS solution. For dopamine in **Figure 4.8 (a)**, we observed a linear increase in electrocatalytic oxidation and reduction currents. The calibration

curves for electro-oxidation peak currents (I_{pa}) gave a linear relationship: I_{pa} (μA) = 0.00991 [DA] (μM) + 0.233 with a correlation coefficient (R^2) = 0.991. The electroreduction peak currents (I_{pc}) gave a linear relationship: I_{pc} (μA) = -0.00892 [DA] (μM) - 0.339 with R^2 = 0.998 was observed with an increase in analyte concentrations. The limit of detection (LoD) was determined using 3σ (σ blank solution without the analyte) to be 1.32 μM for oxidation and 0.95 μM for reduction. For norepinephrine in **Figure 4.8 (b)**, the changes in concentration were linear with electro-oxidation (I_{pa}) and electroreduction (I_{pc}) peak currents with the relationships: I_{pa} (μA) = 0.00622 [NEP] (μM) + 0.232 with R^2 = 0.995 and I_{pc} (μA) = -0.00477 [NEP] (μM) - 0.306 with R^2 = 0.996. The LoD for norepinephrine electro-oxidation was found to be 2.11 μM and 1.78 μM for its electroreduction. For epinephrine in **Figure 4.8 (c)**, the linear curve was observed for the electro-oxidation peak currents (I_{pa}) against concentrations and gave the following relationship: Ipa (μA) = 0.00425 [EP] (μM) + 0.308 with R^2 = 0.990. LoD for epinephrine was found to be 3.08 μM using 3σ. Increasing the concentration of ascorbic acid (AA) between 5.0 – 100.0 μM in **Figure 4.8 (d)** showed no increase in current within the studied potential and concentration range. The limit of quantification (LoQ) was also determined using 10σ (σ background current with no analyte) and was found to be 4.41 μM for electro-oxidation and 3.17 μM for electroreduction of dopamine. For norepinephrine the LoQ was found to be 7.02 μM for electro-oxidation and 5.93 μM for electroreduction and for epinephrine, the LoQ was found to be 10.3 μM for electro-oxidation. The sensitivity of the Au-PEA-CoTCPhOPc towards dopamine was found to be 0.49 $\mu A.\mu M^{-1}.cm^{-2}$ for electro-oxidation and 0.44 $\mu A.\mu M^{-1}.cm^{-2}$ for electroreduction. For norepinephrine the sensitivity was found to be 0.31 $\mu A.\mu M^{-1}.cm^{-2}$ for electro-oxidation and 0.24 $\mu A.\mu M^{-1}.cm^{-2}$ for electroreduction and for epinephrine, it was determined to be 0.22 $\mu A.\mu M^{-1}.cm^{-2}$ for electro-oxidation.

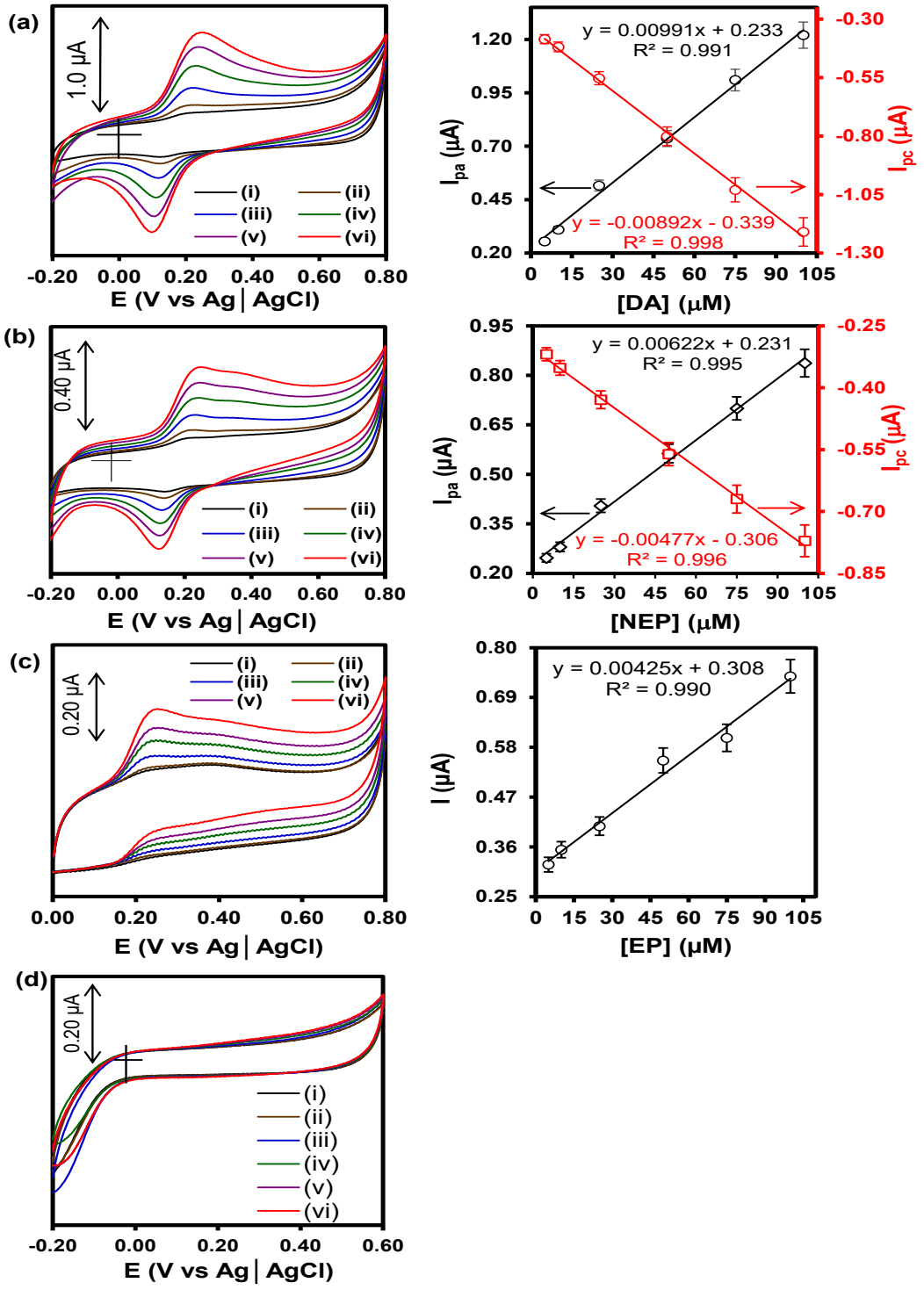

Figure 4.8: Cyclic voltammograms and the corresponding calibration curve of Au-PEA-CoTCPhOPc in the presence of **(i)** 5.0 µM, **(ii)** 10.0 µM, **(iii)** 25.0 µM, **(iv)** 50.0 µM, **(v)** 75.0 µM and **(vi)** 100.0 µM of **(a)** dopamine, **(b)** norepinephrine, **(c)** epinephrine and **(d)** ascorbic acid in pH 7.4 phosphate buffer solution at scan rate 50 $mV.s^{-1}$.

The analytical parameters for Au-PEA-CoTCPhOPc are summarised in **Table 4.2** and are compared with those reported in literature using cobalt phthalocyanine derivatives and their nanomaterial conjugates. Au-PEA-CoTCPhOPc was comparable with various reported methods in that the electrocatalytic peaks for dopamine, norepinephrine and epinephrine were at oxidation potentials less than 0.300 V. The electrocatalytic potentials were also close to the formal oxidation potentials for Co^{II}/Co^{III} which is between 0.00 – 0.60 V. The LoD for Au-PEA-CoTCPhOPc were in μM range. These are higher than those of other CoPc derivatives[76,78] and nanomaterial-CoPc conjugates with graphene[79] and MWCNT.[77] For epinephrine, the LoD value obtained from Au-PEA-CoTCPhOPc (3.08 μM) was lower than the electrode modified with Au-Cys-SWCNT-CoTAPc (6.0 μM) but higher than the electrode modified with MWCNT-CoPc (15.6 nM). Our previous study[106] showed that GCE electrodes give higher electrocatalytic current densities and better LoD when compared to gold electrodes for polymerization of CoTAPc. The comparison conducted was for GCE modified electrodes. There are very few studies conducted with cobalt phthalocyanine modified gold electrode surfaces for the detection of dopamine, norepinephrine and epinephrine. One report by Ozoemena et al.[32] was observed for epinephrine electrochemical detection. The fabrication of the GCE was via electrodeposition and drop-drying of the electrocatalyst or its nanomaterial composite. This method is unstable for long term use. The proposed method in the present study allows for stable thin films fabrication and the gold electrode could be used for months after first preparation. The stability of the method is attributed to electrochemical grafting of the thin PEA film with a strong Au-C bond and covalent amide coupling of the CoTCPhOPc. The studies were reproducible with < 5% (% RSD) during storage and the method was highly reproducible following similar procedure.

Ascorbic acid as a strong interferent for the detection of dopamine, norepinephrine and epinephrine could not be detected within the studied concentration range up to 100.0 μM. The screening off of ascorbic acid was attributed to the carboxylic acid functional groups and the choice of solution pH (7.4) which resulted in the net negative charge ($–COO^-$). At pH 7.4, ascorbic acid exists as an ascorbate anion (pKa = 4.17) and is thus repelled by the negative $–COO^-$. For the catecholamine neurotransmitters, the pKa values were > 8.0 and at pH 7.4 all catecholamine neurotransmitters had a net positive charge due to the ($–NH_3^+$) and therefore could be attracted to the negatively charged $–COO^-$ of Au-PEA-CoTCPhOPc thin monolayer film and get electrochemically oxidized and reduced.

Table 4.2: Summary of the analytical parameters for Au-PEA-CoTCPhOPc towards the detection of dopamine, norepinephrine and epinephrine compared with reported methods using CoPc derivatives and their nanomaterial conjugates.

Analyte	E_p (V)	LoD	LoQ	LCR	Sensitivity	Refs.
DA	0.264	1.32 µM	4.40 µM	5.0 – 100 µM	0.49 µA.µM.cm^{-2} ($e_{ox.}$)	TW
	0.110	0.95 µM	3.17 µM	5.0 – 100 µM	0.44 µA.µM.cm^{-2} ($e_{red.}$)	TW
	[a]0.300	20 nM	-	0.10 – 1.0 µM	0.024 µA.nM^{-1} (CA)	76
		30 nM		0.10 – 0.40 µM	0.016 µA.nM^{-1} (CV)	
	[b]0.490	0.33 nM	10.0 nM	7.5 – 67.5 nM	1.07 µA.µM^{-1}	77
	[c]0.245	0.030 µM	-	2.0 – 10 µM	2.54 µA.µM^{-1}	78
	[d]0.280	0.87 nM	-	20 – 220 nM	0.302 µA.nM^{-1}	79
NEP	0.269	2.11 µM	7.02 µM	5.0 – 100 µM	0.31 µA.µM.cm^{-2} ($e_{ox.}$)	TW
	0.130	1.78 µM	5.93 µM	5.0 – 100 µM	0.24 µA.µM.cm^{-2} ($e_{red.}$)	TW
EP	0.271	3.08 µM	10.3 µM	5.0 – 100 µM	0.22 µA.µM.cm^{-2}	TW
	[e]0.250	15.6 nM	-	1.33 – 5.5 µM	-	15
	[f]0.200	6.0 µM	-	Up to 130 µM	9.4 mA.mM^{-1})	32

TW (this work), [a]GCE-pCoTABAPc (cobalt (II) tetra-[*β*-N-(4-aminophenyl)benzamide] phthalocyanine), [b]GCE-MWCNT-CoTMBANAPc (cobalt (II) tetra[(*E)*-(4-methoxybenzylidene) amino] naphthalene-1-amine phthalocyanine), [c]GCE-CoTGPc (cobalt (II) tetra-ganciclovir phthalocyanine), [d]GCE-Graphene-CoTSPc (cobalt (II) tetrasulfonated phthalocyanine), [e]MWCNT-CoPc (cobalt (II) phthalocyanine), [f]Au-Cys-SWCNT-CoTAPc (cobalt (II) tetra-amino phthalocyanine). CA (chronoamperommetry) and CV (cyclic voltammetry). $e_{ox.}$ (electrocatalytic oxidation) and $e_{red.}$ (electrocatalytic reduction).

4.7 Mechanism for Electrocatalytic Oxidation or Reduction

The Au-PEA-CoTCPhOPc showed good electrocatalytic oxidation and reduction towards dopamine (DA) and norephinephrine (NEP) whilst for epinephrine (EP) only the electrocatalytic oxidation was observed. The electrocatalytic oxidation and reduction at the MPc complex modified electrode is a metal-based process.[107] The computational analysis of the involvement of metal ion of CoPc and oxygen atom of the dopamine was previously reported.[108] The overlap of the frontier orbitals from lowest unoccupied molecular orbital (LUMO+2) for metal d_z^2 orbitals were found datively stronger for dopamine highest occupied molecular orbital (HOMO-2). The frontier orbitals of ascorbic acid (a strong interferent of catecholamine neurotransmitter detection) do not overlap with the LUMO+2 (metal d_z^2 orbitals) hence not electrocatalyzed, and also electrostatic repulsion blocks the interaction with the immobilized CoTCPhOPc at Au-PEA-CoTCPhOPc. **Equations** (**4.3**) and (**4.4**) show the mechanism of dopamine electrocatalytic oxidation and reduction. The metal oxidation first occurs equation (**4.3**), the loss of 2 electrons ($2e^-$) and an increase in oxidation state of Co^{II}TCPhOPc to Co^{III}TCPhOPc. Two CoTCPhOPc molecules are required for the oxidation and reduction of a single dopamine molecule. The Co^{III}TCPhOPc allows for the coordination of dopamine (DA) via O atoms and the oxidation occurs to form dopamine-o-quinone (DAq), equation (**4.4**). Similar results also occur for the efficient detection of norepinephrine and epinephrine.

$$2\,Co^{II}TCPhOPc \rightleftharpoons 2\,Co^{III}TCPhOPc + 2e^- \qquad \textbf{(4.3)}$$

$$2\,Co^{III}TCPhOPc + DA \rightleftharpoons 2\,Co^{II}TCPhOPc + DAq + 2H^+ \qquad \textbf{(4.4)}$$

Chapter Five: Conclusions and Future Perspectives

5. Conclusions and Future Perspectives

This chapter serves to conclude the present study by summarizing its findings and provide an outlook for future studies aimed at carrying the study forward.

5.1 Conclusions

The successful synthesis of CoTCPhOPc through the cyclotetramerization of 4-(3-carboxyphenoxy)phthalonitrile was accomplished. The CoTCPhOPc was confirmed using FT-IR spectroscopy, UV-vis spectroscopy, MCD spectroscopy, elemental analysis and mass spectrometry. CoTCPhOPc was then immobilized onto a phenylethylamino pre-grafted gold electrode surface, Au-PEA, successfully to yield Au-PEA-CoTCPhOPc surface. The Au-PEA-CoTCPhOPc electrode was characterized using electrochemical methods (cyclic voltammetry and impedance spectroscopy) and spectroscopic methods (X-ray photoelectron spectroscopy). The effect of pH was evaluated using negative and positively charged redox probes, $[Fe(CN)_6]^{3-/4-}$ and $[Ru(NH_3)_6]^{2+/3+}$ respectively. Au-PEA-CoTCPhOPc was used to detect dopamine, norepinephrine and epinephrine successfully with electro-oxidation peak potentials observed at 0.264 V, 0.269 V and 0.271 V respectively. The LoD (μM) and LoQ (μM, in bracket) values were obtained to be 1.32 (4.41), 2.11 (7.02) and 3.08 (10.3) respectively for electro-oxidation of dopamine, norepinephrine and epinephrine. For the electroreduction of dopamine and norepinephrine, the reduction peaks were observed at 0.110 V and 0.130 V respectively. The LoD and LoQ (in brackets) based on the electroreduction were obtained to be 0.95 (3.17) and 1.78 (5.63) μM for dopamine and norepinephrine respectively. The Au-PEA-CoTCPhOPc exhibited excellent sensitivity ($\mu A.\mu M^{-1}.cm^{-2}$) with the following trend 0.49 > 0.31 > 0.22 for

dopamine > norepinephrine > epinephrine respectively for electrocatalytic oxidation. For electrocatalytic reduction dopamine gave good sensitivity of 0.44 $\mu A.\mu M^{-1}.cm^{-2}$ compared to 0.24 $\mu A.\mu M^{-1}.cm^{-2}$ for the electroreduction of norepinephrine. The Au-PEA-CoTCPhOPc thin film was shown to screen off ascorbic acid as no electrocatalytic oxidation or reduction peak was observed within the studied potential range and concentration up to 100.0 μM. The potential application of the proposed method is promising as a stable and reproducible Au-PEA-CoTCPhOPcs can be fabricated. Therefore, Au-PEA-CoTCPhOPc can be used for the detection of catecholamine neurotransmitters in various conditions without losing the electrocatalytic CoTCPhOPc thin monolayer film and signal after refreshing through cycling in pH 7.4 PBS solution.

5.2 Future Perspectives

The research is ongoing in an effort to optimize the electrode to enable discrimination between the catecholamine neurotransmitters. Goyal and Bishnoi (2011)[109] designed an electrode that could distinctly discriminate between dopamine, norepinephrine and epinephrine in human plasma and urine samples. This work forms the basis of our continued investigation. In addition, the evaluation of Au-PEA-CoTCPhOPc towards real sample analysis would be conducted once the electrode design can discriminate between the various catecholamine neurotransmitters.

References

1 J. A. Ribeiro, P. M. V. Fernandes, C. M. Pereira and F. Silva, *Talanta*, 2016, **160**, 653 – 679.

2 B. J. Sanghavi, O. S. Wolfbeis, T. Hirsch and N. S. Swami, *Microchim. Acta*, 2015, **182**, 1 – 41.

3 C. Yang, M. E. Denno, P. Pyakurel and B. J. Venton, *Anal. Chim. Acta*, 2015, **887**, 17 – 37.

4 Z. Tavakolian-Ardakani, O. Hosu, C. Cristea, M. Mazloum-Ardakani and G. Marrazza, *Sensors*, 2019, **19**, 1 – 30.

5 S. D. Niyonambaza, P. Kumar, P. Xing, J. Mathault, P. De Koninck, E. Boisselier, M. Boukadoum and A. Miled, *Appli. Sci.*, 2019, **9**, 1 – 31.

6 S. Jung-Klawitter and O. K. Hubschmann, *Cells*, 2019, **8**, 1 – 45.

7 F. Ghasemi, M. R. Hormozi-Nezhad and M. Mahmoudi, *Anal. Chim. Acta*, 2016, **917**, 85 – 92.

8 X. Cao, M. Qin, P. Li, B. Zhou, X. Tang, M. Ge, L. Yang and J. Liu, *Sen. Actuators B Chem*, 2018, **268**, 350 – 358.

9 A. S. Adekunle, B. O. Agboola, J. Pillay and K. I. Ozoemena, *Sen. Actuators B Chem*, 2010, **148**, 93 – 102.

10 Z. Guo, M.-L. Seol, M.-S. Kim, J.-H. Ahn, Y.-K. Choi, J.-H. Liu and X.-J. Huang, *Analyst*, 2013, **138**, 2683 – 2690.

11 X. Ma, M. Chen, X. Li, A. Purushothaman and F. Li, *Int. J. Electrochem. Sci.*, 2012, **7**, 991 – 1000.

12 B. O. Agboola and K. I. Ozoemena, *Electroanalysis*, 2008, **20**, 1696 – 1707.

13 D. M. Fouad and W. A. El-Said, *J. Nanomater.*, 2016, 1 – 8.

14 B. O. Agboola, S. L. Vilakazi and K. I. Ozoemena, *J. Solid State Electrochem.*, 2009, **13**, 1367 – 1379.

15 F. C. Moraes, D. L. C. Golinelli, L. H. Mascaro and S. A. S. Machado, *Sen. Actuators B Chem*, 2010, **148**, 492 – 497.

16 M. V. Gorbunova, S. V. Gutorova, D. A. Berseneva, V. V. Apyari, V. D. Zaitsev, S. G. Dmitrienko and Y. A. Zolotov, *Appl. Spectrosc. Rev.*, 2019, **54**, 631 – 652.

17 L. Xie, L. Chen, P. Gu, L. Wei and X. Kang, *J. Vis. Exp.*, 2018, **133**, 1 – 10.

18 S. Kruss, M. P. Landry, E. V. Ende, B. M. A. Lima, N. F. Reuel, J. Zhang, J. Nelson, B. Mu, A. Hilmer and M. Strano, *J. Am. Chem. Soc.*, 2014, **136**, 713 – 724.

19 J. F. van Staden and R. I. S. van Staden, *Talanta*, 2012, **102**, 34 – 43.

20 H.-C. Lee, T.-H. Chen, W.-L. Tseng and C.-H. Lin, *Analyst*, 2012, **137**, 5352 – 5357.

21 J.-J. Feng, H. Guo, Y.-F. Li, Y.-H. Wang, W.-Y. Chen and A.-J. Wang, *ACS Appl. Mater. Interfaces*, 2013, **5**, 1226 – 1231.

22 S. Jafarinejad, M. Ghazi-Khansari, F. Ghasemi, P. Sasanpour and M. R. Hormozi-Nezhad, *Sci. Rep.*, 2017, **7**, 1 – 8.

23 A. Naseri and M. R. Majidi, *DARU J. of Pharm. Sci.*, 2011, **19**, 270 – 276.

24 N. Elgrishi, K. J. Rountree, B. D. McCarthy, E. S. Rountree, T. T. Eisenhart and J. L. Dempsey, *J. Chem. Educ.*, 2018, **95**, 197 – 206.

25 S. R. Ali, Y. Ma, R. R. Parajuli, Y. Balogun, W. Y.-C. Lai and H. He, *Anal. Chem.*, 2007, **79**, 2583 – 2587.

26 A.-L. Liu, S.-B. Zhang, W. Chen, X.-H. Lin and X.-H. Xia, *Biosens. Bioelectron.*, 2008, **23**, 1488 – 1495.

27 M. Mazloum-Ardakani, H. Beitollahi, B. Ganjipour, H. Naeimi and M. Nejati, *Bioelectrochemistry*, 2009, **75**, 1 – 8.

28 B. O. Agboola and K. I. Ozoemena, *Phys. Chem. Chem. Phys.*, 2008, **10**, 2399 – 2408.

29 S. R. Ali, R. R. Parajuli, Y. Balogun, Y. Ma and H. He, *Sensors*, 2008, **8**, 8423 – 8452.

30 S. Thiagarajan, R.-F. Yang and S.-M. Chen, *Bioelectrochemistry*, 2009, **75**, 163 – 169.

31 R. N. Goyal, V. K. Gupta, M. Oyama and N. Bachheti, *Talanta*, 2007, **72**, 976 – 983.

32 K. I. Ozoemena, D. Nkosi and J. Pillay, *Electrochim. Acta*, 2008, **53**, 2844 – 2851.

33 S. Arslan, *J. of Life Sci.*, 2016, **6**, 188 – 197.

34 G. de la Torre, C. G. Claessens and T Torres, *Chem Comm*, 2007, 2000 – 2015.

35 Z. Neduvhuledza, T. Nkaki, M. Louzada, T. Nyokong and S. Khene, *Opt. Mater.*, 2020, **109**, 1 – 10.

36 A. Hajri, S. Touaiti and B. Jamoussi, *Adv. Optoelectron.*, 2013, 1 – 7.

37 D. Mwanza, S. Khene and P. Mashazi, *Polyhedron*, 2017, **134**, 263 – 274.

38 C. Yagci and A. Bilgin, *J. Porphyr. Phthalocyanines*, 2013, **17**, 573 – 586.

39 M. S. Agirtas, B. Cabir and S. Ozdemir, *Dyes Pigm.*, 2013, **96**, 152 -157.

40 I. Acar, S. Topcu, Z. Biyiklioglu and H. Kantekin, *Color. Technol.*, 2013, **129**, 259 – 266.

41 C. G. Claessens, U. Hahn and T. Torres, *Chem. Rec.*, 2008, **8**, 75 – 97.

42 N. Masilela and T. Nyokong, *Dyes Pigm.*, 2010, **84**, 242 – 248.

43 V. N. Nemykin and E. A. Lukyanets, *Arkivoc*, 2010, **(i)**, 136 – 208.

44 X. Song, Y. She, H. Ji and Y. Zhang, *Org. Process Res. Dev.*, 2005, **9**, 297 – 301.

45 J. Mack and N. Kobayashi, *Chem. Rev.*, 2011, **111**, 281 – 321.

46 S. Centane, O. J. Achadu and T. Nyokong, *Electroanalysis*, 2017, **29**, 2470 – 2482.

47 N. Xiao and B. J. Venton, *Anal. Chem.* 2012, **84**, 7816 – 7822.

48 N. Rapulenyane, E. Antunes, N. Masilela and T. Nyokong, *J. Photochem. Photobio. A*, 2012, **250**, 18 – 24.

49 M. Yanagisawa, F. Korodi, J. Bergquist, A. Holmberg, A. Hagfeldt, B. Akermark and L. Sun, *J. Porphyr. Phthalocyanines*, 2004, **8**, 1228 – 1235.

50 Y. Wan, S. Chen, G. Wang, Q. Liang, Z. Li and S. Xu, *Acta Phys. Pol. A*, 2016, **130**, 785 – 790.

51 O. G. Lutsenko and O. A. Golubchikov, *Russ. J. of Appl. Chem.*, 2011, **84**, 1623 – 1625.

52 M. S. Kahouech, K. Hriz, S. Touaiti and J. Bassem, *Mater. Res. Bull.*, 2016, **75**, 144 – 154.

53 J. H. Zagal and F. Bedioui, *Electrochemistry of N4 Macrocyclic Metal Complexes Volume 2: Biomimesis, Electroanalysis and Electrosynthesis of MN4 Metal Complexes*, Springer International Publishing, Switzerland, 2016.

54 J. Nackiewicz and M. Kliber, *Arkivoc*, 2015, **(i)**, 269 – 299.

55 G. K. Karaoglan, G. Gumrukcu, A. Koca, A. Gul and U. Avciata, *Dyes Pigm.*, 2011, **90**, 11 – 20.

56 R. Bayrak, H. T. Akcay, Z. Biyiklioglu and I. Degirmencioglu, *Synth. Met.*, 2016, **220**, 643 – 652.

57 P. N. Mashazi, K. I. Ozoemena, D. M. Maree and T. Nyokong, *Electrochim. Acta*, 2006, **51**, 3489 – 3494.

58 D. Mwanza, S. Mvango, S. Khene, T. Nyokong and P. Mashazi, *Electrochim. Acta*, 2017, **254**, 89 – 100.

59 M. Shumba and T. Nyokong, *Electrochim. Acta*, 2016, **196**, 457 – 469.

60 D. Akyuz, U. Demirbas, A. Koca, F. Celik and H. Kantekin, *J. Mol. Struct.*, 2020, **1206**, 1 – 7.

61 V. Cakir, F. Demir, Z. Biyiklioglu, A. Koca and H. Kantekin, *Dyes Pigm.*, 2013, **98**, 414 – 421.

62 N. Manjunatha, M. Imadadulla, K. S. Lokesh and K. R. V. Reddy, *Dyes Pigm.*, 2018, **153**, 213 – 224.

63 M. Nemakal, S. Aralekallu, I. Mohammed, S. Swamy and L. K. Sannegowda, *J. Electroanal. Chem.*, 2019, **839**, 238 – 246.

64 S. Khene, D. A. Geraldo, C. A. Togo, J. Limson and T. Nyokong, *Electrochim. Acta*, 2008, **54**, 183 – 191.

65 Z. O. Makinde, M. Louzada, P. Mashazi, T. Nyokong and S. Khene, *Appl. Surf. Sci.*, 2017, **425**, 702 – 712.

66 N. Manjunatha, A. Shambhulinga, M. Imadadulla, K. Prabhu C. P. and K. S. Lokesh, *Microchem. J.*, 2018, **143**, 82 – 91.

67 K. I. Ozoemena and T. Nyokong, *J. Electroanal. Chem.*, 2005, **579**, 283 – 289.

68 D. Belanger and J. Pinson, *Chem. Soc. Rev.*, 2011, **40**, 3995 – 4048.

69 S. Griveau, D. Mercier, C. Vautrin-Ul, A. Chausse, *Electrochem. Commun.*, 2007, **9**, 2768 – 2773.

70 S. Kesavan and S. A. John, *J. Colloid Interface Sci.*, 2014, **428**, 84 – 94.

71 O. K. Adeniyi and P. N. Mashazi, *Electrochem. Acta*, 2020, **331**, 1 – 10.

72 K. E. Berg, Y. R. Leroux, P. Hapiot and C. S. Henry, *ChemElectroChem*, 2019, **6**, 4811 – 4816.

73 S. Kesavan, A. Prabhakaran and S. A. John, *RSC Adv.*, 2014, **4**, 30896 – 30905.

74 R. G. Nuzzo, B. R. Zegarski and L. H. Dubois, *J. Am. Chem. Soc.*, 1987, **109**, 733 – 740.

75 P. Mashazi and T. Nyokong, *Microchim. Acta*, 2010, **171**, 321 – 332.

76 V. A. Sajjan, I. Mohammed, M. Nemakal, S. Aralekallu, H. Kumar K. R., S. Swamy and L. K. Sannegowda, *J. Electroanal. Chem.*, 2019, **838**, 33 – 40.

77 Mounesh, B. S. Jilani, M. Pari, K. R. V. Reddy and K. S. Lokesh, *Microchem. J.*, 2019, **147**, 755 – 763.

78 Mounesh, P. Malathesh, N. Y. P. Kumara, B. S. Jilani, C. D. Mruthyunjayachari and K. R. V. Reddy, *Heliyon*, 2019, **5**, 1 – 14.

79 N. Diab, D. M. Morales, C. Andronescu, M. Masoud and W. Schuhmann, *Sens. Actuat. B Chem.*, 2019, **285**, 17 – 23.

80 N. G. Mphuthi, A. S. Adekunle and E. E. Ebenso, *Sci. Rep.*, 2016, **6**, 1 – 20.

81 S. R. Nxele, D. O. Oluwole and T. Nyokong, *Electrochim. Acta*, 2019, **326**, 1 – 13.

82 D. Rudolph, S. Neuhuber, C. Kranz, M. Taillefert and B. Mizaikoff, *Analyst*, 2004, **129**, 443 – 448.

83 M. N. Abbas, A. A. Saeed, M. B. Ali, A. Errachid, N. Zine, A. Baraket and B. Singh, *J. Solid State Electrochem.*, 2019, **23**, 1129 – 1144.

84 A. G. Shard, *J. Vac. Sci. Technol. A*, 2020, **38**, 1 – 13.

85 G. Greczynski and L. Hultman, *Prog. Mater Sci.*, 2020, **107**, 1 – 46.

86 P. N. Mashazi, K. I. Ozoemena and T. Nyokong, *Electrochim. Acta*, 2006, **52**, 177 – 186.

87 D. Martel, N. Sojic and A. Kuhn, *J. Chem. Ed.*, 2002, **79**, 349 – 352.

88 B. O. Agboola, A. Mocheko, J. Pillay and K. I. Ozoemena, *J. Porphyr. Phthalocyanines*, 2008, **12**, 1289 – 1299.

89 A. Sacco, *Renew. Sust. Energ. Rev.*, 2017, **79**, 814 – 829.

90 A. Yahyazadeh and V. Azimi, *Elixir Appl. Chem.*, 2012, **49**, 9991 – 9993.

91 D. O. Oluwole and T. Nyokong, *J. of Photochem. Photobiol. A*, 2015, **312**, 34 – 44.

92 A. Fashina, E. Amuhaya and T. Nyokong, *Spectrochim. Acta A Mol. Biomol. Spectrosc*, 2015, **137**, 294 – 299.

93 Y. Li, T. M. Pritchett, J. Huang, M. Ke, P. Shao and W. Sun, *J. Phys. Chem. A*, 2008, **112**, 7200 – 7207.

94 J. Mack and M. J. Stillman, *Encyclopedia of Inorganic and Bioinorganic Chemistry*, 2011, 1 – 16.

95 G. N. Ngubeni, J. Britton, J. Mack, E. New, I. Hancox, M. Walker, T. Nyokong, T. S. Jones and S. Khene, *J. Mater. Chem. C.*, 2015, **3**, 10705 – 10714.

96 N. Kobayashi and K. Nakai, *Chem. Commun.*, 2007, 4077 – 4092.

97 K. P. Kabwe, M. Louzada, J. Britton, T. O. Olomola, T. Nyokong and S. Khene, *Dyes Pigm.*, 2019, **168**, 347 – 356.

98 S. Colak, M. Durmus and S. Z. Yildiz, *Dalton Trans.*, 2016, **45**, 10402 – 10410.

99 P. Mashazi, E. Antunes and T. Nyokong, *J. Porphyr. Phthalocyanines*, 2010, **14**, 932 – 947.

100 P. Mashazi, P. Tetyana, S. Vilakazi and T. Nyokong, *Biosens. Bioelectron*, 2013, **49**, 32 – 38.

101 K. Ozoemena and T. Nyokong, *Electrochim. Acta*, 2002, **47**, 4035 – 4043.

102 B. O. Agboola, K. I. Ozoemena, T. Nyokong, T. Fukuda and N. Kobayashi, *Carbon*, 2010, **48**, 763 – 773.

103 P. N. Mashazi, P. Westbroek, K. I. Ozoemena and T. Nyokong, *Electrochim. Acta*, 2007, **53**, 1858 – 1869.

104 H. O. Finklea, *Electroanalytical Chemistry*, **19**, Marcel Dekker, New York, 1996.

105 K. I. Ozoemena, T. Nyokong and P. Westbroek, *Electroanalysis*, 2003, **15**, 1762 – 1770.

106 P. Mashazi, C. Togo, J. Limson and T. Nyokong, *J. Porphyr. Phthalocyanines*, 2010, **14**, 252 – 263.

107 H. Xu, J. Xiao, L. Yan, L. Zhu and B. Liu, *J. Electroanal. Chem.*, 2016, **779**, 92 – 98.

108 N. Fourati, M. Seydou, C. Zerrouki, A. Singh, S. Samanta, F. Maurel, D. K. Aswal and M. Chehimi, *ACS Appl. Mater. Interf.*, 2014, **6**, 22378 – 22386.

109 R. N. Goyal and S. Bishnoi, *Talanta*, 2011, **84**, 78 – 83.